
DOCTORAL THESIS

**SIZE EFFECT
OF CONCRETE AND SANDSTONE
IN COMPRESSION**

DISSERTATION

**SIZE EFFECT
VON BETON UND SANDSTEIN
UNTER DRUCKBEANSPRUCHUNG**

ausgeführt zum Zwecke der Erlangung des akademischen Grades eines
Doktors der technischen Wissenschaften

eingereicht an der Technischen Universität Wien
Fakultät für Bauingenieurwesen

von

Dipl.-Ing. Stefan L. Burtscher
Matrikelnummer 8925844
Apollogasse 3/26, 1070 Wien, Österreich

Referent: O.Univ.Prof. Dipl.-Ing. Dr.-Ing. Johann Kollegger, M.Eng.
Institut für Stahlbeton- und Massivbau, Technische Universität Wien
Karlsplatz 13/212, 1040 Wien, Österreich

Koreferent: Prof. Ing. Zdeněk Bittnar, DrSc.
Department of Structural Mechanics, CTU Prague
Thákurova 7, 166 29 Praha 6, Czech Republic

Wien, im Dezember 2002

.....

Abstract

It is well known from literature that heterogeneous materials like concrete or rock show different strength and ductility for small and large sizes. Thus the experimental determined strength is not a material property. Numerous experiments were performed regarding the size effect in tension, very few experiments were performed in compression.

In structural systems concrete is applied to carry in compression and not tension. Compressive loading is very important in structural engineering, especially in unreinforced structures. The compressive failure in a load carrying member is brittle and in most cases more dangerous. Experimental investigations are therefore needed. Experiments from literature on column like specimens under compressive loading were performed up to a size range of 1:4. The size range of a series of geometrically equal specimens is given by the amplification factor of a characteristic dimension from the smallest to the largest specimen size. Large size ranges are advantageous, because the data can be fitted more accurately. The largest size range of the experiments under compressive loading will be presented in this thesis. These series were performed in one of the largest testing facilities available. The tests on sandstone were performed on a size range of 1:32 and the concrete series on a size range of 1:16. These test series have the largest size ranges of tests on granular materials under compression published so far.

Three sandstone test series were performed. Special attention was paid to minimize influences of testing facilities, determine an appropriate specimen machine interface, a suitable notch for compressive loading and the influence of strength between centric and eccentric loading.

A test series on concrete specimens was carried out. To eliminate additional sources of size effect in the molding process, the formwork and the concrete mixture were considered in the preparation of specimens. The influence between the different testing machines was determined. The increase of strength due to hardening of concrete during testing period was evaluated. A size effect was detected for both materials and the results are compared to the two most common size effect laws.

Contents

1	Introduction	1
1.1	Motivation and aim of this study	1
1.2	The size effect phenomenon	4
1.3	Outline of the thesis	4
2	State of the art	6
2.1	Short historical review of size effect	6
2.2	Sources for size effect on structural strength	7
2.3	Size effect laws	9
2.3.1	The Size Effect Law by Bažant	9
2.3.2	The Multifractal Scaling Law by Carpinteri	10
2.4	Size effect in compression	10
2.5	Size effect tests	12
3	The sandstone material	18
3.1	Introduction	18
3.2	Why is sandstone the material of choice	19
3.3	Density, grains and pores of the different series	20
3.3.1	Sandstone of the preliminary series	20
3.3.2	Sandstone of the test series on sizes XS to XXL	20
3.3.3	Sandstone of the verification series	20
4	Preliminary test series on sandstone	23
4.1	Introduction	23
4.2	Specimen dimensions and geometry	23
4.3	Compressive tests under centric and eccentric loading	26
4.3.1	Investigations on the notches for specimens tested under eccentric compression	26
4.3.2	Investigations on the interface between loading platen and specimen	28
4.3.3	Compressive loading	29

4.3.4	Arrangement of displacement transducers and AE-sensors .	30
4.3.5	Test control	31
4.4	Data preparation and parameter extraction	36
4.4.1	Correction of the load displacement plots	36
4.4.2	Determination of material parameters from displacements and loads	36
4.5	Results of preliminary series	39
4.5.1	Centric and eccentric loading	39
4.5.2	Performance of notches and interfaces	39
4.5.3	Strength versus density	39
4.5.4	Strength versus eccentricity of loading	40
4.5.5	Notched specimens after testing	40
4.6	Four Point bending test	42
5	Test series on sandstone	44
5.1	Introduction	44
5.2	Specimen dimensions and geometry	44
5.3	Homogeneity of sandstone specimens	47
5.4	Boundary conditions and testing machines	48
5.4.1	Loading arrangement	48
5.4.2	Interface between loading platen and specimen	49
5.5	Arrangement of displacement transducers	51
5.6	Acoustic Emission Measurements	51
5.6.1	Aim and set-up of acoustic emission measurements	51
5.7	Test control	52
5.8	Results of test series on sizes XS to XXL	52
5.8.1	Strength versus specimen size	54
5.8.2	Strength versus loading rate	55
5.8.3	Strength and Young's modulus versus wave speed	57
5.8.4	Classification of fracture pattern	57
5.8.5	Specimens after testing	59
5.8.6	Influence of the notch on stresses and strains over specimen height	62
5.8.7	Strength versus eccentricity	62
5.8.8	Tabular results of individual specimens	63
5.8.9	Stress strain plots for every specimen	66
5.8.10	Acoustic emission (AE) results	66
6	Verification series on sandstone	71
6.1	Introduction	71
6.2	Specimen dimensions and geometry	71

6.3	Homogeneity of specimen	71
6.4	Boundary conditions and testing machines	74
6.4.1	Loading arrangement	74
6.4.2	Interface between loading platen and specimen	74
6.5	Arrangement of displacement transducers	74
6.6	Test control	74
6.7	Results of verification series on sizes XS to L	75
6.7.1	Specimens after testing	75
6.7.2	Strength versus loading rate	75
6.7.3	Density versus strength	75
6.7.4	Density versus Young's modulus	76
6.7.5	Strength versus specimen size	76
6.7.6	Stress strain plots for each size	78
7	Size effect in compression of sandstone	81
7.1	Collection of strength versus size data	81
7.1.1	Scatter of experimental results	81
7.2	Normalized strength versus size of all series	83
7.3	Fitting of data to SEL and MFSL	83
8	Test series on concrete	85
8.1	Introduction	85
8.2	Specimen dimensions	85
8.2.1	Concrete cylinders for determination of strength	86
8.3	Specimen preparation	87
8.3.1	Concrete formwork and concreting	87
8.3.2	Placing the reinforcement and attaching the steel plate	91
8.3.3	Concrete batch	91
8.3.4	Concreting of specimens	93
8.4	Boundary conditions and loading	94
8.4.1	Loading arrangement	94
8.4.2	Interface between loading platen and specimen	94
8.5	Test set-up	94
8.5.1	Set-up for sizes XXL, XL and L tested in the Column Tester	94
8.5.2	Setup for sizes M and S tested in the D2 machine	96
8.5.3	Set-up for sizes M and L tested in the Inova machine	96
8.5.4	Set-up for tests on the concrete cylinders	99
8.6	Test control	99
8.7	Determination of material parameters from displacements and loads	101

9	Size effect in compression of concrete	103
9.1	Strength versus specimen size	103
9.2	Strength versus loading rate	103
9.3	Development of cylinder strength with time	105
9.4	Influence of age on strength of specimen	105
9.5	Influence of testing machine	109
9.6	Fitting of data to SEL and MFSL	111
9.7	Stress strain diagrams	111
9.8	Tabular results for individual specimens	115
9.9	Specimens after testing and crack patterns	115
10	Summary of main results	121
10.1	Sandstone experiments	121
10.2	Concrete experiments	123
	Bibliography	125

Chapter 1

Introduction

1.1 Motivation and aim of this study

Experimental results on materials like concrete or rock showed that the specimen size has an influence on nominal strength and ductility. Therefore the experimentally determined strength is not a material property, but is dependent on the size of the structure. In the case of concrete, cylinders with a diameter of 15cm and a length of 30cm are often used. With the strength determined on these small specimens structures that are many scales larger are designed. The strength of the structure could only be determined by testing of the structure itself. Usually the size of structures exceeds the capability of testing machines. In the laboratory structures are usually scaled versions of real structure. The experimental results of small scale specimen can give information or insight into the structural behavior, but the influence of the size on the structural strength and ductility cannot be captured. This demand is often not fulfilled. It is interesting to note that this phenomena is known since Leonardo da Vinci, but till today open questions remained. Several different sources influence this phenomena at the same time.

In the last three decades size effect has been studied intensively by numerous researchers. Most of the experiments were performed on various specimen geometries on concrete under tensile loading. The experiments were used to verify the size effect models. The most important models are the Size Effect Law by Bažant (Bažant, 1984) and the Multifractal Scaling Law by Carpinteri (Carpinteri, 1994) or (Carpinteri and Ferro, 1994). One main disadvantage of these laws are that they have to be fitted for each material, geometry and each type of test.

The purpose of this experimental investigation was the further investigation of the size influence. Such phenomena can be observed on large size ranges more clearly than on small size ranges. Due to the fact that the smallest size has to be limited by the representative volume. The largest size is limited by the maximum

load and dimension of the testing machine. The Column Tester at the Vienna University of Technology allows to increase the size range because of its high testing load and large dimensions.

The experimental investigation on the size effect is a difficult task, because one has to deal with different sizes of geometrically equal specimens, where the same boundary conditions have to be met for all specimens and specimen sizes. All geometric dimensions of the specimens have to be scaled by the same factor. The larger the factor from the smallest to the largest specimen, the more pronounced is the effect of size on the observed quantity. When multiplying all the specimen dimensions by a scale factor the length changes linearly with the size factor, the cross section changes by the order of two with the size factor and the volume by the order of three. This means practically that the testing frame has to be adapted to the length of each specimen type and that the maximum load changes by the order of two with the size factor from one size to the other (disregarding the size effect). Due to strongly varying maximum loads different testing frames had to be used. For the investigations a huge (Column Tester) a medium (Inova, TU Prague) and a small (D2) testing machine was used.

It is stated in literature (Van Mier et al., 1997) that different testing machines produce different results. In the concrete series an investigation of machine influence was performed as well. For this purpose tests in the Inova machine at the Institute of Structural Mechanics at the Technical University in Prague were performed.

To determine the size effect in the concrete material it is important that the material is the same in the whole volume of each specimen. Special attention was paid to the molding process and the formwork to prevent alternations of the concrete in specimen with different sizes, e.g. different concrete mixtures, microcracks due to diffusion phenomena or hydration and other phenomena, see sections 2.2 and 8.3.

Several size effect test series for concrete loaded in tension are available. A series with a size range of 1:32 was performed by Van Vliet (2000). Very few experimental investigations were performed on the size effect of concrete under compressive loading. Size effect series for larger size ranges on concrete in compression were performed by Bažant and Kwon on microconcrete (Bažant and Kwon, 1994), Hollingworth and Sener et.al. on plain concrete columns (Hollingworth, 1998; Sener et al., 1999) and Nemeček on reinforced concrete (Nemeček, 2000). The largest size range in all the test series performed on concrete under compression was 1:4. Within the scope of this thesis very large experimental investigations were performed on sandstone and concrete. This concrete size effect series had the largest size range (1:16) of the performed size effect experiments on concrete under compressive loading and the sandstone size effect series had the



(a) Specimen of concrete series on sizes S (diameter 5cm) to XXL (diameter 80cm) (b) Specimen of test series on sizes XS to XXL (smallest specimen in hand)

Figure 1.1: Overview of specimen of the concrete series and the test series on sizes XS to XXL on sandstone

largest size range (1:32) that was performed under compressive loading. All together three experimental series on sandstone under compression were performed, namely the *preliminary series*, the *test series on sizes XS to XXL* and the *verification series*. A detailed report describing the sandstone series and presenting the results for every individual specimen is given in Burtscher et al. (2003a) and for the concrete series in Burtscher et al. (2003b). An overview of the specimens tested in the *test series on sizes XS to XXL* on sandstone and the *concrete size effect series* is given in figure 1.1. The experiments were performed with the Column Tester and the D2 machine in the joint Laboratory of the Institute for Structural Concrete and the Institute for Steel Structures at the Vienna University of Technology. Additional tests were performed in the Inova machine at the Department of Structural Mechanics at CTU Prague.

At the Institute of Structural Concrete at the University of Technology, Vienna a massive frame structure (Schwarz, 1987) is available. In order to carry out the size effect tests the frame was equipped with 4 servo hydraulic actuators, a computer supported data acquisition system, equipment for implementation of the actuators and setup for column testing. It is now possible to perform experiments with closed loop control on specimens with a length from 40cm to 5m, a cross section up to 120x100cm and with a maximum load of 17000kN, see Burtscher et al. (2003a) or Burtscher et al. (2003b) for details. A similar

experimental set-up was used for spun concrete columns, see Burtscher et al. (2002). This testing frame allows to test real size structures. Hence it is possible to compare the structural behavior of real size structures with laboratory size structures. This knowledge is of major importance because structures can then be designed with the strength and ductility determined on real scale laboratory tests.

The failure and the size effect in compression are less understood than in tension. In most cases it is the more important and dangerous failure, which is highly brittle, showing no ductility. This might be even more important for high strength concrete columns.

1.2 The size effect phenomenon

In general terms, the *scale* or *size effect* is the variation of material parameters with specimen size, where the smallest specimen may not be smaller than the representative volume of the material. The size effect vanishes when the representative volume has been reached. The *scale effects* are due to the fact that with increasing size the number of weak spots in the material volume increases as well. Additionally the specimen shape influences the experimental result, which is called *shape effect*. In this investigation all specimen dimensions and eccentricities of loading were scaled by the same factor. Therefore the test series performed in this investigation represent the influence of size and scale but not the influence of shape. A study on the influence of shape is given in (Schickert, 1980).

The available theoretical size effect models describe the variation of strength with size. They are based on different physical assumptions and show different behavior with increasing size. These models are not linear, therefore, large size ranges are advantageous.

1.3 Outline of the thesis

First the *state of the art* is shortly summarized in chapter 2. The sources of the size effect and the most important models describing the size effect are presented. Additionally the tests found in literature are shortly summarized. In chapter 3 the sandstone is described and the quarry is presented.

The experimental investigation started with the *preliminary series* on sandstone specimen on sizes $100x100x200mm$, see chapter 4. First the influence of the interface between the loading platen and the specimen was studied. Four different interfaces were investigated. Additionally an optimal notch was searched, that is not sharp (infinite stresses), does inhibit fracture on the specimen-machine inter-

face and initiates fracture determined by a transversally propagating crack band. Additionally different eccentricities were tested and the suitable control for the tests was determined. Additionally the flexural strength was also determined.

In the *test series on sizes XS to XXL* a size range of 1:32 was tested on notched specimen under eccentric compressive loading, see chapter 5 for a description of the experiments and section 5.8 for the results. The two most common size effect laws were also fitted to the test data.

The last series on sandstone was the *verification series*, see chapter 6 for a description of the tests and section 6.7 for results. This test series was performed on a vast number of specimens to clarify open questions that came up after the *test series on sizes XS to XXL*. The size range was 1:8.

Finally the concrete series was carried out on a size range of 1:16. In chapter 8 the formwork, the concrete mixture, solutions to minimize unwanted influences that can arise during the molding process are described. The results are presented in chapter 9. The experimental data was also fitted to the most common size effect laws.

Chapter 2

State of the art

2.1 Short historical review of size effect

In this section a short summary of the history of size effect is presented, for more information see the detailed articles from Bažant (1999), Bažant and Chen (1997), the book written by Bažant and Planas (1998) and the thesis from Müller (2001).

It is known for a long time that materials exhibit size effect. The references date back to Leonardo da Vinci (16th century, in the notebooks of Leonardo da Vinci) and Galileo Galilei (Williams, 1957). In these early years Leonardo da Vinci stated that "among cords of equal thickness the longest is the least strong". A century later Galileo argued that Leonardo's size effect cannot be true. Important was the development found by Mariotte (Mariotte, 1718). From experiments he concluded that "a long rope and a short one always support the same weight, unless that in a long rope there happen to be some faulty place in which it will break sooner than in a shorter". Based on this he proposed the principle of "the inequality of matter whose absolute resistance is less in one place than another". Namely, the longer the rope the greater the probability of encountering an element of low strength.

Two centuries later Griffith (Griffith, 1921) showed experimentally that the strength of glass fibers could be raised 11 times, when the diameter of the glass fiber was decreased 32 times. From this observation he concluded that "the weakness of isotropic solids... is due to the presence of discontinuities or flaws... The effective strength of technical materials could be increased 10 or 20 times at least if these flaws could be eliminated". In 1926 Peirce formulated the weakest-link model for a chain. Due to lack of statistical distributions that adequately represent low strengths with an extremely small probability, Weibull presented in 1939 what is called today the Weibull distribution (Weibull, 1939). This is one of the first main theories of size effect which today still receives a lot of attention.

In these days Gonnerman (Gonnerman, 1925) performed a test series on 1755 concrete cylinders of different size, concrete mixture and age. He detected that the strength decreases with increasing size.

In 1972 Walsh (Walsh, 1972) tested three-point bending beams with notches. He was the first who plotted strength versus size in a double logarithmic diagram. He detected that the nominal strength of the beams decreased with increasing size of geometrically equal specimen. He also detected that this decrease was only determined above a certain threshold. This threshold can be seen as the critical or transitional depth d_0 .

Important advances were made due to the work of Hillerborg (1976) (Hillerborg et al., 1976) who introduced the cohesive crack model. He showed with finite element analyses that unnotched beams under three-point bending exhibit size effect on the modulus of rupture.

In the year 1984 Bažant presented the Size Effect Law (SEL) (Bažant, 1984) for the so-called deterministic or fracture mechanics size effect, see section 2.3.1. Until 1984 the size effect was attributed to the statistical size effect and not deterministic size effect. Therefore statisticians worked on that topic and not mechanicians, see section 2.3.1.

Beside statistical and deterministic approach there is a third approach to size effect, that was presented by Carpinteri (1994), Carpinteri and Ferro (1994) that is based on the multifractality of a fracture surface at ultimate load, see section 2.3.2.

2.2 Sources for size effect on structural strength

According to (Bažant and Planas, 1998, section 1.3) there are six different sources for size effect in concrete:

Boundary layer effect is due to the fact that at the concrete surface layer adjacent to the formwork has a smaller relative content of large aggregates, in comparison to the interior of the member. This layer has different properties, most important is the smaller stiffness. The thickness of this layer is dependent on the maximum aggregate and is independent of the structure size. The size effect is due to the fact that in a smaller member the boundary occupies a large portion of the cross section, while in a large member it occupies a small part of the cross section.

A second type of boundary layer effect arises because of the different elastic properties between the boundary layer and the interior. Normal stresses parallel to the boundary cause transverse stresses in the interior, while at the surface these stresses are zero.

The third type is due to the Poisson effect, that causes the surface layer to be nearly in plane stress, while the interior is nearly in plane strain.

Diffusions phenomena such as heat conduction or pore water transfer. Their size effect is because the diffusion half times are proportional to the square of the size of the structure. The diffusion process changes the material properties, produces inelastic strains and cracking, e.g. drying may lead to cracking in the surface layer. Due to different drying times the extent and density of cracking could be different in small and large members.

Hydration heat or phenomena associated with chemical reactions. This effect is related to the previous one due to the half times of dissipation of the hydration heat. Thicker members heat to higher temperatures and may cause cracking, induce drying, accelerate chemical reactions and alter the material properties.

The statistical size effect is the oldest known source of size effect and is based on the statistical distribution of the strength in the material. This size effect is originated by Weibull (1939) and is based on the model of the chain, whose maximum load is determined by the lowest strength in the chain. Therefore the longer the chain the lower the maximum load of the chain.

Fracture mechanics size effect is due to the release of stored energy into the fracture front. It is stated in literature that this effect is the most important source of size effect and is discussed in more detail for tension in section 2.3.1 and for compression in section 2.4.

Fractal nature of crack surface. The size effect due to fractality of the fracture surface is still controversially discussed.

Additionally due to preparation of specimens an additional source especially for small concreting heights (below 20 to 30 cm) is the

Top layer strength. When fresh concrete is poured into a formwork the layer below the top surface has lower strength after hydration. After casting the water ascends from the concrete to the top of the surface. Thus more water is in the top layer, which is a source for lower strength.

This source can affect the strength of concrete columns that were produced in horizontal position.

2.3 Size effect laws

2.3.1 The Size Effect Law by Bažant

The Size Effect Law (SEL) was presented by Bažant (1984). This theory is not based on statistical distributions of material parameters, it is dependent on stress redistributions. In this theory small sizes were bound to plasticity limit, and large sizes follow the Linear Elastic Fracture Mechanics. The SEL was derived for geometrically similar structures with notches using energy arguments and alternatively dimensional analysis and was found as

$$\sigma_N = \frac{B f_t}{\sqrt{1 + \frac{D}{D_0}}} \quad , \quad (2.1)$$

where f_t was the tensile strength, D is a characteristic dimension of the structure, B is constant and D_0 is the transition size from plasticity limit to Linear Fracture Mechanics, which is also constant. The constants B and D_0 have to be determined by fitting of experimental data.

The Size Effect Law in equation 2.1 was derived for notched specimens made of quasibrittle materials under tensile loading, but was also used for fitting of materials under compressive loading. Quasibrittle materials were defined (Bažant, 1999) as materials that obey on a small scale the theory of plasticity (or strength theory), characterized by material strength or yield limit and on a large scale the Linear Elastic Fracture Mechanics (LEFM) characterized by fracture energy. Plasticity theory and LEFM do not possess a characteristic length. For the bridging of plasticity theory and LEFM a characteristic length is necessary. A combination of plasticity and LEFM parameters leads to the Irwin's (1958) characteristic length or material length

$$l_0 = \frac{EG_f}{\sigma_0^2} \quad , \quad (2.2)$$

where E is the Young's modulus, G_f is the fracture energy and σ_0 is the yield or strength limit. l_0 is approximately the length of the fracture process zone. The key to the deterministic quasibrittle size effect is a combination of the concept of strength or yield with fracture mechanics.

Additional formulations were developed for structures with large notches and without notches, which resulted in the Universal Size Effect Law (Bažant, 1997; Bažant and Planas, 1998, section 9.1.7). The variation of strength with specimen size is plotted in figure 2.1a for the size effect law.

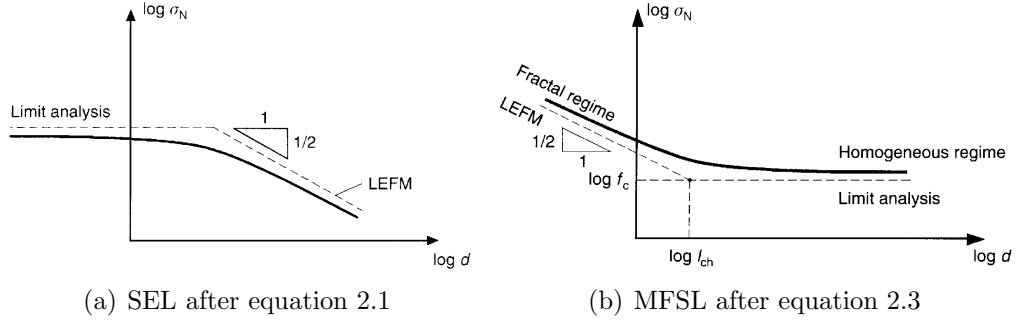


Figure 2.1: Size (scale) effects according to Size Effect Law (SEL) and Multifractal Scaling Law (MFSL), from (Carpinteri et al., 1999)

2.3.2 The Multifractal Scaling Law by Carpinteri

The Multifractal Scaling Law (MFSL) proposed by Carpinteri (Carpinteri, 1994; Carpinteri and Ferro, 1994) writes as

$$\sigma_N = f_c \sqrt{1 + \frac{l_{ch}}{d}} = \sqrt{A + \frac{B}{D}} \quad , \quad (2.3)$$

where σ_N is the nominal compressive stress, f_c is the compressive strength of an infinitely large specimen and l_0 represents a internal material length. Alternatively the second expression can be used for data fitting, where A and B are the constants that have to be fitted from experimental data.

In this model the mechanical properties are strictly connected with the considered scale of observation. For larger scales, the influence of disorder progressively vanishes. The trend of the law is plotted in figure 2.1b. The law predicts a different trend for small and large sizes than the SEL. This law was developed for the variation of tensile strength with size. In Carpinteri et al. (1999) was argued that the failure mode of compressed concrete specimens can be considered as resulting from local tensile mechanisms, or from a combination of tensile and shear mechanisms depending on specimen geometry. With this argument the same law was used for tension and compression (Carpinteri et al., 1999). The same was also often done with the SEL.

2.4 Size effect in compression

Compression failure of ductile metals is caused by plastic slip on inclined shear bands. This failure is ductile, without any significant post peak decrease of the applied load and causes no size effect. In quasibrittle materials such ductile failure

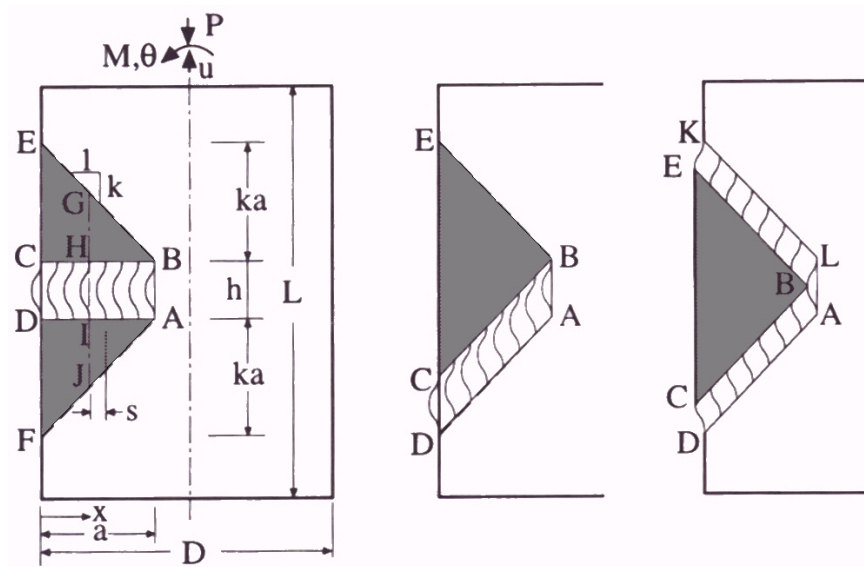


Figure 2.2: Three kinds of transversally propagating crack bands of axial splitting cracks with stress relief zone, from (Bažant and Xiang, 1997)

is only possible under high lateral confining stresses, which is a case beyond the scope of this thesis. In experiments under compressive loading shear failures are often observed on the macroscopic scale. But their microscopic mechanism is different, because the interlock of rough surfaces inclined to the compressive stress prevents any slip. Slip is only possible, when the cracks are open and the material is heavily damaged. This cannot be the case, because the cracks are inclined to the principal compressive stress, that keep the cracks closed. The microscopic mechanism of the shear like failures is often axial tensile microcracking inclined to shear direction. For eccentric compressive loading the failure mode of the column is transverse propagation of a band of axial splitting cracks from the surface into the material volume (Bažant and Xiang, 1997), see figure 2.2. The crack band can propagate orthogonal or inclined to the direction of compression. Several alternatives that all lead to equivalent results are given in figure 2.2. Axial splitting macro-cracks do not change the global stress field and cause no global energy release, but the transversely propagating crack band does. A deterministic size effect exists only, when the propagation of the crack causes a global energy release. Thus the failure by propagation of a transversally propagating band must show a size effect of deterministic type. In contrary under centric compression and low friction boundaries the specimen fails in form of an axial splitting macrocrack. A splitting macrocrack does not change the macroscopic stress field and causes no

release of global energy. No size effect is accompanied with that type of fracture and therefore the centric compression is not of interest for this thesis.

Compression failure is often fitted to the SEL, see equation 2.1. As already discussed the failure in compression follows different mechanisms. In a paper by Bažant and Xiang (1997) a dependence of the strength on size was derived as

$$\sigma_N = k_c D^{-2/5} \quad . \quad (2.4)$$

In the analysis of Bažant and Xiang (1997) it was assumed that the crack width is proportional to the material length and therefore constant and that the spacing of axial micro cracks is proportional to $D^{-1/5}$ (Bažant et al., 1993), which leads to a slope of 2/5 for the LEFM asymptote in the logarithmic plot. The experiments from Bažant and Kwon (1994) were again fitted with the new power law and it was found that this model represents the trend better than the original SEL (Bažant and Xiang, 1997). Thus in the double logarithmic plot the asymptotic size effect in compression follows a less steep slope of $-2/5$, and not $-1/2$ as in the SEL.

2.5 Size effect tests

Most of the investigations were performed under tensile loading on compact test specimens (e.g. Slowik, 1995; Linsbauer and Šanjna, 1999) and direct tension on dog bone specimens (e.g. Van Vliet, 2000). The biggest size range on compact test specimen was 1:160. This series was performed by Dempsey et al. on first year sea ice (Dempsey et al., 1995). The series of Van Vliet (2000) was performed on concrete and sandstone. The tests series is the largest performed on dog bone specimen made of plain concrete, with a size range of 1:32.

Fewer tests were performed under compression on geometrically equal specimens. Tests on a size range of at least 1:4 were performed on columns by Bažant and Kwon (1994), Sener et al. (1999), Hollingworth (1998), Němeček (2000), on concrete cylinders by Sener (1997) and Kim et al. (1999). The double punch tests by Marti (1989) have to be mentioned also. The compression tests on concrete columns and on notched PEEK specimen (Bažant et al., 1999) are discussed in this section.

In this thesis tests under compressive loading on sandstone and concrete are described. The experiments on sandstone are presented in the chapters 4 to 7 and for concrete in chapter 8 and 9. A detailed test report with listings and graphs for every individual specimen is given in Burtscher et al. (2003a) for the sandstone series and in Burtscher et al. (2003b) for the concrete series.

The main parameters from the tests in literature and the test series performed in this thesis are listed in table 2.1. The specimens are drawn in figure 2.3. The

Table 2.1: Experimental work on the size effect in compression

Reference	Size Range	h/d	e	Material	Strength [N/mm^2]	ϱ [%]
Bažant, Kwon 1994	1:4	5, 10, 15	D/4	Microcon.	29	4.9
Sener, et.al 1999	1:4	2.5, 5, 10	0	Concrete	28	0
Hollingworth 1998	1:4	2.9, 5.2, 10.4	0	Concrete	33-117	0, 4.5
Nemeček 2000	1:4	6.7	D/5	Concrete	27	2.1
Bažant et.al 1999	1:4	2.5	>0	PEEK	-	-
Sandstone Series	1:32	2	D/22	Sandstone	25	-
Concrete Series	1:16	4	D/40	Concrete	35	0

e = eccentricity of loading

ϱ = reinforcement content

PEEK = poly-ether-ether-keton

dimensions and the reinforcements of the specimen were all scaled by a factor for every size, thus geometrical similarity was fulfilled. The largest size range of specimens were tested in the sandstone and the concrete series performed as part of this thesis.

Tests on micro-concrete columns by Bažant and Kwon (1994)

The specimens were cast in a impregnated formwork. After one day the formwork was removed and the specimens were stored for 28 days in water at 20°C. They were removed from the water bath prior to testing, to prevent drying and shrinkage cracks. The tests were performed with a predefined eccentricity. Most of the columns broke in the center, half of the stocky columns broke at 1/4 of the specimen length and some at the ends. According to bending theory the specimens would have been expected to break in the middle where the highest moment occurred. The results were fitted to the Size Effect Law, see equation 2.1.

Three years later the data was analyzed again. In this investigation (Bažant and Xiang, 1997) it was assumed that the crack width h is constant. As already discussed in section 2.4, the slope in the double logarithmic size effect plot be-

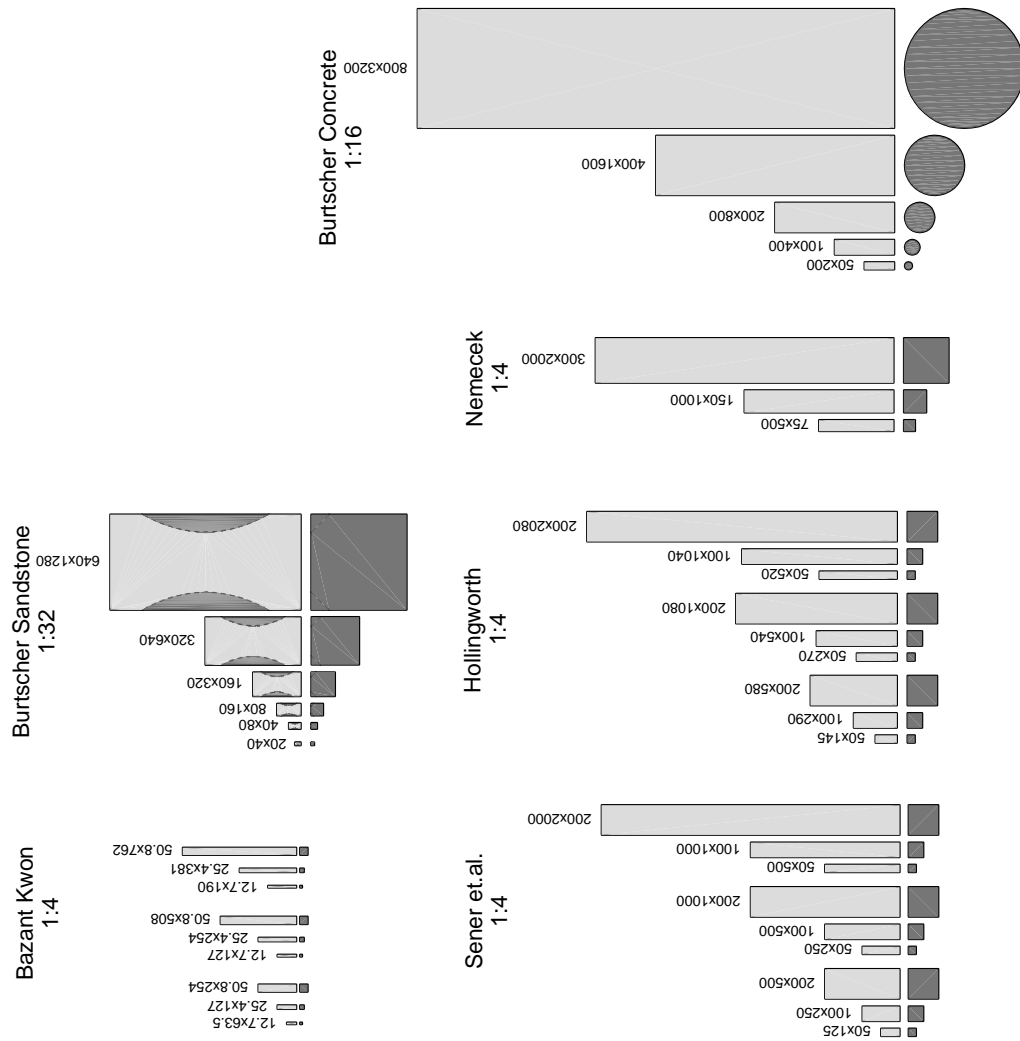


Figure 2.3: Comparison of different specimens for size of effect tests in compression [mm]

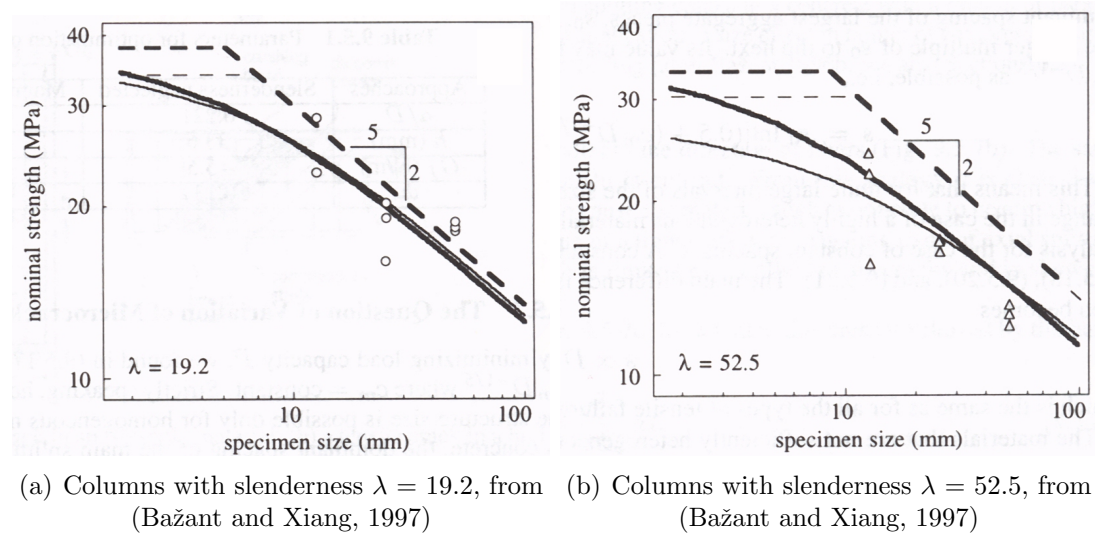


Figure 2.4: Results of size effect tests in compression (Bažant and Kwon, 1994)

comes $-2/5$, see figure 2.4 for a column slenderness of $\lambda = 19.2$ (left) and $\lambda = 52.5$ (right).

Tests on plain concrete by Sener et al. (1999)

These tests were performed on plain concrete columns with quadratic cross section, where only the ends were reinforced to ensure proper load transfer from the testing machine to the specimen. The column could rotate freely on both ends and the loading was applied in the centroid of the specimen. The displacements were measured over the whole specimen length, on all four sides over half of the length in the middle and in the horizontal direction in the middle. With these measurements it was also possible to determine the uniformity of loading. The tests showed that with increasing load the specimen deflection in the middle increased, which is attributed to internal cracking and the heterogeneity of the material. Due to the different eccentricities the energy release may be different. This effect was more pronounced in smaller specimen than in larger ones. In figure 2.5 the strength of the specimen versus specimen size is plotted for column slenderness $\lambda = 9.7$ (left) and $\lambda = 34.7$ (right). The plots show that the strength is increasing first with increasing size and afterwards decreasing. Arguing as discussed previously that the smallest specimen were problematic in the tests, it could be still concluded on the remaining data that a size effect on the strength was present.

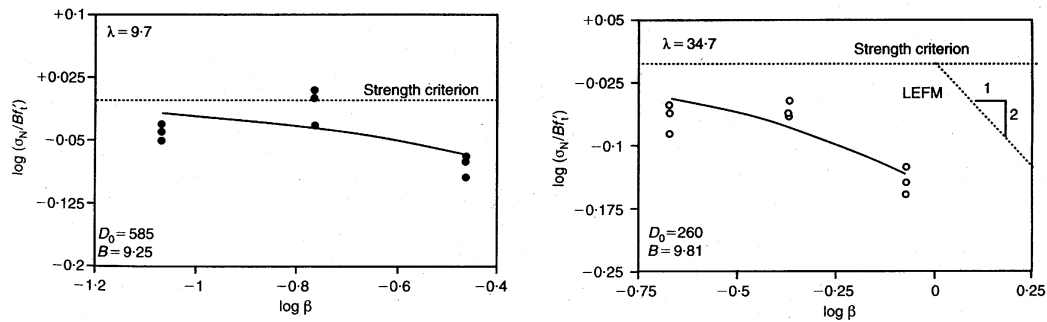


Figure 2.5: Strength versus specimen size in logarithmic plot for stocky (left) and slender (right) column, from (Sener et al., 1999)

Tests on plain and reinforced concrete columns by Hollingworth (1998)

These experiments were similar to the experiments of (Sener et al., 1999). The specimens were produced as described there and the specimens were loaded under centric loading, but in this investigation, the rotation on the specimen ends was inhibited. Again specimens with different slenderness and also different concrete strength were tested, see table 2.1. A size effect on the strength for geometrically equal specimens could not be determined. An investigation of the specimen length on the nominal strength of the structure was influenced by loading eccentricities.

Remarks on the tests by Sener et al. (1999) and Hollingworth (1998)

The tests of (Sener et al., 1999) showed that performing tests on columns under centric loading with freely rotating ends is difficult to perform, because eccentricities are easily induced due to the heterogeneity of the material. In the tests of (Hollingworth, 1998) the ends were not allowed to rotate freely and the centric loading could be easier maintained up to peak load. However testing columns under centric loading is always influenced by the random distribution of the material strength, which means that after initiation of cracking the propagation is influenced by the fixed boundaries. Additionally, Bažant and Ožbolt (1992) showed numerically that the centric loading of a cylinder fails by an axial splitting macrocrack and produces no size effect. Such cracks were observed in the tests. On the other hand real structures are always loaded under eccentric loading. The strengths of heterogeneous materials tend to be higher under eccentric loading. This was also observed in the Preliminary Test Series, see figure 4.13 on page 40.

Tests on reinforced concrete columns by Němeček (2000)

The tests were performed under eccentric loading of $e = D/5$, this means that from the beginning of the test tensile stresses were present on the backside of the specimen. Most of the specimens failed in the middle. The failure was initiated by softening of the concrete on the compressed side, then the reinforcement buckled between the stirrups. On the compressed side a damage zone in form of a wedge developed. With ongoing loading in the post-peak branch one or more sharp cracks developed on the tensed side. In the tests a size effect on the ductility was determined. A size effect on the nominal strength was not observed in the tested size range. A reason could be that the concrete was confined with stirrups that induced a higher ductility to the concrete. Additionally the longitudinal reinforcement that does not exhibit a size effect carried parts of the load.

Tests on PEEK columns by Bažant et al. (1999)

The tests were performed under eccentric compression, with rotation fixed boundaries. The specimens were notched in the direction orthogonal to the longitudinal axis, as normally used in fracture testing. The experiments showed that these notches start a failure by axial splitting shear cracks, which was followed by a transversally propagating band. Thus the specimens were provided with a slanted notch on the compressed side to prevent the initiation by axial splitting shear cracks. The inclination of the notch with respect to the longitudinal axis was determined experimentally. The axial splitting cracks could then be avoided, see figure 2.6 (left). The experimental results in figure 2.6 (right) show that a size effect on the nominal strength was determined.

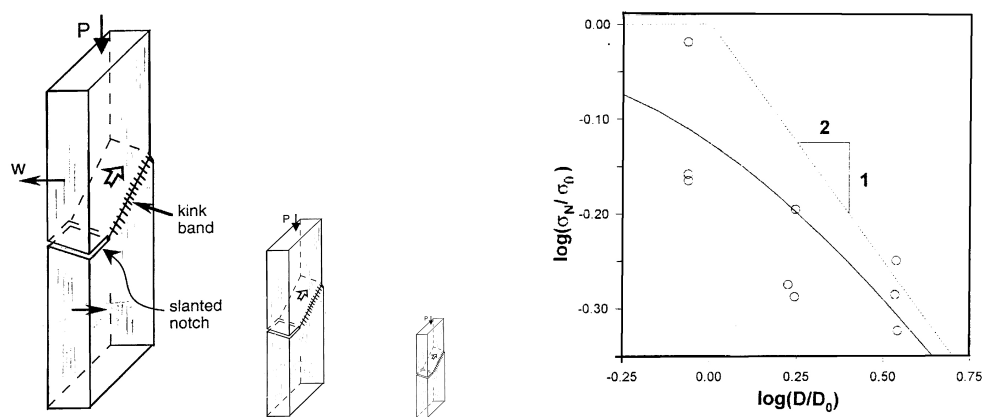


Figure 2.6: Specimen and nominal strength versus Size, from (Bažant et al., 1999)

Chapter 3

The sandstone material

3.1 Introduction

In the area of St. Margarethen in the province Burgenland, Austria, there were numerous quarries where sandstone was exploited. Since very early ages the sandstone from the famous *Römersteinbruch* was used for sculptures and masonry. The sandstone can be seen at the St. Stephen's cathedral, the Dominican, the Franciscan church, the Musikverein, the building of the Vienna Stock Exchange and other places (Piller and Vavra, 1991). Today only few quarries are still in use. The sandstone of these test series was from the quarry *Hummel*, which is next to the *Römersteinbruch*. The stone is gained by first sawing in vertical direction, see figure 3.1 and afterwards the block is separated at the bottom. For this purpose holes are drilled at the bottom and the whole block is lifted with special devices. With this method blocks with dimensions 1.3x1.3x5m are gained. From these blocks slabs or prisms are sawed.

The sandstone is a porous Leithakalk. The material was formed 15 million years ago by sedimentation in a warm and shallow subtropical lagoon. The sediments were bound with fine-grained calcite, for details see Rohatsch (1997).

All sandstone specimens tested in the three series were from the quarry *Hummel*. For every series one block was selected and the specimens were cut from the smallest possible volume. This was done to keep the variation in the material as small as possible. The specimens for each series were gained at different dates, the blocks and thus material was not the same from one series to the other. In the following subsections important parameters determined prior to testing are listed for every series.



Figure 3.1: Sandstone in the quarry "Hummel". Left: Vertical cuts after sawing. Right: block of sandstone

3.2 Why is sandstone the material of choice

In order to determine the fracture mechanics size effect of a granular material it is important that the material is the same in the whole volume of each specimen. In the case of concrete this is difficult to achieve because of the boundary layer effect, the microcracks due to hydration effects and due to diffusion phenomena, see section 2.2. These phenomena have different influence for different sizes and therefore may change the material response, which is not wanted for such kind of tests.

These effects are introduced into the concrete during the moulding process. To avoid such unwanted effects, tests on sandstone were performed. This material has several advantages.

- The material shows no or a vanishing boundary layer effect (of first type in section 2.2). No hydration or diffusion effects of different kind took place in the material.
- The preliminary tests showed that the strength values only scatter by 10%.
- The average grain size is 0.5 mm (average pore size is 0.6 mm), which allows to test very small specimen sizes, without going beyond the conditions for a representative volume.
- The stress-strain response is nearly linear up to peak load.

The influence of the stratification was investigated in the preliminary tests by ultrasonic testing, but also in compressive tests and was found to be very small in the investigated sandstone. The big disadvantage of sandstone is that the material parameters can scatter strongly, due to inclusions or other inhomogeneities. The sandstone of the preliminary series was very homogeneous and showed, as just mentioned, low scatter for a granular material. However for the *test series on sizes XS to XXL* and the *verification series* the scatter was higher.

3.3 Density, grains and pores of the different series

3.3.1 Sandstone of the preliminary series

The density of all specimens varied from 1.97 to 2.08 g/cm^3 . In tables 4.2 and 4.3 on page 41 the densities for every individual specimen are listed. The true density of the sandstone was 2.71 g/cm^3 .

To determine the structure of the material and to distinguish differences from one series to the other 100 pore and grain diameter were measured on the surface of specimen number 11. The measurement was done with a microscope. The histograms of the pores and the grains are given in figure 3.2.

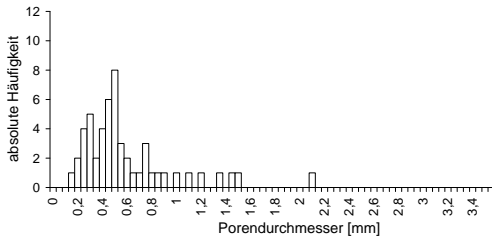
3.3.2 Sandstone of the test series on sizes XS to XXL

A relation between strength and density was not determined in the preliminary series. Instead of the density the wave speed was measured with the acoustic emission equipment in longitudinal and transversal direction. Alternations from one specimen to the other can be determined with the wave speed measurement. On the surface of specimen 64a 100 diameters of grains and pores were determined and the histogram is given in figure 3.3.

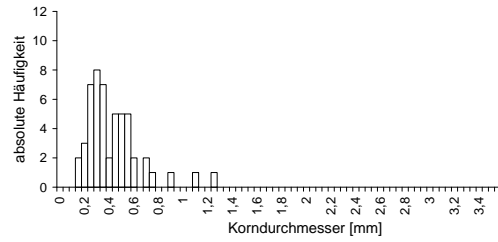
3.3.3 Sandstone of the verification series

Some specimens of this series had porous regions, see figure 3.5, therefore they were separated into dense and porous specimens. The true density was determined in the preliminary series as 2.71 g/cm^3 . The density of the dense specimen was between 2.02 and 2.27 g/cm^3 . In the dense and the porous region of specimen 08-01 50 pore and grain diameter were measured. The histograms showing the distribution are given in figure 3.4.

The sandstone material was also investigated by microscopic observations. Specimen 08-01 from the *verification series* (see chapter 6) had a dense region

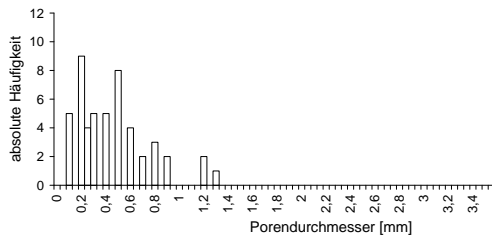


(a) Histogram of pore diameter
($d_{mean} = 0.59mm$)

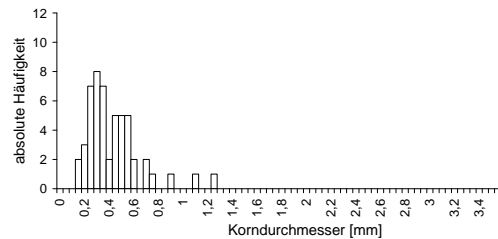


(b) Histogram of grain diameter
($d_{mean} = 0.43mm$)

Figure 3.2: Histogram of pore and grain diameter of preliminary series

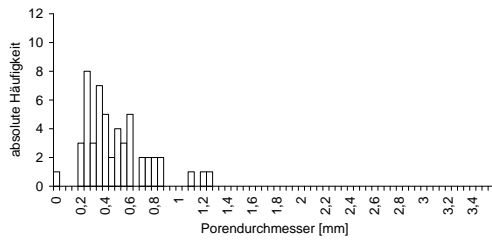


(a) Histogram of pore diameter
($d_{mean} = 0.45mm$)

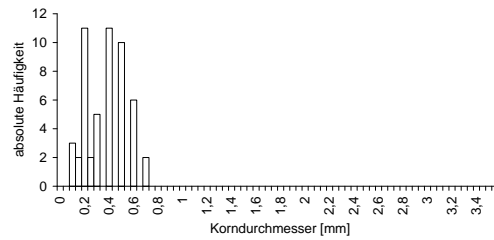


(b) Histogram of grain diameter
($d_{mean} = 0.70mm$)

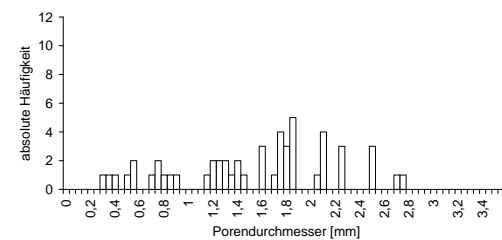
Figure 3.3: Histogram of pore and grain diameter of test series



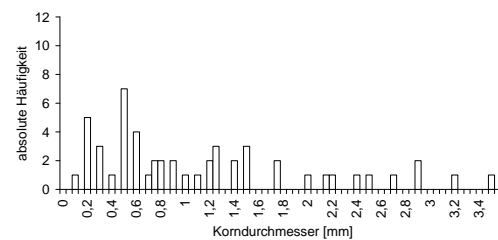
(a) Histogram of pore diameter
($d_{mean} = 0.49mm$) in dense region



(b) Histogram of grain diameter
($d_{mean} = 0.37mm$) in dense region



(c) Histogram of pore diameter
($d_{mean} = 1.54mm$) in porous region



(d) Histogram of grain diameter
($d_{mean} = 1.14mm$) in porous region

Figure 3.4: Histogram of pore and grain diameter for porous and dense region of sandstone 08-01 tested in the verification series

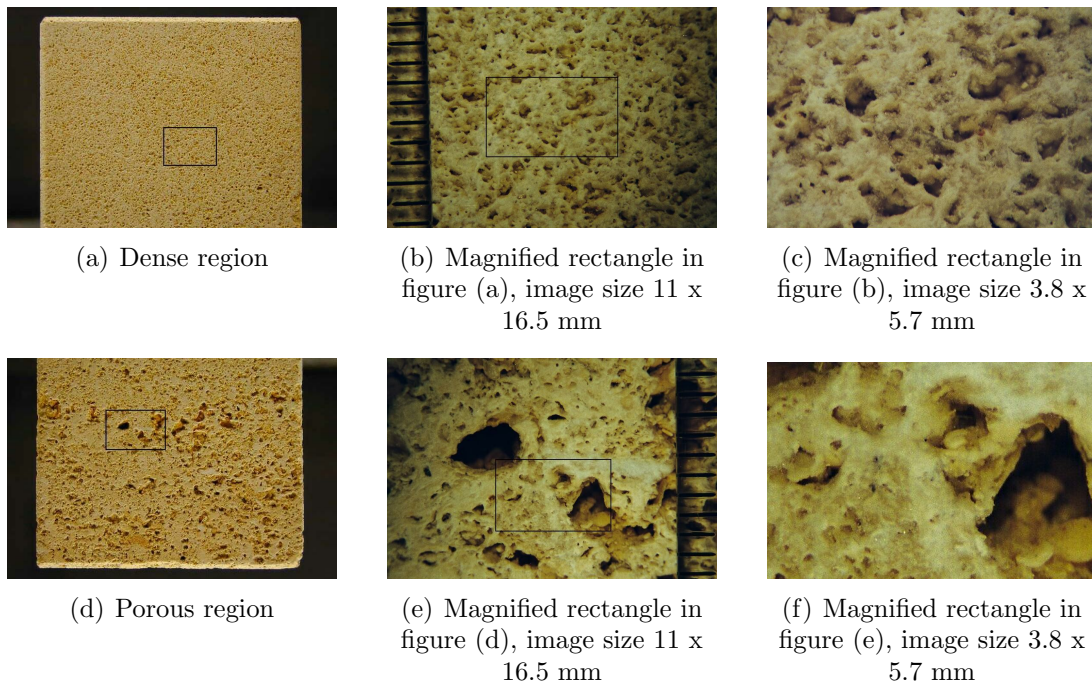


Figure 3.5: Microscopic observation of sandstone 08-01 maximum magnification factor 14. Top: dense region. Bottom: porous region

at the top of the specimen and a porous region at the bottom. Microscopic observation were performed at three magnification scales, see figure 3.5.

Chapter 4

Preliminary test series on sandstone

4.1 Introduction

In this *preliminary test series* the compressive strength and the scatter of compressive strength were determined in tests performed under centric and eccentric loading. Four point bending tests were performed to determine the flexural strength. The influence of stratification on the compressive and flexural strength was also studied. Very important were the investigations on the interface between loading platen and specimen, the amount of eccentricity, the proper test control and the notch that led to the desired fracture type.

4.2 Specimen dimensions and geometry

The specimen behavior can be strongly influenced by friction between loading platen and specimen, because this friction induces a triaxially confined zone at the specimen ends. The constitutive behavior under triaxial confinement is different than for uniaxial conditions. In a compression test triaxial conditions on the specimen ends can be introduced by high friction between the loading platen and specimen. For low height to dept ratios the triaxial zones can occupy most of the specimen volume and influence the stress strain response (van Vliet and van Mier, 1996), see figure 4.1. By testing with different end constraints and slenderness it was found that the influence of end constraint reduces strongly if the specimen has a height to depth ratio of $h/d=2$ (Van Mier et al., 1997). The specimens in the three sandstone series were tested under eccentric loading, thus friction free boundary conditions could not be fulfilled and the specimens were produced with a height to diameter ratio of $h/d=2$.

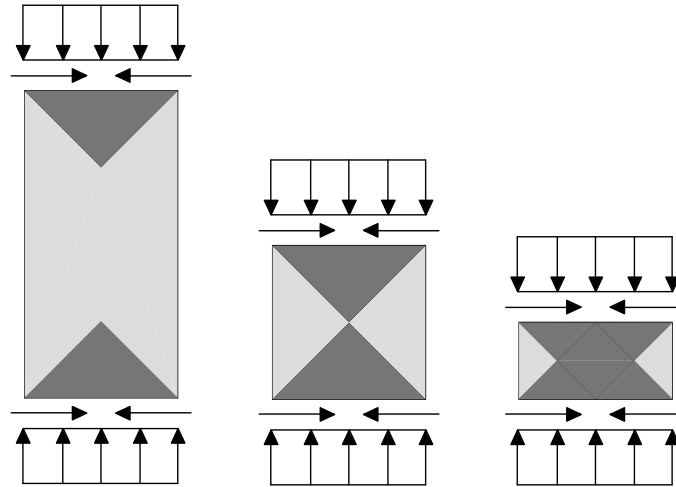


Figure 4.1: Confined zones due to frictional restraint for specimen of different slenderness, after (van Vliet and van Mier, 1996)

The specimens had dimensions of 100x100x200 mm and were sawed from one sandstone slab with thickness 100 mm. The stratification of the sandstone was in the plane of the slab. During preparation of the specimens special attention was paid to the precise geometric dimensions, plain surfaces and the stratification. The specimens were homogeneous and did not show a pronounced stratification. Only four specimen had inclusions. They were also tested to investigate the influence of the inhomogeneities. In this *preliminary test series* 28 specimen were tested under compressive loading. 24 of the specimens had the strata plane in the 100x100 cross section (transversal stratification) and 4 had the strata along the longitudinal axes in the 100x200 dimension (longitudinal stratification). A listing of the notches, the loading type and the eccentricity is given in table 4.1. Additionally to the compressive tests four-point bending tests were performed on 8 specimens, with dimensions 48x48x200 mm. Four specimens had the strata in the longitudinal and four in transversal direction. The tests are described in section 4.6.

Table 4.1: Specimens tested in *preliminary test series* with different interfaces and notches

Specimen number	Bearing of loading device	Eccentricity [mm]	Type of Notch	Interface	Comment
3	spherical	0	no	steel plate	
6	spherical	0	no	grout, teflon	
8	spherical	0	no	steel plate	
9	spherical	0	no	grout, teflon	spalling of edges
15	spherical	0	no	steel plate	spalling of edges
16	spherical	0	no	carton	
26	spherical	0	no	grout, teflon	inclusions
14	rot. fixed	0	no	grout, teflon	
4	rot. fixed	0	no	grout	uneven surface
1	tilting	5	no	grout	
13	tilting	5	no	grout	spalling of edges
20	tilting	5	no	grout	program error
22	tilting	5	no	grout	spalling of edges
24	tilting	5	no	teflon	uneven surface
25	tilting	5	no	grout	
27	tilting	5	no	grout	inclusions
28	tilting	5	no	grout	inclusions
7	tilting	5	1	grout	spalling of edges
19	tilting	5	2	grout	
2	tilting	5	3	teflon	
5	tilting	5	3	teflon	
10	tilting	5	3	teflon	
12	tilting	5	3	teflon	
17	tilting	5	3	grout	
18	tilting	5	3	teflon	
21	tilting	10	no	grout	

4.3 Compressive tests under centric and eccentric loading

4.3.1 Investigations on the notches for specimens tested under eccentric compression

When a prismatic specimen is tested under compression the failure mode often is the spalling of edges near the loading surface. The specimen is influenced in that region by the boundary conditions. If failure occurs in that region the damage that precedes the failure is influenced by the interface and thus may affect the maximum load or the post peak behavior. Additionally and even more important is that it cannot be distinguished if the failure is due to improper boundary conditions (e.g. uneven loading surface) or by exceeding the material strength. Thus the specimen should be notched, that the location where fracture starts is predefined and is not located on the specimen ends. This makes assessing and in certain cases the control of the test easier. For tests on specimens loaded in tension or for three point bending tests notches are often used. In compression this is more problematic because the fracture band propagates inclined to the loading direction (Bažant et al., 1999), see figure 2.6 on page 17. The inclination of the notch has to be equal to the propagating crack band. In this investigation smooth notches were used to circumvent this problem. In a smooth notch the conditions are also closer to a real structure, because there is no sharp notch tip where the stresses become theoretically infinite.

In this *preliminary test program* 8 specimens without notches were tested under eccentric loading. Three different types of smooth notches were investigated, see figure 4.2. One specimen was tested with notch type 1 and one with notch type 2 and the remaining 6 specimens were tested with notch type 3. The notch was always on the more compressed side of the specimen. The performance of the notch was determined by the kind of fracture of the specimen, see figure 4.3. The specimen with notch type 1 showed a spalling of the edges at the loading face. The notches 2 and 3 initiated the fracture in the notch and a inclined crack band propagated towards the specimen centroid. In specimen with notch type 2 the edges at the loading faces showed also some fracture. The notch type 3 performed best in the experiments and the specimens of the *test series on sandstone* and the *verification series* were provided with that notch. A drawing of a specimen with this notch is displayed in more detail in figure 5.1 on page 45.

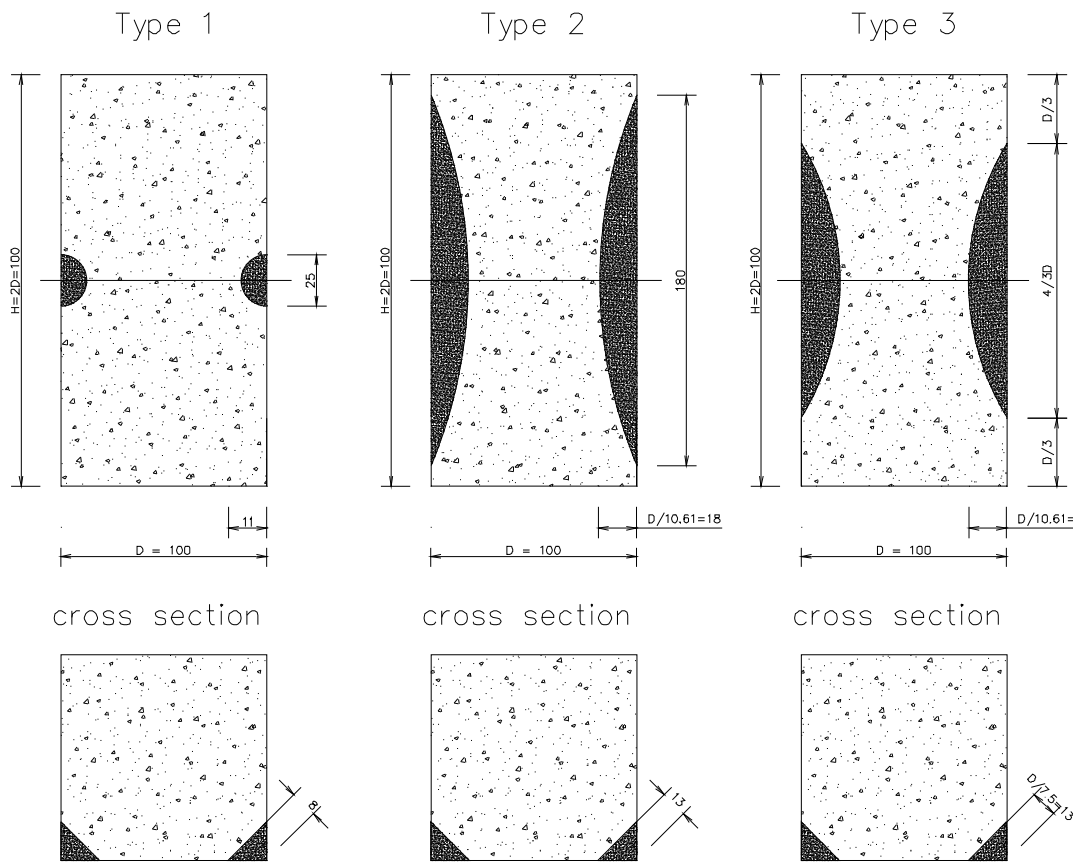


Figure 4.2: The three notches investigated in compressive tests

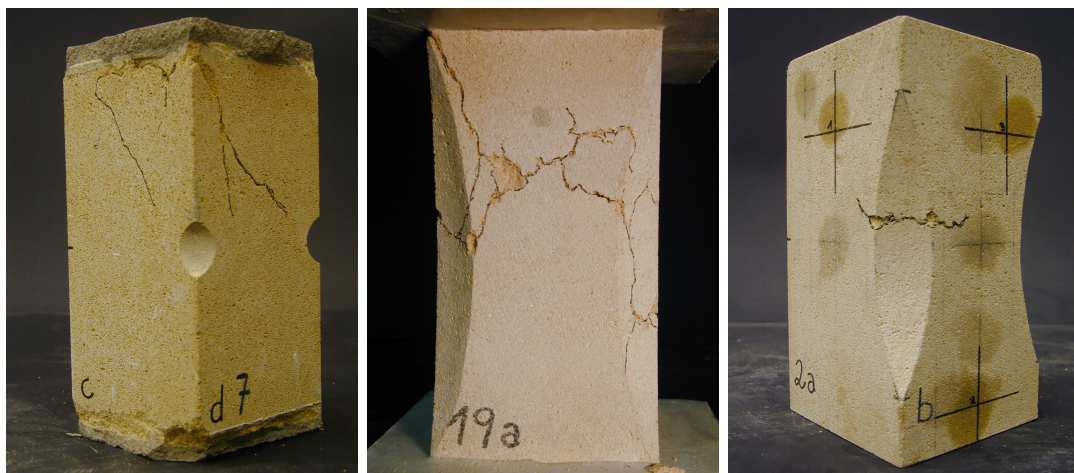


Figure 4.3: Specimen with different notches after testing

4.3.2 Investigations on the interface between loading platen and specimen

The influence of different interfaces was investigated in a extensive Round Robin test program (Van Mier et al., 1997; Zisopoulos et al., 2000) on concrete. In this test program brush platens, MGA pads (Aluminium, Grease and polyester film), but mostly teflon sheets were used. The main purpose of these sheets was to reduce the friction between loading platen and specimen, that would build up triaxially confined zones at the specimen ends. In this series it was also important that the load was transferred uniformly into the specimen and that a slightly uneven loading surface did not lead to spalling of the edges. All specimen surfaces were sawed in the quarry and were therefore not as even as the steel platens loading the specimen. For the smaller specimens the loading surface was polished, but for the large specimen (XXL and XL of the test series) this was not possible. To transfer the load uniformly into the specimen the interface had to compensate possible bumps in the loading surface. To determine the best possible solution four different interfaces were investigated:

- Specimen were positioned directly on the loading plates, without any interface.
- A layer of fine grout with a thickness of approximately 5 mm was placed between specimen and loading platen. The layer at the bottom of the specimen had to be cast in the testing machine.
- A cardboard layer was placed between specimen and loading platen, as also used by Tschegg et al. (1995) for biaxial tests.
- A teflon layer (thickness 0.75 mm) and double sided sand paper was placed between specimen and loading platen.

When no additional interface was used between sandstone and steel platen, then nearly invisible unevenness could lead to a spalling of the edges, see figure 4.4.

Nearly half of the specimens were prepared with a layer of fine grout on both ends of the specimen. One half was always grouted outside while the other was grouted directly in the testing machine. The big disadvantage of the grout layer was the different shrinkage of the grout layer directly below the sandstone specimen and around the specimen. This could be due to the different thickness of grout layer below and around the specimen. Additionally the porosity of the sandstone lead to a very high water absorption of the sandstone and therefore the grout attached to sandstone showed different shrinkage than the rest outside.



Figure 4.4: Spalling of edges when tested directly on steel plates (left) and when fine grout layer was used (right)

The different shrinkage produced an uneven surface, which was nearly invisible with naked eye, but caused improper boundary conditions between the steel plate and the specimen. It was observed after the experiment that the load was not uniformly transferred from the steel loading platen to the grout layer. There was a stress concentration below the edges of the prism and the specimen failed by spalling of edges, see figure 4.4.

The cardboard layer performed well during the experiment. However using teflon at this point seemed to be even more promising, especially for the big specimen of the size effect series. Teflon reduces strongly the friction, therefore double sided sand paper was laid between teflon and loading platen. On the other hand teflon starts to yield at low stresses and therefore eliminates stress concentrations at the interface. All experiments with teflon and double sided sand paper were successful.

4.3.3 Compressive loading

In this preliminary investigation the strength of the sandstone as well as its post-peak response was investigated. Stable experiments were difficult to perform, because for some specimens the failure was highly brittle. Due to proper test control it was possible to end up with stable experiments. The specimen were tested under

- centric compression,

- eccentric compression on longitudinal and transversal stratified specimens with different eccentricities $e = D/20 = 5 \text{ mm}$ and $e = D/10 = 10 \text{ mm}$ (no notch) and
- eccentric compression $e_{notch} = 3.3 \text{ mm}$ with smooth notches, see figure 4.2.

In the centric compression tests spherical hinges with a teflon layer were used on both sides to apply the load, see Figure 4.5 right. The spherical hinges could rotate freely during the whole experiment. In the eccentric test a longitudinal hinge in the axis of the machine was used and the eccentricity was applied by moving the test specimen apart from the axis, see figure 4.5 left. The position of the force was defined by the position of the cylinder axis. Due to the rotating capability in one direction no moment could be transferred or generated during the experiment, i.e. rotation of the loading platen was possible, without moment build up. Additionally, the load did not change the position and did not rotate. In the experiment the specimen was shifted laterally to the cylinder axis and the load was introduced with the eccentricity defined by the lateral shift, see figure 4.5 left. The performance of the spherical hinges and the longitudinal hinges was good for all experiments.

4.3.4 Arrangement of displacement transducers and AE-sensors

The total displacements during the experiments were below 1 mm. For accurate measurement of the displacement digital incremental transducers with an resolution and accuracy of $1\mu\text{m}$ were used. The transducers measuring the longitudinal displacements were fixed to the specimen with sharp steel needles and had an initial measuring length between 145 mm and 200 mm, see figure 4.6. The lateral displacement was measured using two rectangular aluminum sheets that were pressed to the surface of the specimen and the displacement of the sheets was measured using a displacement transducer that was fixed to one of the sheets. In the centric experiments three displacement transducers were used to measure the longitudinal displacements and one for the lateral displacement. In the eccentric tests two longitudinal displacements and two lateral displacement were recorded, see figure 4.6.

For the acoustic emission measurements 5 sensors were positioned on the specimen surface. The sensor positions are shown in figure 4.6. To ensure an appropriate acoustic coupling between sensor and specimen a thin film of grease was used. The sensors were attached to the specimen using rubber bands. The position of the sensors was not always in the middle of the specimen, therefore the distance of the rubber bands to the edge of the specimen was not the same. This

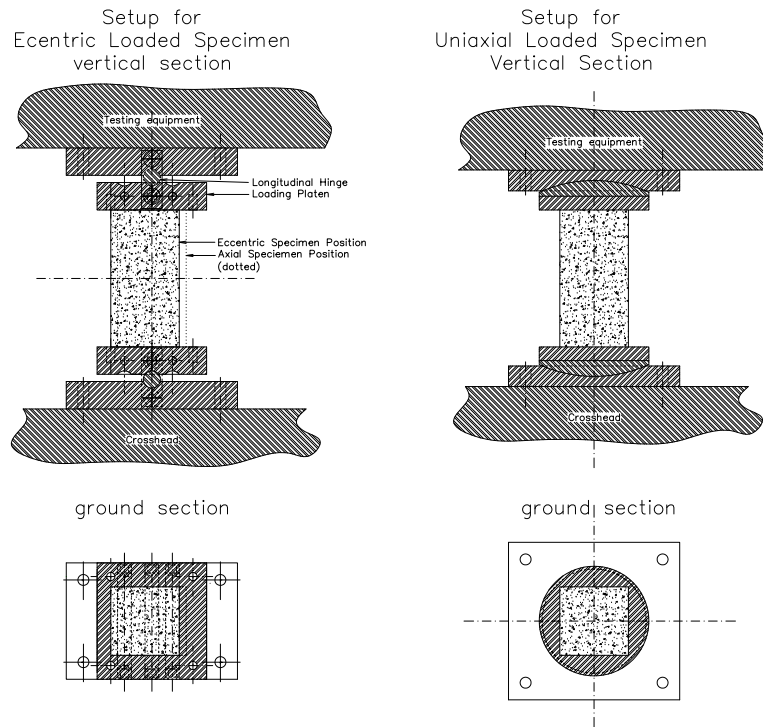


Figure 4.5: Experimental setup for eccentric and centric compression test of sandstone prism

produced a non-uniform pressure of the sensor against the specimen, see figure 4.7. The *preliminary experiments* showed that the attachment of the sensors was not completely satisfactory. There were problems with the accurate positioning, but also with the non-uniform pressure. The acoustic emission measurements in the preliminary series were performed to collect experience with AE-equipment, software, attachment of sensors. For the size effect test series the sensors were mounted on the specimens using steel stirrups with a screw, see section 5.6.1.

4.3.5 Test control

The displacement transducers used for measuring and test control are working on an optoelectronic basis, with a measuring rod made of glass. The glass makes the transducers vulnerable to damage. First, the test control was performed by displacement control of the longitudinal displacement transducer on the compressed side (*DT 1*, in figure 4.6). The experiments showed that for some specimens the failure was sudden and with high energy dissipation. This could damage the

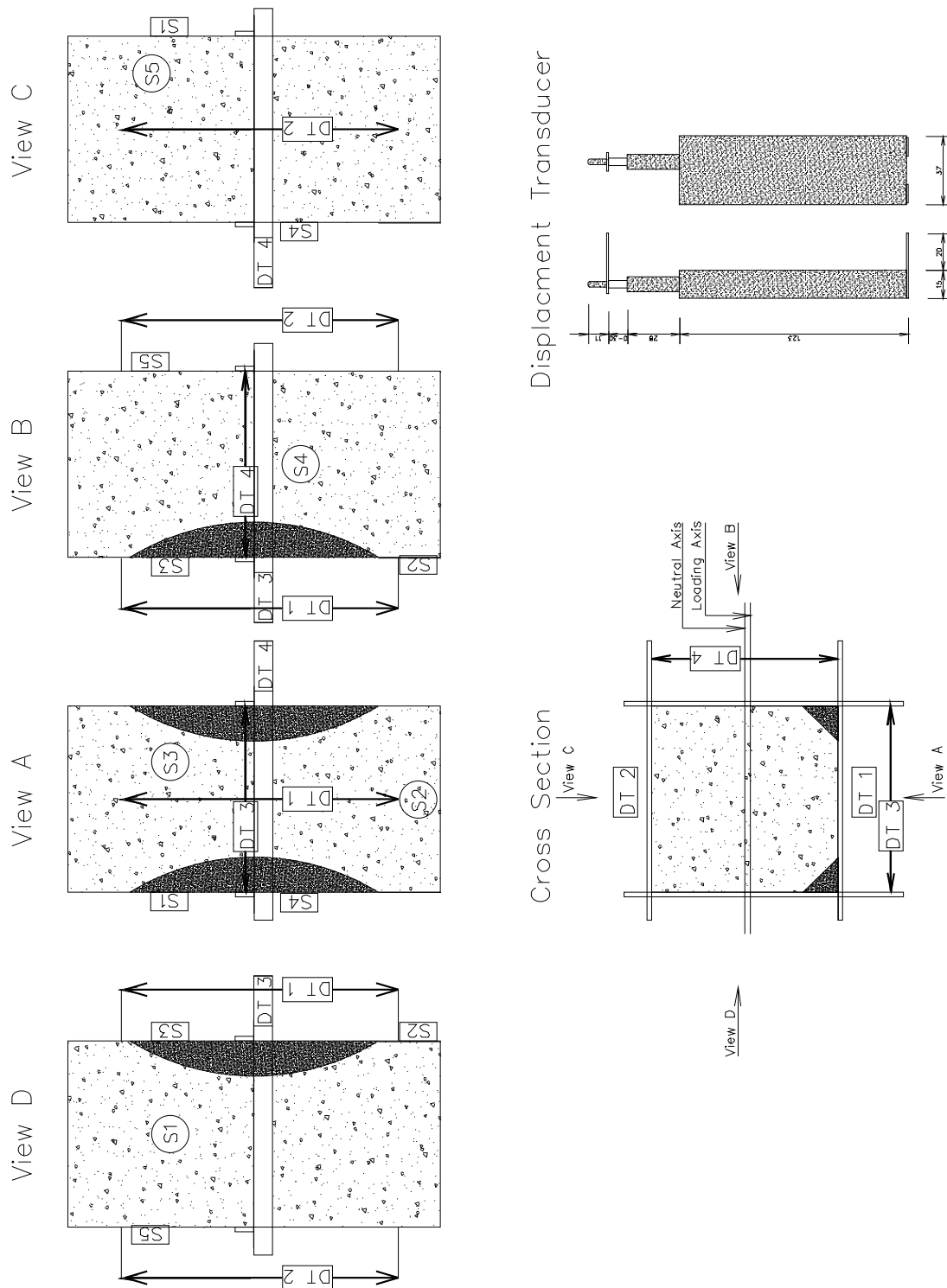


Figure 4.6: Arrangement of displacement transducers (DT1 to DT 4) and sensors (S1 to S5) for acoustic emission measurements on specimen. Dimensions of the digital displacement transducers

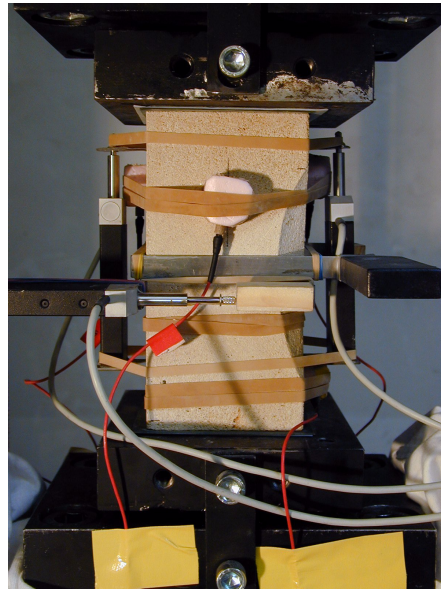


Figure 4.7: Photograph of displacement transducers and sensors on notched specimen. Between the specimen and the loading platens the interface was established using double sided sand paper and a teflon sheet

displacement transducers and therefore control by longitudinal displacement was not sufficient. A test control that could ensure stable conditions throughout the whole experiment was needed.

In a displacement controlled experiment of a strain softening material it is often sufficient to have a powerful hydraulic aggregate and a quick control equipment. When the material enters the softening region, the hydraulic actuator needs to be supplied very quickly with a large amount of oil. In that case the load reduces, while the deformation is still growing. When the experiment is performed with displacement control the experiment can be performed stable without sudden failure. Additionally a stiff frame relaxes the machine requirements a little. The longitudinal displacement is permanently increased by the deformation rate. In a softening material the displacement over the whole specimen length changes much less than in the softening band, because outside the softening band the material unloads (elastically), see figure 4.8. If the softening band is very small compared to the surrounding region, the displacement due to unloading of the surrounding material becomes more pronounced and the load displacement curve shows very brittle behavior. The feedback signal from the displacement transducer changes only little, but the load changes strongly. This makes displacement control difficult and could lead to sudden failure. Therefore a different control

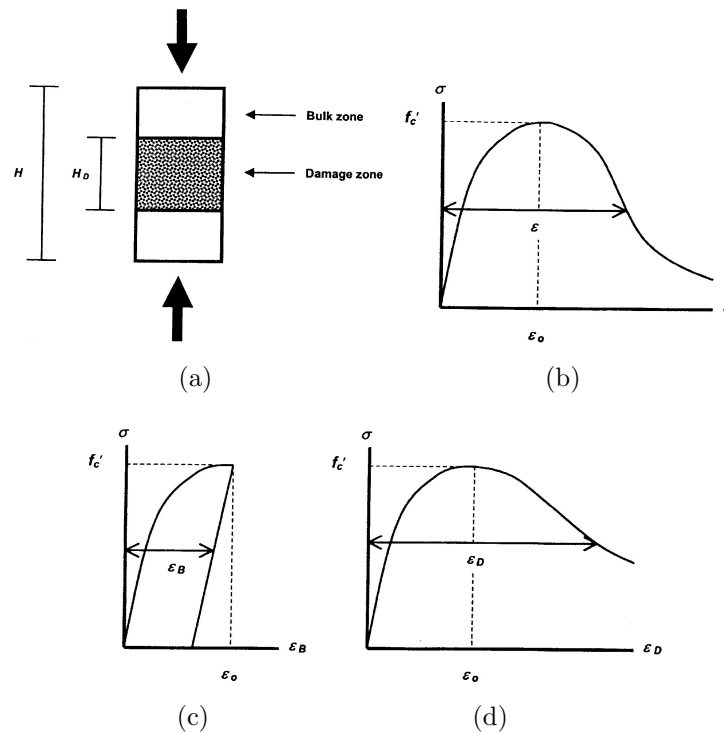


Figure 4.8: Response of a softening material under compression. (a) the softening band and the "elastic" region (b) stress strain curve of whole specimen, (c) stress strain in the "elastic" region (d) stress strain in the softening region, from Palmquist and Jansen (2001)

had to be found, whose control value would increase before and after peak. One option was to use LVDT's with a small measuring length at the position where the cracks are expected to occur. This was successfully done by Van Vliet (2000) for tensile tests.

In compression it is not that simple, because parts can separate from the specimen and the *crack band* is running usually inclined to the loading direction. When the crack is running outside the zone measured by the displacement transducer or when parts, where the displacement transducer is fixed separately, the measurement is not any longer usable for control of the experiment.

In literature different methods were used to circumvent this. One is the so called Partial-Elastic-Subtraction-Method (PESM), which uses a linear combination of displacement and force that partially subtracts the elastic response and leads to a stable feedback signal (Okubo and Nishimatsu, 1985; Jansen and Shah, 1997), see figure 4.9. Choi et al. (1996) used a constant circumferential loading

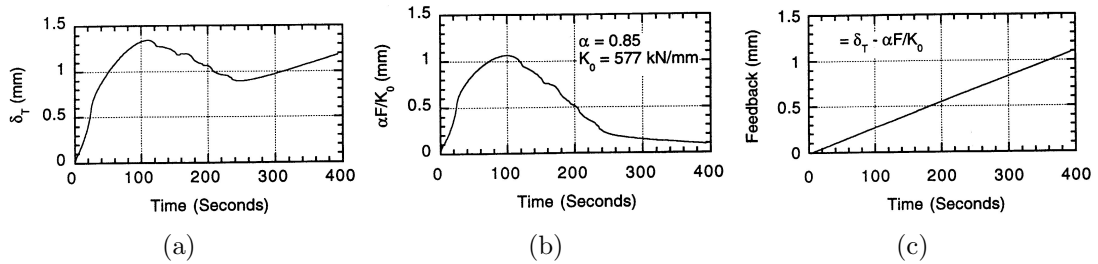


Figure 4.9: PESH Method, curve (c) follows from (a) minus (b), from Jansen and Shah (1997)

rate (circumferential displacement divided by the undeformed circumference) for control. This stabilizes the experiment because the lateral displacement increases before peak and also after peak load stronger as the longitudinal displacement. In the tests of Choi et al. (1996) the axial loading rate was very high at the beginning of the experiment, but decreased with increasing load, see figure 4.10. Prior to maximum load (indicated by a circle) the circumferential loading became higher than the axial in figure 4.10.

This test control was also applied to the sandstone experiments to prevent sudden failure. To circumvent the high loading rate at the beginning of the experiment a combination of axial and circumferential loading rate was used for control of the experiments. The tests were controlled by the longitudinal displacement on the compressed side (*DT1*) and the lateral displacement transducers (*DT3*, *DT4*), see figure 4.6. The lateral displacement transducers were multiplied by a factor of 10. This factor resulted from an earlier measured Poisson's ratio of 0.2 and a height to depth ratio of 2. In a linear elastic deformation state the longitudinal displacement is therefore 10 times the lateral displacement. The larger value of the longitudinal or the multiplied lateral deformation signal was used for control of the experiment. During testing it turned out that a factor of 7 was better. The prescribed loading rate was $1 \mu\text{m}/\text{s}$.

At the start of the experiment the longitudinal displacement transducer on the compressed side was responsible for control, but with increasing load the control changed to one of the lateral displacement transducers. In most experiments this change was very early in the experiment. With this control technique it was possible to perform a stable experiment although the material responded very brittle.

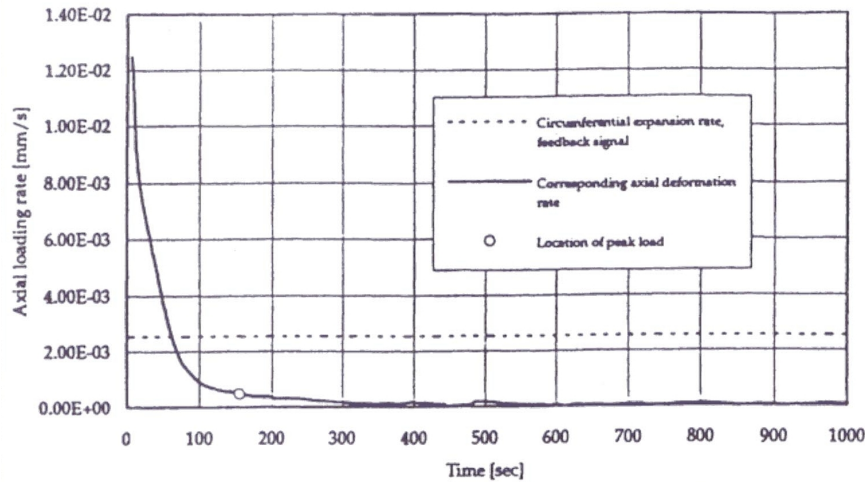


Figure 4.10: Axial and circumferential displacement rate in compressive test performed by circumferential control. Maximum load indicated by circle, from Choi et al. (1996)

4.4 Data preparation and parameter extraction

4.4.1 Correction of the load displacement plots

At the beginning of the experiment the measured displacements were larger than the displacements of the specimen. Therefore the measured data below a certain level had to be corrected. Here this was done below $1/6$ of the maximum load. For the correct determination of the origin of the diagram the points at $1/6$ and $1/3$ of the maximum load were determined, see figure 4.11. A straight line was placed through these points and intersected with the time axis. The distance to zero was determined and the curve was moved to this position.

4.4.2 Determination of material parameters from displacements and loads

Cross section parameters at notch

All material and cross section parameters were determined in the notched cross section in the middle of the specimen, see figure 4.12. The stresses σ_{notch} were calculated in the center of the notched region on the compressed and tensile side according to linear elasticity theory. The area A , the moment of inertia I and the distances of the centroid y were determined on the notched cross section.

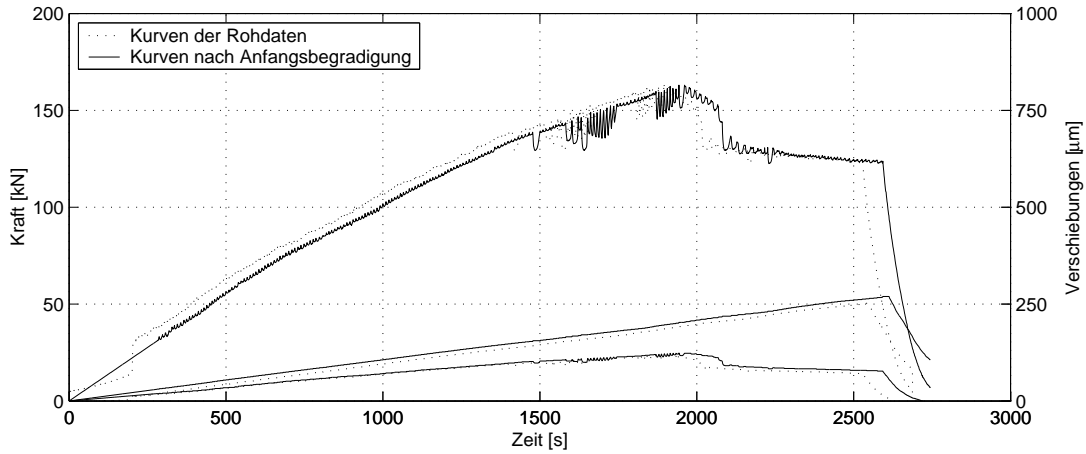


Figure 4.11: Original measured displacement w_1 (dotted line), moved data (solid line)

The cross section dimensions b_1 and b_2 were measured for each specimen. In all three series the deviations were very small. The area of the cross section in the notched region was calculated as

$$A = b_1 \cdot b_2 - slk^2 = b_1 \cdot b_2 - (D/7.5 \cdot \sqrt{2})^2 \quad (4.1)$$

the width of the notch slk was calculated as

$$slk = \frac{D}{7.5} \sqrt{2} \quad . \quad (4.2)$$

The distance of the centroid from the tensed side in the notched cross section y_{st} was calculated as

$$y_{st} = [b_1 \cdot b_2^2/2 - slk^2 (b_2 - slk/3)]/A \quad (4.3)$$

and from the compressed side as

$$y_{sc} = b_2 - y_{st} \quad . \quad (4.4)$$

The moment of inertia writes

$$I = (y_{sc}^3 + y_{st}^3) \frac{b_1}{12} + (y_{sc}^3 + y_{st}^3) \frac{b_1}{4} - slk^2 \left(y_{sc} - \frac{slk}{3} \right)^2 - \frac{slk^4}{36} \quad . \quad (4.5)$$

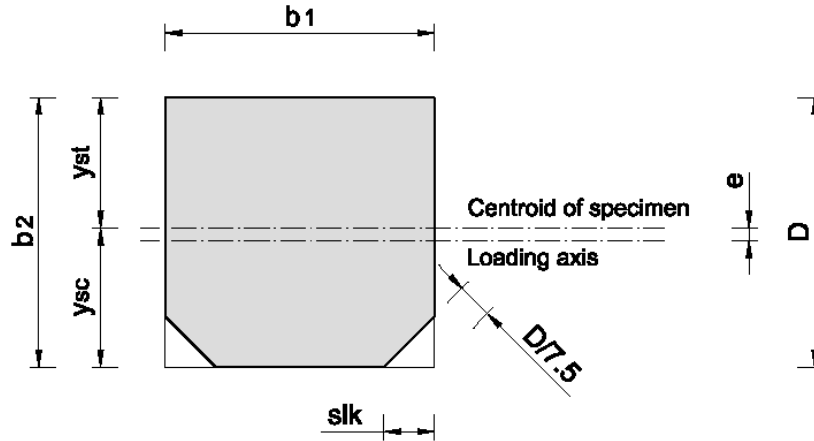


Figure 4.12: Cross section of sandstone specimen with notch type 3 loaded with eccentricity e

Calculation of stresses and strains from data

The stresses in the notched cross section at the center of the specimen σ_{notch} were calculated according to theory of linear elasticity as

$$\sigma_{notch} = \frac{F}{A_{notch}} \pm \frac{F \cdot e_{notch} \cdot y_{notch}}{I_{notch}} \quad (4.6)$$

The strains were calculated on the compressive and tensile side. The calculated strains did not consider the varying cross section. From the displacement transducers $DT1$ and $DT2$ the strains were determined as mean strains ε_{mean} over the whole specimen length by dividing the measured displacement Δl by the measuring length l_0 . The measuring length l_0 of the displacement transducers $DT 1$ and $DT 2$ was 0.9 times the specimen length. The strains were calculated as

$$\varepsilon_{mean} = \frac{\Delta l}{l_0}, \quad \varepsilon_c = \frac{w_1}{0.9 \cdot h}, \quad \varepsilon_t = \frac{w_2}{0.9 \cdot h} \quad (4.7)$$

For the modulus of elasticity the stresses and strains were determined at $\frac{1}{3}$ and $\frac{1}{6}$ of the maximum load. The modulus of elasticity E_{mean} was calculated as

$$E_{mean} = \frac{\sigma_{\frac{1}{3}F_{max}} - \sigma_{\frac{1}{6}F_{max}}}{\varepsilon_{\frac{1}{3}F_{max}} - \varepsilon_{\frac{1}{6}F_{max}}} \quad (4.8)$$

4.5 Results of preliminary series

4.5.1 Centric and eccentric loading

The specimens loaded centrically failed by axial splitting, which is not the desired failure mode for the size effect series. The longitudinal axial splitting crack does not change the global stress field, and so it causes no global release of energy. This failure mode does not exhibit a size effect (Bažant and Planas, 1998, section 9.5.9) and was for this investigation not of interest.

There are other fractures that lead to a release of global strain energy. Such fractures are the failure by a transversal splitting crack band that starts from one side of the specimen edge and propagates towards the center. By the formation and propagation of the crack, global strain energy was released and a size effect was expected for a sufficient range of sizes.

For this purpose the specimens were not loaded centrically, but with a small eccentricity. To further intensify the failure mode and to predefine the position of the failure mode a notch was introduced into the specimen.

4.5.2 Performance of notches and interfaces

The specimens were tested with no notch and with three different notches under compressive loading, see section 4.3.1. The interface between the loading platen and the specimen was also varied, see section 4.3.2. It turned out during the *preliminary testing* that the interface and the notch type were of major importance for proper performance of the tests and for obtaining reliable data. It was very difficult to find a suitable interface between loading platen and specimen, that was easy to establish at reasonable time and did not lead to the spalling of the edges. To prevent spalling of edges on the specimen a proper interface and a notch that predefines the fracture were necessary. In table 4.1 on page 25 the performance of the notches and interfaces were summarized. In this section only specimens with numbers 3, 6, 8, 16, 14, 1, 25, 19, 2, 5, 10, 12, 17, 18, 21 were considered.

4.5.3 Strength versus density

The strength values of the specimens are compared in figure 4.13 (left) with the density of the material. One can see that the density is varying for the specimens tested under centric loading from 1.98 to 2.08 g/cm^3 (5%). For the specimens tested under centric loading and rotation free boundaries ($e=0$, rot. free) the strength increased with increasing density, see figure 4.13 (left). For the eccentrically loaded specimens such behavior was not detected. For the tests performed

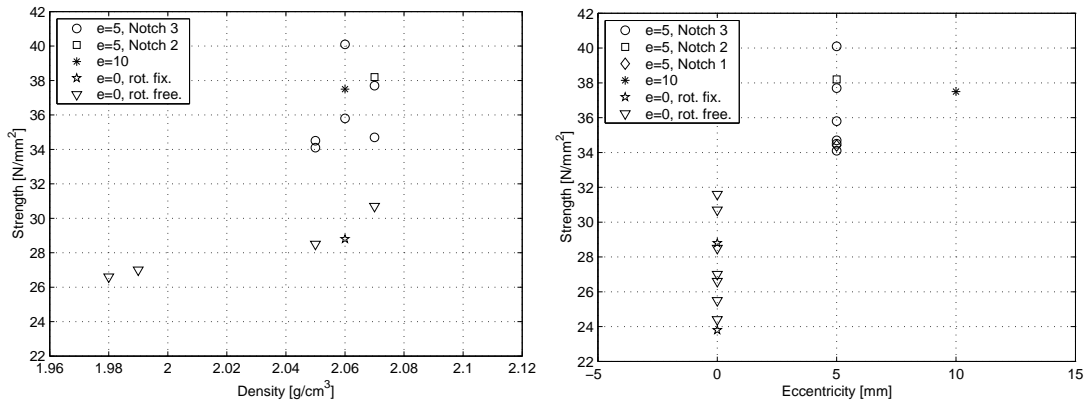


Table 4.2: Strengths from centric tests of the preliminary series in N/mm^2

boundary	quantity	$f_{c,mean}$ [N/mm^2]	E-modulus [N/mm^2]	density [g/cm^3]	notch	strat.	comment
rot. free	4	28.2	18333	2.02	no	trans.	
rot. free	1	24.4	19400	2.02	no	trans.	inclusions
rot. fixed	2	26.2	23650	2.07	no	trans.	

Table 4.3: Eccentric strength of sandstone of the preliminary series in N/mm^2

e	quantity	$f_{c,mean}$ [N/mm^2]	E-modulus [N/mm^2]	density [g/cm^3]	notch	strat.	comment
D/20	1	31.6	30500	2.06	no	trans.	
D/20	1	31.8	28400	1.97	no	long.	
D/20	2	26.6	24050	1.99	no	trans.	inclusions
D/10	1	37.5	37000	2.06	no	trans.	sudden failure
D/20	7	36.4	27470	2.07	type 3	trans.	see figure 5.1



Figure 4.14: Specimen 19 after testing and opening the existing cracks (from left to right)

testing the specimen did not show severe damage. The surface was brushed and the cracks became visible. The cracks on the surface were colored with a black pen. It was carefully tried to open the existing cracks with a screwdriver and to remove the broken parts, to see how the crack propagated inside the specimen. After removal of every fractured piece the crack surface was cleaned again with a smooth brush. The picture sequence in figure 4.14 shows this very nicely. In figure 4.14 one can easily see that the cracks start from one side (the compressive side) of the specimen and propagates from the surface into the material.

4.6 Four Point bending test

A specimen with transversal (specimen 11) and a specimen with longitudinal stratification (specimen 23) were cut in longitudinal direction into four pieces. The new specimens had dimensions of $45 \times 45 \times 200$ mm. These specimens were tested under four point bending. The span of the specimen was 18 cm and the distance of the two load points was 6 cm from the support, see figure 4.15 for test setup. For every test specimen the load and the deflection in the middle of the specimen was used for application of displacement rate. The strengths are presented in table 4.4.

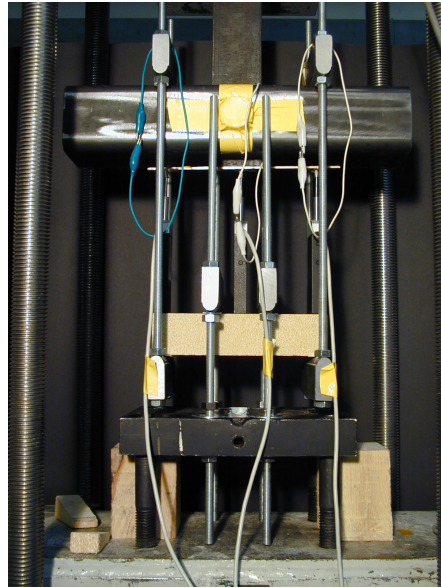


Figure 4.15: Experimental setup for four point bending test

Table 4.4: Four point bending strength of sandstone of the preliminary series in N/mm^2

quantity	$f_{c,mean}$ [N/mm^2]	$f_{c,max}$ [N/mm^2]	$f_{c,min}$ [N/mm^2]	strat.	comment
4	6.6	6.9	6.4	transversal	
1	6.7	-	-	longitudinal	

Chapter 5

Test series on sandstone

5.1 Introduction

In the *test series* specimen of 6 different sizes from XS to XXL with a total size range of 1:32 were tested. All dimensions were scaled for every size by the same factor, thus geometric similarity was provided. The aim of the series was to find the influence of size on strength, namely the size effect.

5.2 Specimen dimensions and geometry

All specimens for the *test series on sizes XS to XXL* were sawed in the quarry at St. Margarethen im Burgenland from one block with the dimensions $5.0 \times 1.3 \times 1.3$ m. The sandstone used for this test series was not from the same block as the specimens for the *preliminary test series*. The dimensions of the specimens varied from 20x20x40 mm (XS-size specimens) to 640x640x1280 mm (XXL-size specimens), see table 5.1. All specimens had the stratification transversal to the direction of loading (longitudinal stratification) and the same geometric dimensions just scaled by a factor (similarity in three dimensions), see table 5.1.

All specimen sizes from XS to XXL are drawn in figure 5.2 and one can see the impressive size range in figure 1.1 (smallest specimen in hand). The size range that was covered in the experiment was 1:32. From the XXL and the XL size 3 specimens were tested and 6 from the L and M sizes. The number of S and the XS size specimens was increased to 12, because higher scatter was expected. The total number of specimens was 42, all specimens were provided with a notch that was previously investigated in the *preliminary test series*, see figure 5.1. The notch was formed in longitudinal direction as a smooth notch that produces no high stress gradients in the longitudinal specimen axis. The advantages of providing the specimen with a notch was to predefine the location

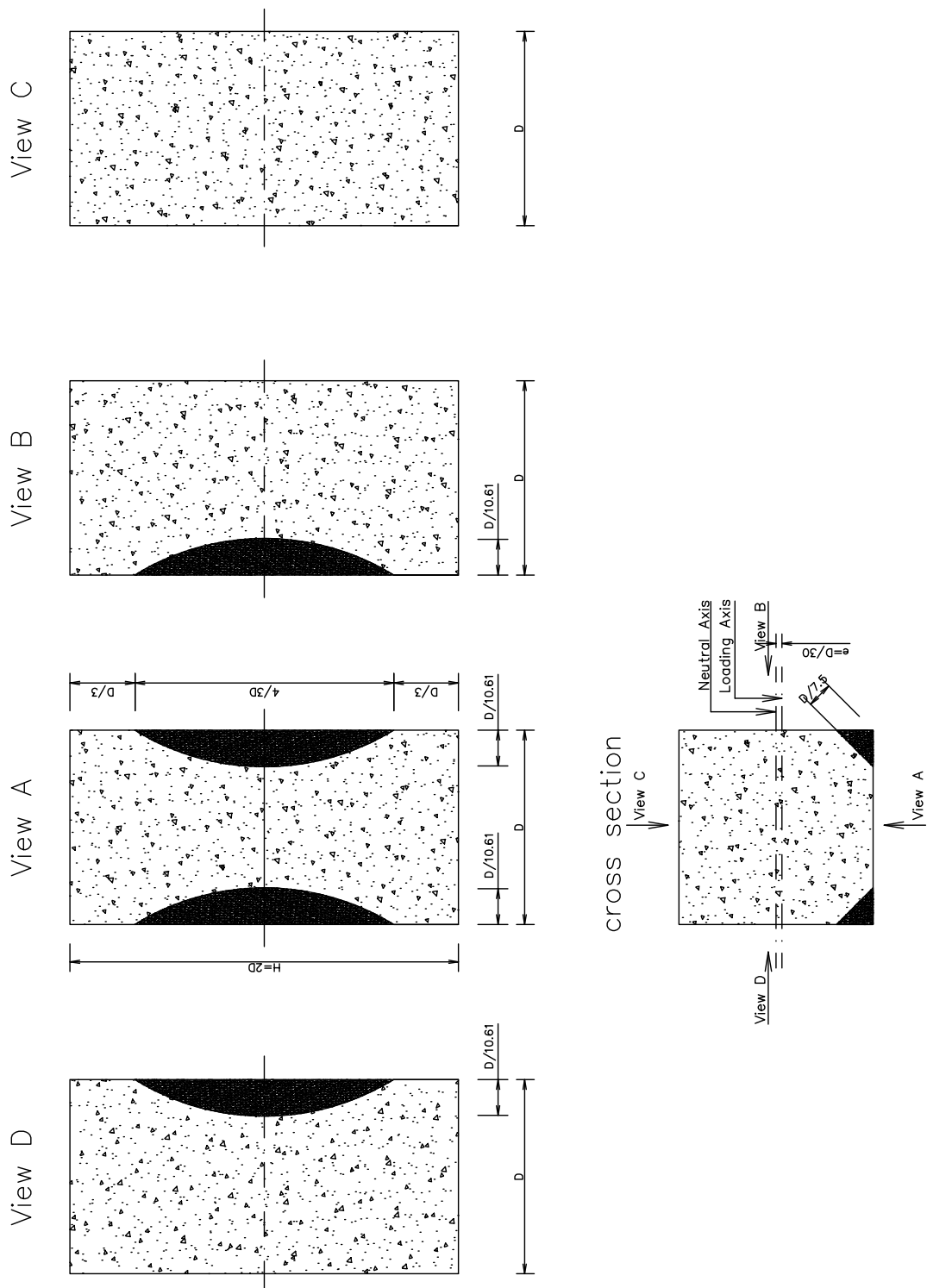


Figure 5.1: Geometry of the specimens with notch

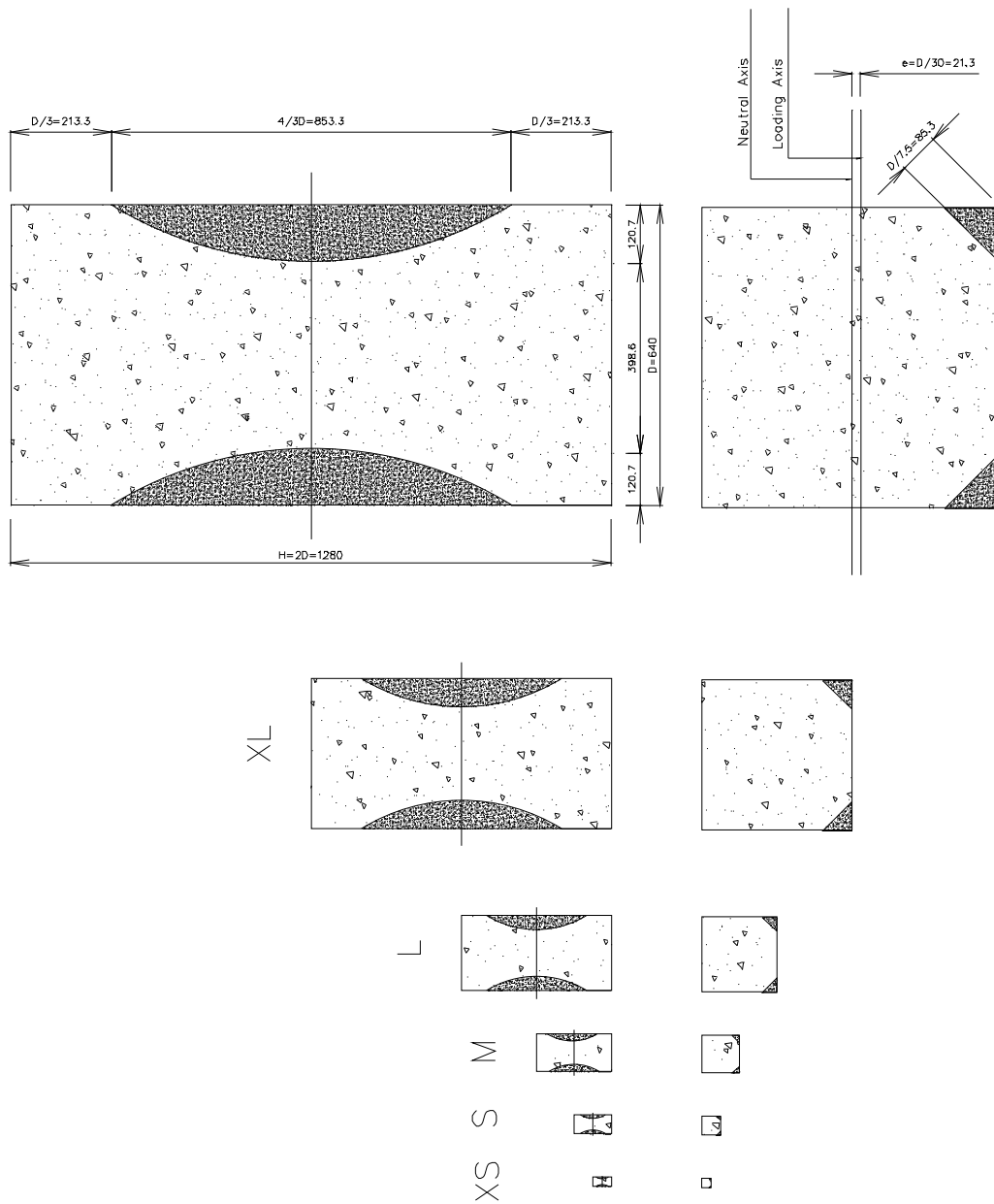


Figure 5.2: Dimensions of the 6 sandstone specimen sizes for size effect test series from XS to XXL in mm

Table 5.1: Sandstone specimens used for size effect tests

Specimen	Number	Dimensions [mm]	Cross section [cm ²]	weight kg	Testing frame
XXL	3	640x640x1280	4096	1150	Column Tester
XL	3	320x320x640	1024	145	Column Tester
L	6	160x160x320	256	18	D2
M	6	80x80x160	64	2.3	D2
S	12	40x40x80	16	0.3	D2
XS	12	20x20x40	4	0.04	D2

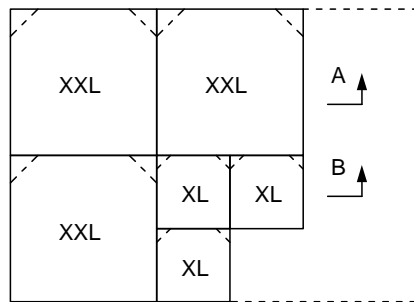
were the fracture did start, to make it more easy to control the test, prevent spalling of edges and to observe fracture of the specimen, see section 4.3.1 for an investigation on the notches. Another advantage of the notch was to reduce the influence of visible inhomogeneities, see chapter 5.3.

5.3 Homogeneity of sandstone specimens

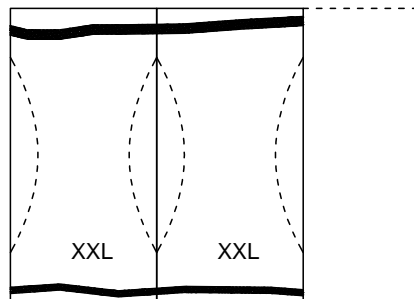
The sandstone block in the quarry was homogeneous in the center, but had one compaction band close to the top and one close to the bottom face. The specimens were cut such that the more compacted material was in the region without notch towards the faces where loading was applied, see figure 5.3. The notch was between the highly compacted bands, where the sandstone appeared homogeneous. The notch reduced the cross section and determined the location where the fracture started. Due to special attention prior to cutting it was possible to have visible inhomogeneities outside the notched region.

The discussed compaction bands occurred only in the XXL, but also in some XL specimens. Except of these two bands the specimen showed a very homogeneous structure on the specimen surface.

VERTICAL SECTION



SECTION A A



SECTION B B

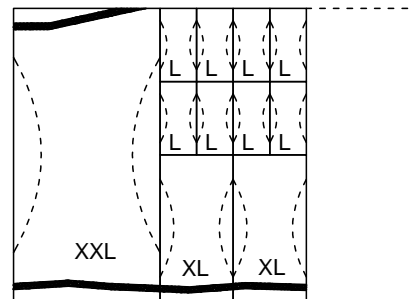


Figure 5.3: Compaction bands in the sandstone block, with sawing scheme

5.4 Boundary conditions and testing machines

5.4.1 Loading arrangement

All the specimens were loaded with a predefined eccentricity. This was done for various reasons

- The centric tests in the preliminary series failed by axial splitting, see section 4.5.1. The compressive failure due to axial splitting does not produce a size effect (Bažant and Planas, 1998, section 9.5.9). This was numerically shown by Bažant and Ožbolt (1992).
- Exact centric loading of a column is difficult to establish experimentally and due to the heterogeneity of the material the stress states in the cross section are never uniform, see section 2.5.

- Due to the higher stress concentration the surface where the failure starts was predefined and could be observed during experiment, see section 4.3.1.
- The test could be controlled by the displacement in the region where the fracture started, see section 4.3.5.

In all experimental set-ups the loading platens were placed on longitudinal hinges on both ends of the specimen. For sizes XS, S, M, L the D2 frame was used. The experimental set-up was the same as in the preliminary tests. The position of the force was defined by the axis of the hinge. Due to the rotating capability in one direction no moment could be transferred or generated during the experiment, i.e. rotation of the loading platen was possible without moment build up. To introduce the eccentricity the specimen was shifted in direction normal to the hinge axis by the amount of the desired eccentricity. The load did not change the position and did not rotate during experiment. For the XS, S, M and L size specimens different thicknesses of loading platens and diameters of cylinders were necessary.

The XL and XXL specimen were tested in the Column Tester, see figures 5.4, 5.5 and figure 5.7 for a photo. A longitudinal hinge in form of a cylindrical bearing on one side of the specimen was used. On the other side were four hydraulic actuators that applied the load. The control of the cylinders during experiment was twofold. First, all four cylinders were controlled to apply the same load through the loading platen and to the specimen during experiment. Secondly, they applied the defined strain (or displacement) to the specimen. The cylinders were equipped with spherical hinges on both sides of the hydraulic actuator and the central axis of this experimental setup goes through the center of all four hydraulic jacks. The longitudinal axis of the specimen was positioned below the axis of the experimental setup by the predefined eccentricity. Due to this shift the eccentricity was established. A detailed description of the Column Tester can be found in Burtscher et al. (2003a) or Burtscher et al. (2003b).

5.4.2 Interface between loading platen and specimen

In section 4.3.2 of the *preliminary test series* various systems were investigated to provide a proper load transfer from loading platen to the specimen. For the size effect tests a layer of teflon and double sided sandpaper was used. The thickness of the teflon was 0.75 mm. The teflon layer was used to prevent stress peaks on the sandstone loading face, due to a eventually bumpy surface of the sandstone. In the locations of the bumps stress peaks could arise. Teflon yields at very low stresses and therefore prevents stress concentrations on the loading surfaces of the specimen. The friction between steel and teflon was very low, which could

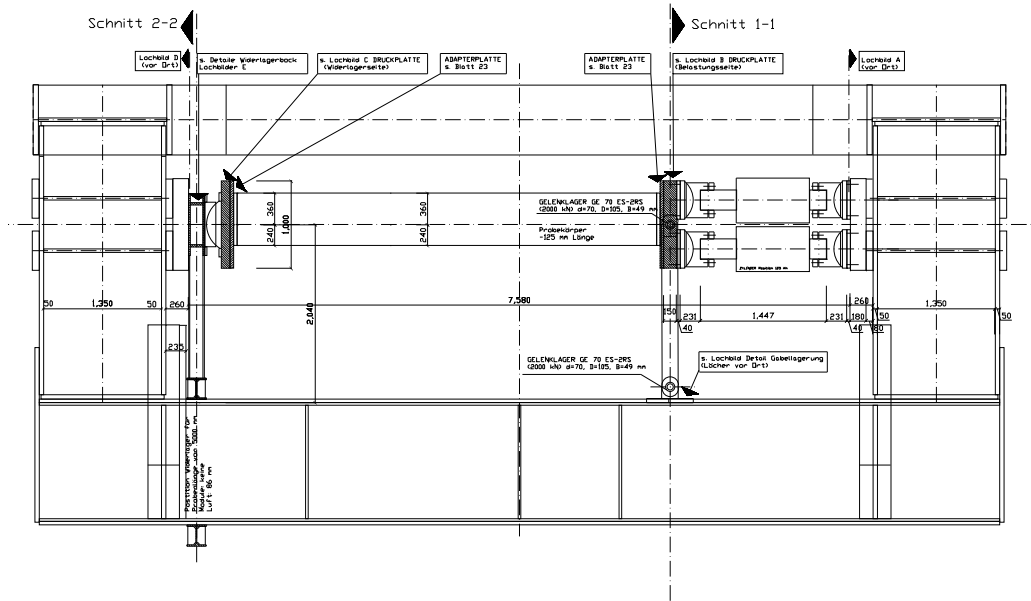


Figure 5.4: Longitudinal Section of Column Tester with equipment for a column length of 5.0m

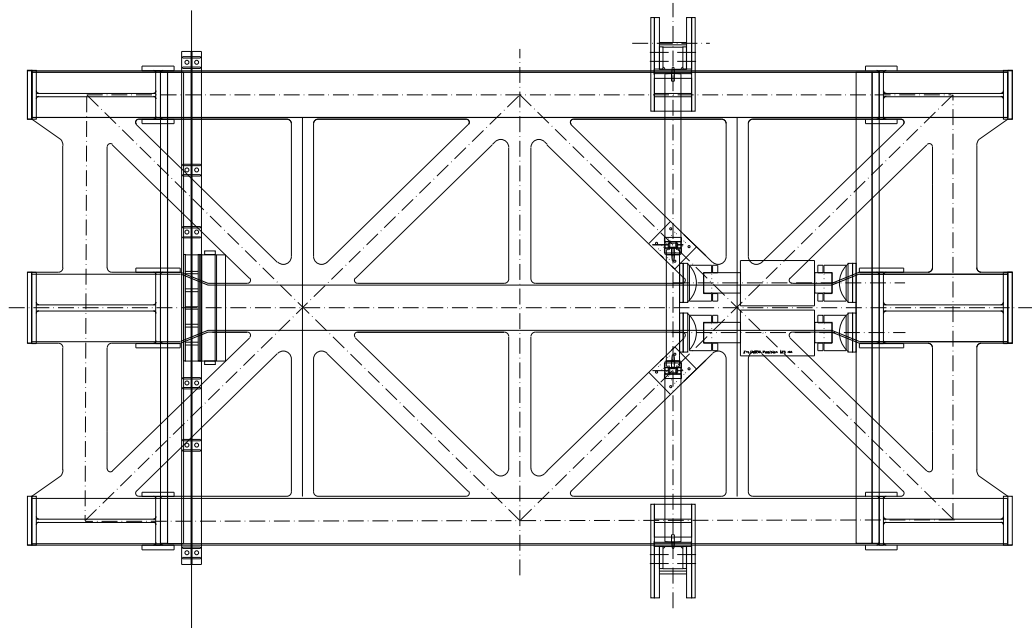


Figure 5.5: Horizontal Section of Column Tester with equipment for a column length of 5.0m

lead to a translation of the specimen on the interface during experiment. This was intensified by eccentric loading of the specimen, especially when the post peak region was entered. Therefore the double sided sand paper was positioned between the loading plates and the teflon layer. The thickness of the teflon layer was not changed with specimen size, because the unevenness of the surface was assumed to be the same for all specimens.

5.5 Arrangement of displacement transducers

The displacements in the sandstone specimens were very low, especially for the smaller sizes. The accuracy of usual LVDT's is about 0.1mm , which was not precise enough. For accurate measurements of the displacements digital incremental transducers with an resolution and accuracy of $1\mu\text{m}$ were used instead. The arrangement of the displacement transducers and the AE-sensors was equal for all specimens and was scaled with the specimen size, see figure 5.6. The measuring length of the longitudinal displacement transducers *DT 1* and *DT 2* (see figure 5.6) was always 90% of the total specimen length. For the XXL- and the XL-size specimens a carbon fiber rod was used to measure the displacement over the pre-defined length. For the L- and M-series the displacement transducers were fixed to the specimen with sharp steel needles. The longitudinal displacements and the lateral displacements of the S- and the XS-size specimen were not recorded. Just one displacement transducer was attached to the crosshead to control the experiment. The lateral displacement *DT 4* (see figure 5.6) between the compressive and the tensile surface was measured using two rectangular aluminum rods for the L- and M-size and wooden rods for the XL- and XXL-size. The rods were pressed with rubber bands to both specimen surfaces and the displacement of the sheets were measured using a displacement transducer that was fixed to one of the rods. The lateral displacement *DT 3* (see figure 5.6) was also measured using two rods, but they were working like a seesaw, see figure 5.6.

5.6 Acoustic Emission Measurements

5.6.1 Aim and set-up of acoustic emission measurements

The aim of the acoustic emission measurement was to investigate the onset of damage. Due to limited space on the specimen surface for placement of sensors the acoustic emission measurements were only possible for the sizes XXL, XL and L. 5 sensors with a resonant frequency of 150 kHz were used. The positions of the sensors are displayed in figure 5.6.

The sensors were attached to the specimen surface using a stirrup made of aluminum, see figure 5.7 for a fully instrumented specimen of size XXL. The stirrups were glued to the specimen and a screw was used to press the sensor onto the specimen surface. Between screw and sensor a layer of cork was attached. With the screw and the cork the sensor was pressed to the specimen with a uniform pressure that was approximately equal for all sensors and specimens. To ensure an appropriate acoustic coupling between sensor and specimen a thin film of grease was used.

The gain was 40 dB and the threshold was 30.7 dB (Valen Systeme, 2000, 1994; Leaird, 1997; Miller and McIntire, 1987). The wave speed was determined prior to testing and was between 360 and 410 cm/ms . The wave speed in longitudinal and lateral specimen direction was determined for every specimen.

The location algorithm for determination of acoustic emission source was a 3-D algorithm. Due to the very high activity during testing the sources could not be determined.

5.7 Test control

Proper test control was investigated in the *preliminary series* in section 4.3.5. For this test series the longitudinal (*DT 1*) and the multiplied lateral displacement (*DT 3* and *DT 4*) were used for control as described at the end of section 4.3.5. The displacement rate was changed for the different sizes, that a prescribed strain rate of $1E - 6$ *strain/s* was applied to every specimen.

For specimens XS and S the displacements were not measured on the specimen surface. The control of the test was done by displacement of the crosshead transducer.

5.8 Results of test series on sizes XS to XXL

In the experiments the AE-signals, the load, the longitudinal and lateral displacements were recorded. The arrangement of the displacement transducers and the AE sensors is displayed in figure 5.1. In section 4.4.1 on page 36 the correction of the load displacement plots and in section 4.4.2 the determination of material parameters are described. The experimental results are listed in tabular form in table 5.2 as mean values for the different sizes. In chapter 5.16 the stress strain plots of the different sizes are given.

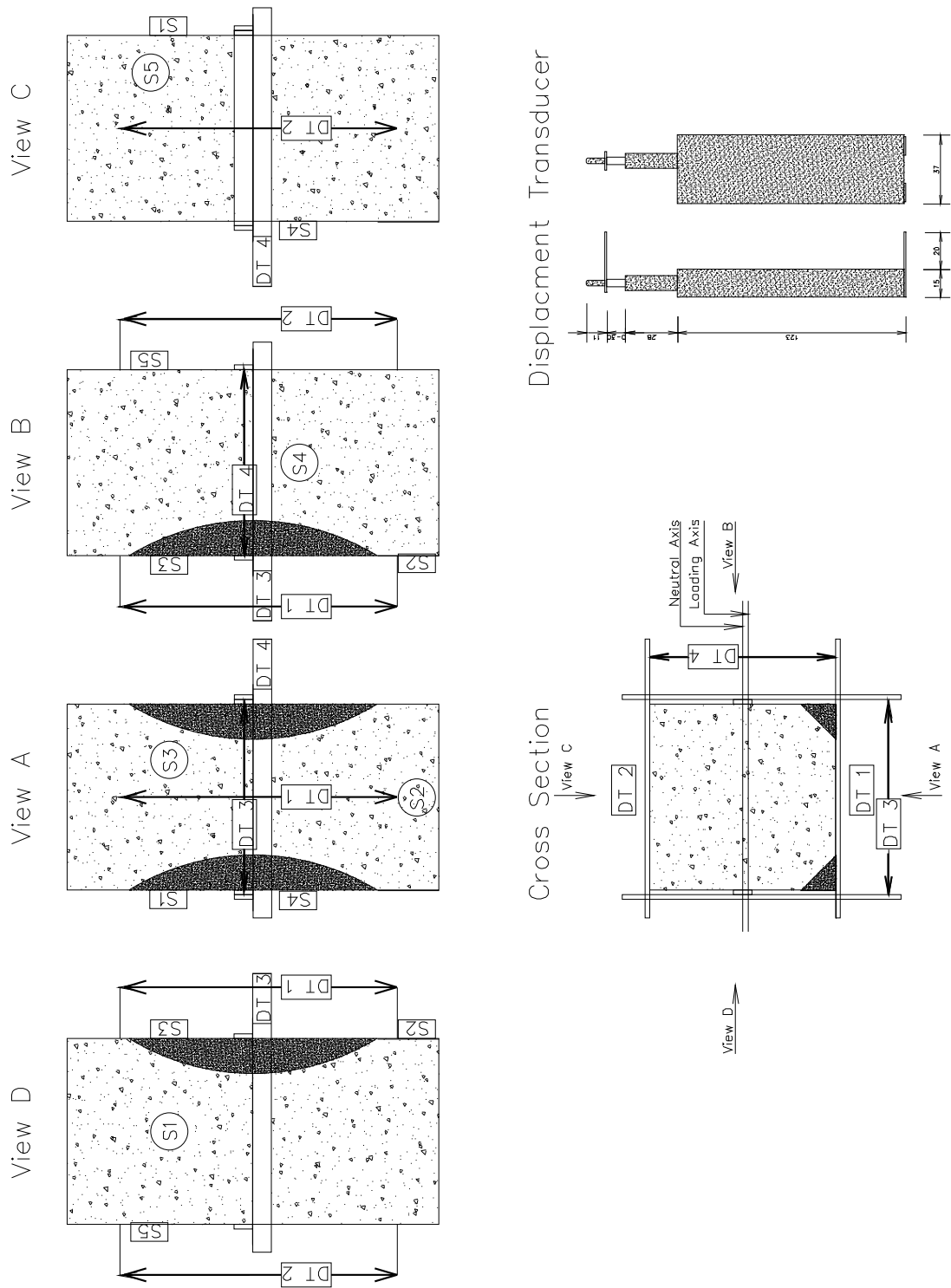


Figure 5.6: Arrangement of displacement transducers DT1 to DT4 and acoustic emission sensors S1 to S5

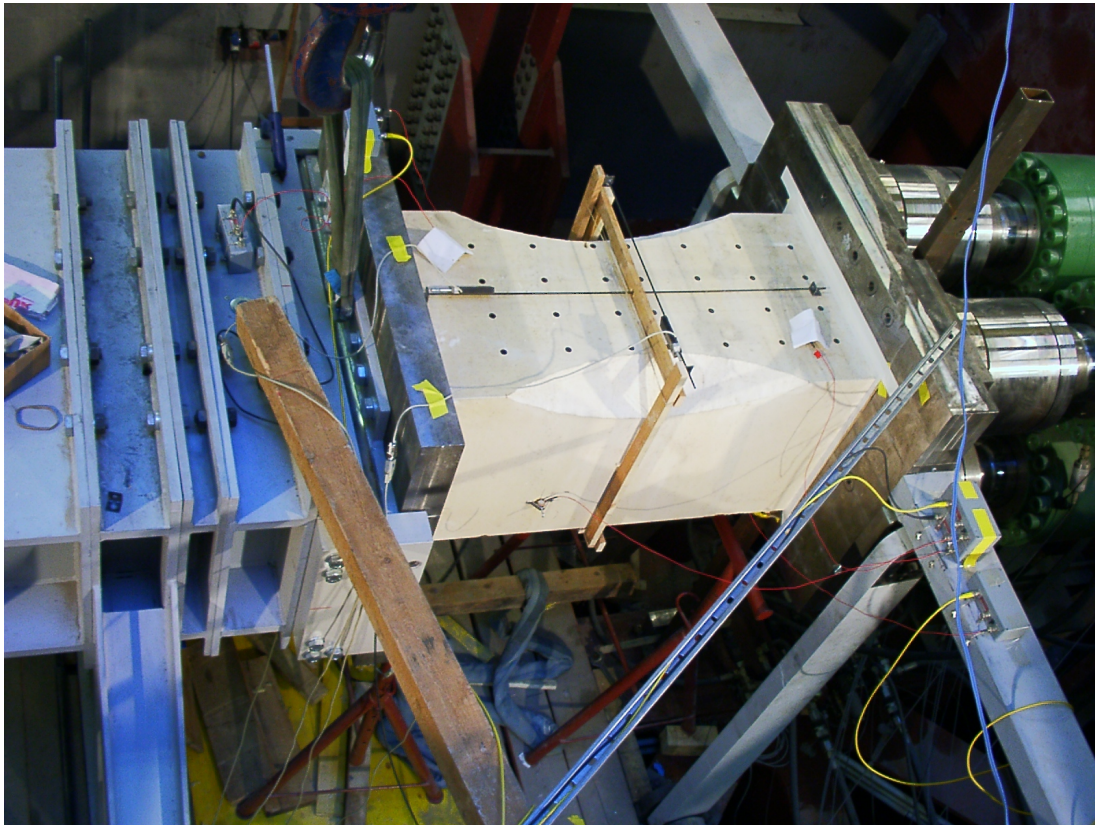


Figure 5.7: Specimen XXL (64x64x128 cm) equipped with displacement transducers and acoustic emission sensors

5.8.1 Strength versus specimen size

One of the main issues of the size effect theory is the influence of strength on the size of the specimen. The strength was determined as maximum stress according to equation 4.6 on page 38. In figure 5.8 the strength determined as maximum stress is plotted versus specimen size. The results are displayed with linear (left) and logarithmic scaling (right) of the axis. In the plots a decrease of strength with increasing specimen size could be determined. Thus a size effect was present in this *test series*. The mean strength decreases from the XS (2cm) to the XXL (64cm) series from 43.0 Mpa to 19.4 Mpa, see table 5.2 for mean values. The mean strengths of the sizes XS and S (4cm) are 43.0 Mpa and 39.2 Mpa, which is much higher than for the other sizes. The mean strength decreases from the M (8cm) to the XXL (64cm) sizes from 23.1 Mpa to 19.4 Mpa, which corresponds to a strength decrease of 16% for a size range of 1:8.

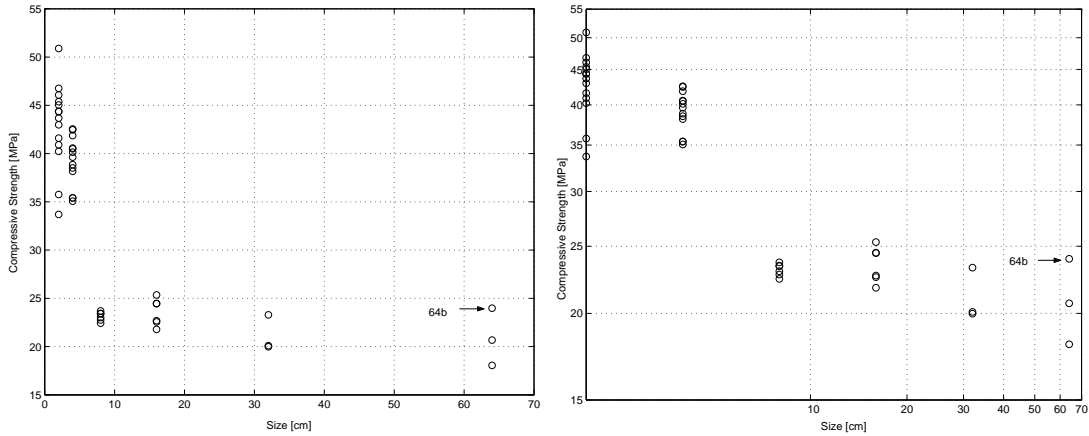


Figure 5.8: Strength vs Specimen size in linear (left) and logarithmic scale(right).

To clarify this drastic increase in strength of the XS and the S sizes, the *verification series* on sizes XS to L was performed. This additional investigation was performed on a high number of specimen. The XS and S specimen in the *test series* were loaded with a higher loading rate, see section 5.8.2. In the *verification series* the range of different loading rates was investigated and it was found that there was no influence of the loading rate, see figure 6.3. Additionally it was found that the density has a pronounced influence on the strength, see section 6.7.3. The strength for equal densities, but different sizes was approximately constant. Thus the trend in figure 5.8 for sizes XS and S was not confirmed. Following from the observations in the *verification series* in sections 6.7.2 and 6.7.3 the high strength values of the sizes XS and S have to be attributed to material inhomogeneities that became crucial for the small sizes.

5.8.2 Strength versus loading rate

It is described in literature that the loading rate affects the strength of specimens. For easier comparison the loading rate for the different sizes was calculated as normalized loading in terms of applied strain per second $\dot{\epsilon}$ and stress per second $\dot{\sigma}$. The loading rate was determined between $\frac{2}{3}$ of maximum load and maximum load. The stress rate is calculated by

$$\dot{\sigma} = \frac{\sigma_{F_{\max}} - \sigma_{\frac{2}{3}F_{\max}}}{t_{F_{\max}} - t_{\frac{2}{3}F_{\max}}} \quad (5.1)$$

and the strain rate by

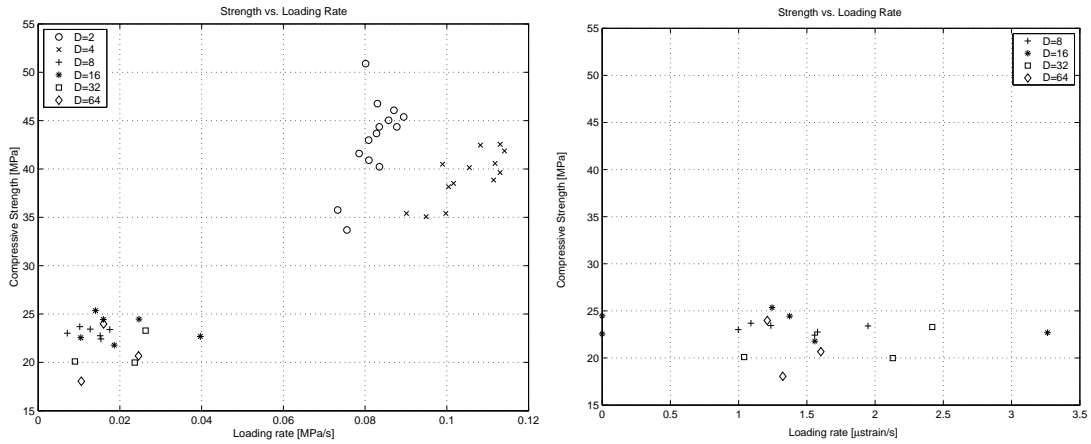


Figure 5.9: Strength vs. loading rate as stress per second (left) and strain per second (right)

$$\dot{\varepsilon} = \frac{\varepsilon_{F_{\max}} - \varepsilon_{\frac{2}{3}F_{\max}}}{t_{F_{\max}} - t_{\frac{2}{3}F_{\max}}} \quad (5.2)$$

This rate should be the same for all specimen sizes. For the sizes $D=2$ cm (XS) and 4 cm (S) only the stress per second could be compared, because the displacements were not measured on the specimen. In figure 5.9 the strength versus loading rate is displayed. The strain rate in figure 5.9 (right) shows a mean strain rate of $1.5 \mu\text{strain}/s$. The deviations from the mean value were small for the specimen sizes from 8 (M) to 64 cm (XXL). The loading rate was so small that it can be assumed that the deviations in loading did not affect the strength of the specimens. Additionally, the plot shows no trend of increasing or decreasing strength with strain rate. For comparison of the stress rates all sizes are considered in figure 5.9 (left). The mean loading rate was $0.02 \text{ MPa}/s$. The loading rate of the sizes $D=2$ (XS) and 4 (S) was four to five times higher than for the other specimen. Also the specimen strength was higher. It was questionable if this effect was due to size effect, loading rate, inhomogeneity or any other effect. To clarify this the *verification series* was performed covering the size range from $D = 2$ (XS) to 16 (L) to validate the results for these sizes and to determine the influence of loading rate on strength. The investigations clearly showed that there was no influence of the loading rate, but of the inhomogeneities in the material, see section 6.7 for the results. A tabular presentation of the results of the *test series* on sandstone can be found in table 5.2 on page 57.

Table 5.2: Mean values of experimental data for specimen of the same size

Specimen [cm]	E [MPa]	F_{max} [kN]	f_c [MPa]	w_{peak} [μm]	$\dot{\sigma}$ [MPa/s]	$\dot{\epsilon}$ [$10^6/s$]	v_{long} [cm/s]	v_{lat} [cm/s]
XS: 2	-	12	43.0	-	0.082	-	-	-
S: 4	-	45	39.2	-	0.105	-	373	-
M: 8	21566	107	23.1	254	0.013	1.40	333	-
L: 16	34982	438	23.6	242	0.021	1.86	336	361
XL: 32	20013	1572	21.1	813	0.019	1.86	342	318
XXL: 64	22380	6225	19.4	1404	0.017	1.46	327	350

5.8.3 Strength and Young's modulus versus wave speed

Prior to testing the wave speed was determined with the acoustic emission equipment. In rock mechanics the wave speed is used to quantify constitutive parameters, like the Young's modulus. In figure 5.10 the Young's modulus and the compressive strength determined in the experiment are plotted versus the wave speed. No trend of Young' modulus and strength could be distinguished with wave speed.

5.8.4 Classification of fracture pattern

To compare results of different specimens and sizes it was important that all specimens showed the same fracture type. Due to the fact that the specimens were notched and should fail at the weakest cross section in the middle of the notch, any other fracture type gave rise to the fact that the fracture was initiated by another effect, e.g. local inhomogeneities or improper boundary conditions. The observed fracture patterns were classed into different types, that give information if the experiment performed well or not. 6 fracture patterns were identified, see figure 5.11. The fracture patterns were defined as

Fracture pattern A Most of the specimens showed this fracture pattern. This fracture pattern indicates that the experiment performed well.

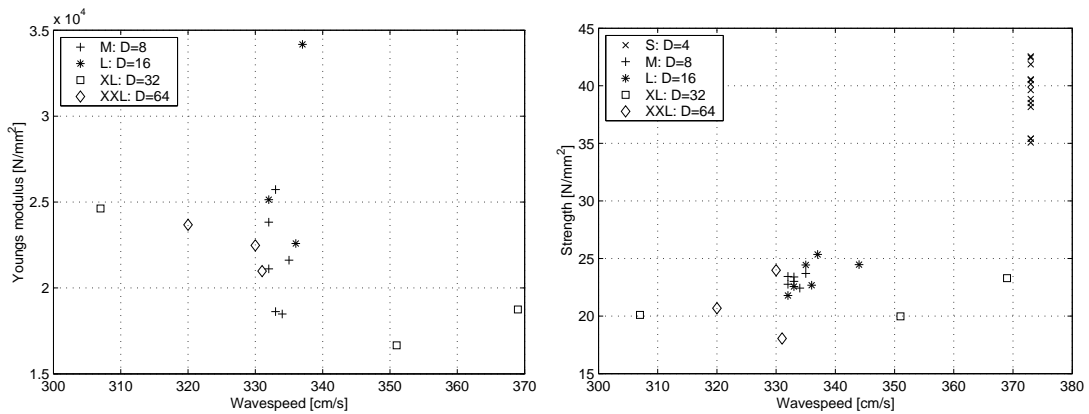


Figure 5.10: Young's modulus and strength versus wave speed in longitudinal direction

Fracture pattern B The same was valid as in fracture pattern A. The difference was that a crack in longitudinal direction over the whole specimen was present after the test. It was assumed that the second part of the crack developed at the final stage of the experiment and did not influence the experiment prior to complete failure.

Fracture pattern C The same was valid as in fracture pattern B. Additionally to the longitudinal crack a tensile crack on the tensile side developed. It could be assured that the tensile crack developed at the final stage of the experiment after the longitudinal cracks were formed.

Fracture pattern D The crack was close to the loading plate. This indicates that improper boundary conditions were responsible for a (most often) lower strength. Another reason could be a porous region that has lower strength.

Fracture pattern E The same as in fracture pattern D applies. For this fracture type it was more likely that the lower strength regions initiated the fracture.

Fracture pattern F Only small parts at the edges were spalling from the specimen. The reason was most often an uneven loading face of the specimen

The experiments that showed fracture pattern A, B and C, performed well and the material parameters extracted were compared in the summarization of the results. The specimen that showed fracture patterns D, E and F were excluded from comparison of results, because their fracture pattern indicated that inhomogeneities or improper boundary conditions were dominating.

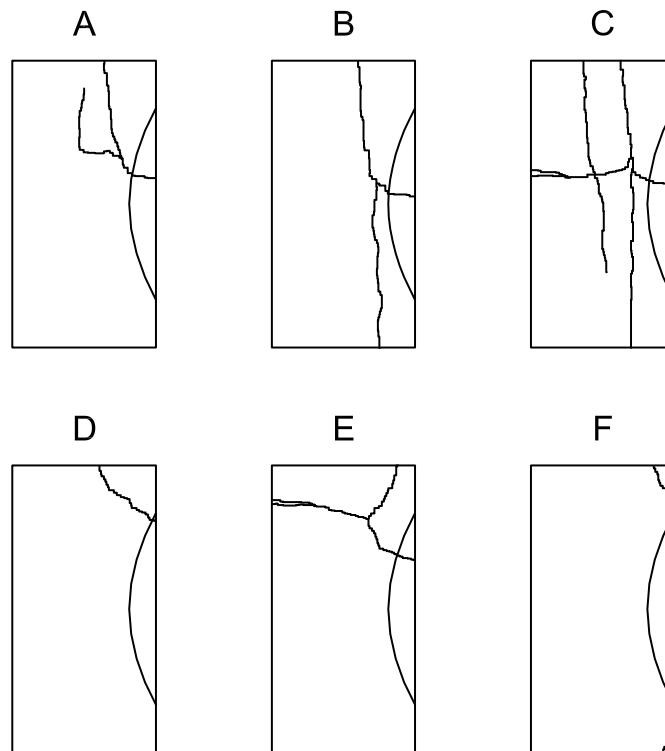


Figure 5.11: Identified fracture pattern

5.8.5 Specimens after testing

After testing the fracture patterns of the specimens were determined. All specimens of this series showed fracture patterns A, B or C and were therefore used for comparison of the results, except specimen 64b. This specimen showed fracture pattern E or F. 64b had no cracks in the notched region, only at the specimen ends. It was concluded that a inhomogeneity with higher strength (possibly a compaction band) was in the notched region. Thus the specimen did not fail in the weaker cross section, but towards the ends. The specimen 64b was excluded for further comparison of results.

The specimen of size XXL and XL were photographed after testing, see figures 5.12 and 5.13. The cracks were colored with a black pencil. All specimen surfaces were brushed with a smooth brush after testing to make cracks visible.



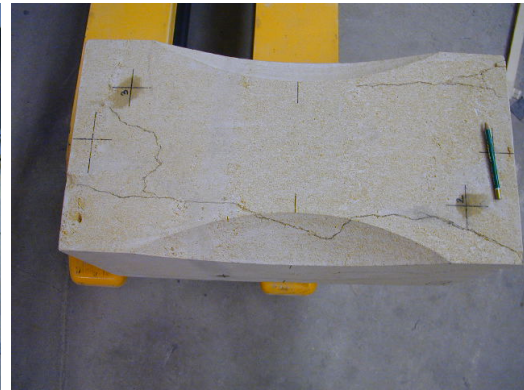
(a) Fractured specimen 32a side view, fracture pattern B



(b) Fractured specimen 32a top view, fracture pattern B



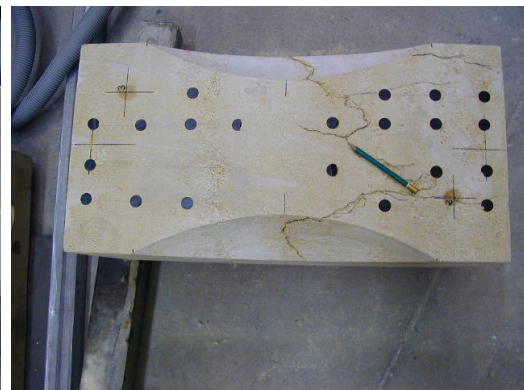
(c) Fractured specimen 32b side view, fracture pattern A



(d) Fractured specimen 32b top view, fracture pattern A



(e) Fractured specimen 32c side view, fracture pattern A

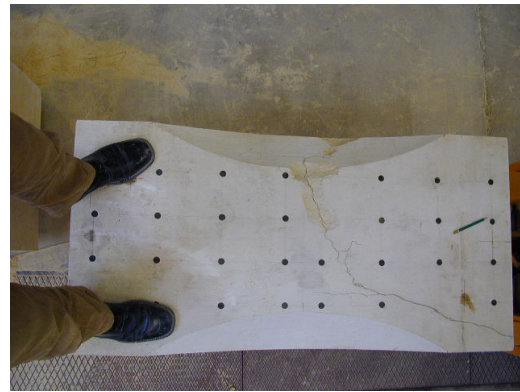


(f) Fractured specimen 32c top view, fracture pattern A

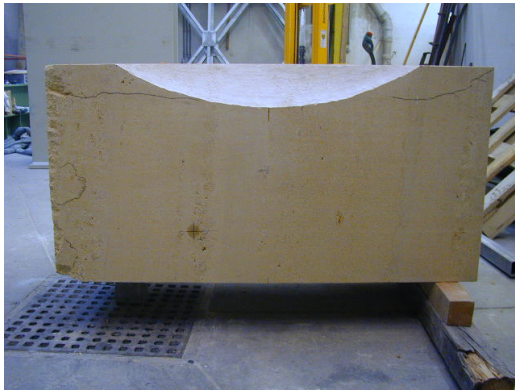
Figure 5.12: Pictures of specimen 32x32x64 cm after testing



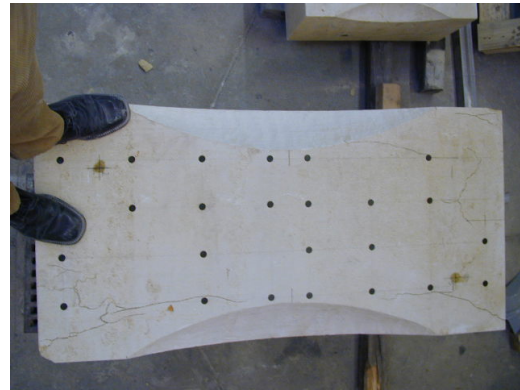
(a) Fractured specimen 64a side view, fracture pattern A



(b) Fractured specimen 64a top view, fracture pattern A



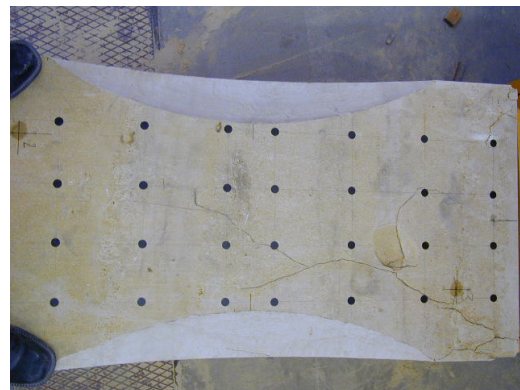
(c) Fractured specimen 64b side view, fracture pattern E



(d) Fractured specimen 64b top view, fracture pattern E



(e) Fractured specimen 64c side view, fracture pattern B



(f) Fractured specimen 64c top view, fracture pattern B

Figure 5.13: Pictures of specimen 64x64x128 cm after testing

5.8.6 Influence of the notch on stresses and strains over specimen height

The notch used was smooth and the cross section changed gradually with height. The stresses and strains varied over the specimen height. With the equations 4.6 and 4.7 the mean stresses and strains were calculated. In this section the stress distribution for a specimen of size M with dimensions $8x8x16cm$, which was loaded by an eccentricity of $e_{notch} = D/20$ (*test series*) was calculated. The change of notch length with height was described by a parabolic function. The variation of notch width slk over height was described as

$$slk(x) = 4x \frac{slk_0}{4D/3} \left(1 - \frac{x}{4D/3}\right) . \quad (5.3)$$

The stresses were calculated and plotted in figure 5.14 over the whole specimen height. In linear elasticity the stresses are directly related to the strains. In the experiment the mean strain over the measuring length of $0.9 \cdot h$ were calculated using equation 4.7. The strain in the middle of the notch was higher by the ratio k of the maximum stress σ_{max} and the mean stress σ_{mean} and writes

$$k = \frac{\sigma_{max}}{\sigma_m} = \frac{21.49}{20.73} = 1.037 . \quad (5.4)$$

In the data evaluation the mean strains were plotted, but the stress was calculated according to equation 4.6, as stress in the notch. The strains in the notch are as calculated in equation 5.4 to be 3.7 % higher than the mean strains.

5.8.7 Strength versus eccentricity

The specimens were loaded with a predefined eccentricity of $e_0 = D/20$, due to second order effects the eccentricity increased by e_2 . e_2 was determined from the strains on the front and back side of the specimen. The longitudinal measurements w_1 , w_2 were used to calculate the additional eccentricity due to loading. The curvature κ and the eccentricity due to second order theory e_2 were determined with

$$\varepsilon_i = \frac{w_i}{l_0} , \quad \kappa = \frac{d^2y}{dx^2} = -\frac{M}{EI} = -\frac{\varepsilon_1 - \varepsilon_2}{D} , \quad e_2 = \frac{\kappa l_0^2}{8} , \quad (5.5)$$

where l_0 was the measuring length. The measurements of the displacements w_1 and w_2 include the deformation due to second order theory and the bending line was approximated by a quadratic function.

This increase of e_2 is dependent on e_0 . Thus the ratio of $e_0 + e_2$ and e_0 has to be constant for all specimen and this ratio may serve as an indicator for the accuracy of the preset eccentricity e_0 in the test. In figure 5.15 the ratios are

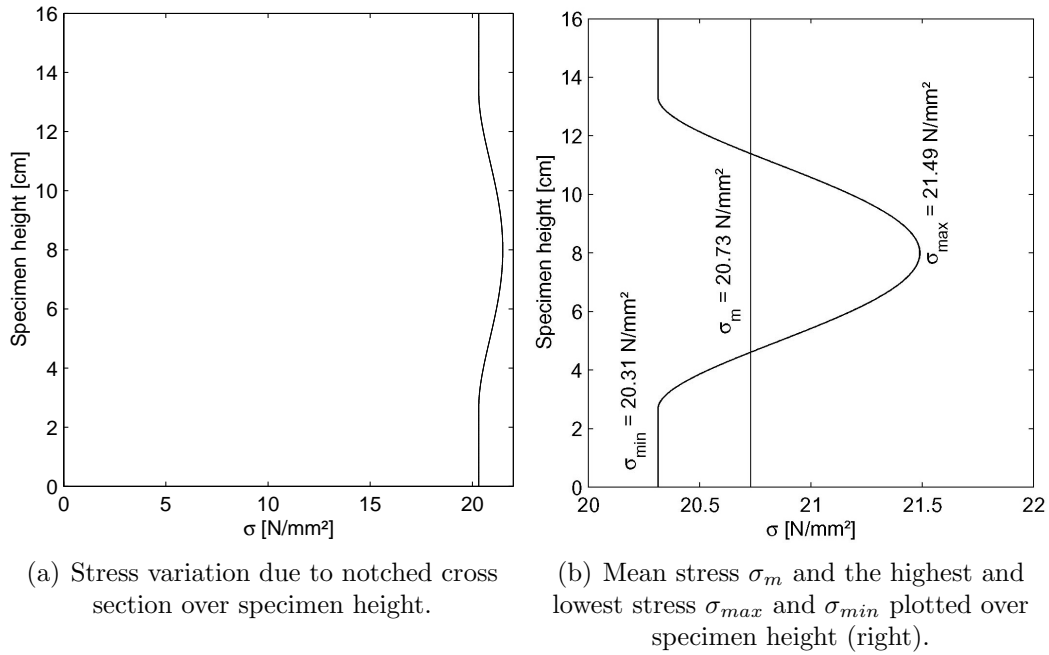


Figure 5.14: Stresses over specimen height in *test series* performed with an eccentricity of $e=D/20$

plotted. The maximum increase of this ratio was below 4%. If we conclude that the maximum variation of the preset e_0 is approximately 4%, the strength gets reduced by less than 1%, when using equation 4.6. Thus the specimen in the tests were positioned with sufficient accuracy. The variation of e_0 was so small that it did not influence strength.

5.8.8 Tabular results of individual specimens

In table 5.3 the results for all specimens are summarized. The listed results are the Young's modulus E , the load at peak F_{max} , the strength f_c , the displacement at peak load w_{peak} , the stress rate $\dot{\sigma}$, the strain rate $\dot{\epsilon}$, the wave speed in longitudinal direction v_{long} and information about the homogeneity of the specimens.

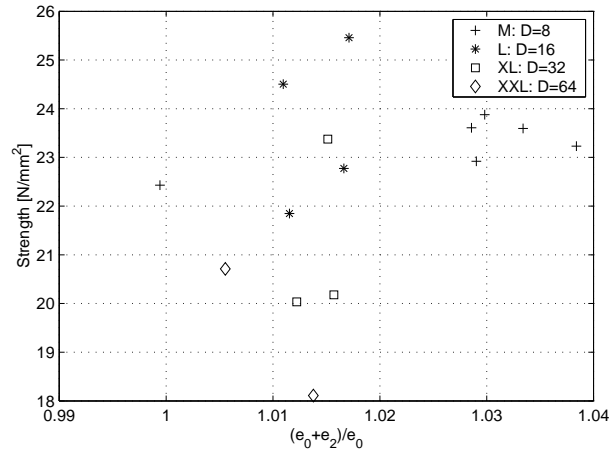


Figure 5.15: Strength versus ratio of eccentricity at maximum load $e_0 + e_2$ and preset eccentricity e_0

Table 5.3: Experimental data for the individual specimen of all tested sandstone specimen

	E	F_{max}	f_c	w_{peak}	$\dot{\sigma}$	$\dot{\epsilon}$	v_{long}	hom.
	[MPa]	[kN]	[MPa]	[μm]	[MPa/s]	[$10^6/s$]	[cm/s]	[cm/s]
2a	-	14.8	50.89	-	0.080	-	-	hom
2b	-	13.2	45.38	-	0.090	-	-	hom
2c	-	12.7	43.67	-	0.083	-	-	hom
2d	-	12.1	41.6	-	0.079	-	-	hom
2e	-	13.6	46.76	-	0.083	-	-	hom
2f	-	12.9	44.35	-	0.088	-	-	hom
2g	-	13.1	45.04	-	0.086	-	-	hom
2h	-	12.9	44.35	-	0.083	-	-	hom
2i	-	10.4	35.76	-	0.073	-	-	hom
2j	-	12.5	42.98	-	0.081	-	-	hom
2k	-	9.8	33.69	-	0.076	-	-	hom
2l	-	11.9	40.91	-	0.081	-	-	hom
2m	-	11.7	40.23	-	0.084	-	-	hom
2n	-	13.4	46.07	-	0.087	-	-	hom
4a	-	41.2	35.41	-	0.090	-	373	hom

Table 5.3: Experimental data for the individual specimen of all tested sandstone specimen

	E	F_{max}	f_c	w_{peak}	$\dot{\sigma}$	$\dot{\epsilon}$	v_{long}	hom.
	[MPa]	[kN]	[MPa]	[μm]	[MPa/s]	[$10^6/s$]	[cm/s]	[cm/s]
4c	-	46.7	40.14	-	0.105	-	373	hom
4d	-	46.1	39.63	-	0.113	-	373	hom
4e	-	44.8	38.51	-	0.101	-	373	hom
4f	-	49.5	42.55	-	0.113	-	373	hom
4g	-	49.4	42.46	-	0.108	-	373	hom
4i	-	44.4	38.16	-	0.100	-	373	hom
4j	-	47.2	40.57	-	0.112	-	373	hom
4k	-	48.7	41.86	-	0.114	-	373	hom
4l	-	41.2	35.41	-	0.099	-	373	hom
4m	-	45.2	38.85	-	0.111	-	373	hom
4o	-	47.1	40.49	-	0.098	-	373	hom
4p	-	40.8	35.07	-	0.094	-	373	hom
8a	21616	110.3	23.7	254	0.010	1.09	335	hom
8b	23829	109.1	23.44	228	0.012	1.23	332	hom
8c	21112	105.9	22.76	240	0.015	1.57	332	hom
8d	25726	107.1	23.01	296	0.007	0.99	333	hom
8e	18624	108.9	23.4	266	0.017	1.94	333	hom
8f	18486	104.4	22.43	240	0.015	1.55	334	hom
16a	34181	471.9	25.35	396	0.014	1.24	337	hom
16b	58020	454.9	24.44	345	0.016	1.37	335	inhom
16c	25136	405.5	21.78	347	0.019	1.55	332	hom
16d	-	455.5	24.47	-	0.025	-	344	inhom
16e	22589	422.2	22.68	366	0.040	3.26	336	inhom
16f	-	419.9	22.56	-	0.010	-	333	inhom
32a	16662	1487.3	19.98	751	0.023	2.12	351	hom
32b	24629	1496.7	20.1	830	0.008	1.04	307	hom
32c	18748	1734.1	23.29	859	0.026	2.41	369	hom
64a	23677	6159.6	20.68	1116	0.024	1.60	320	hom
64b	22480	(7140.8)	(23.98)	1458	0.016	1.20	330	inhom

Table 5.3: Experimental data for the individual specimen of all tested sandstone specimen

	E [MPa]	F_{max} [kN]	f_c [MPa]	w_{peak} [μm]	$\dot{\sigma}$ [MPa/s]	$\dot{\epsilon}$ [$10^6/s$]	v_{long} [cm/s]	hom. [cm/s]
64c	20982	5375.6	18.05	1638	0.010	1.32	331	hom

5.8.9 Stress strain plots for every specimen

The stresses and strains were determined according to equation 4.6 and 4.7 on page 38. In figure 5.16 the stresses and strains on the front were plotted for every specimen size in one graph.

5.8.10 Acoustic emission (AE) results

A physical event like cracking produces a transient elastic wave generated by release of (elastic) energy. This wave is recorded by a sensor and converted to an electronic signal. If the signal exceeds a preset threshold it is detected as hit and stored to the harddisk. The energy content of the acoustic emission signal is attributed to the rapid energy release of the material (damage) and is directly proportional to the area of the acoustic emission wave. An acoustic emission signal has often a clearly identifiable beginning and end. For processes with very active AE emissions it is not possible to determine the exact arriving time of subsequent hits in a hit cascade and the signals cannot be stored as hits. The exact arriving time is important for location calculations. Storing the exact arriving time only makes sense with discrete hits and for first hits of hit-cascades. A hit is terminated after some certain time period and a new hit will be started when the threshold will be reached the next time. Between termination and beginning of a new hit a short duration only reduced data can be stored, e.g. energy, which is then called cascaded energy. In very active processes differences arise between the energy and cascaded energy. For the investigated sandstones the cumulative cascaded hits were for most specimen two times the cumulative hits at maximum load. The AE-activity was very high, thus the cascaded energy represents much better the damage.

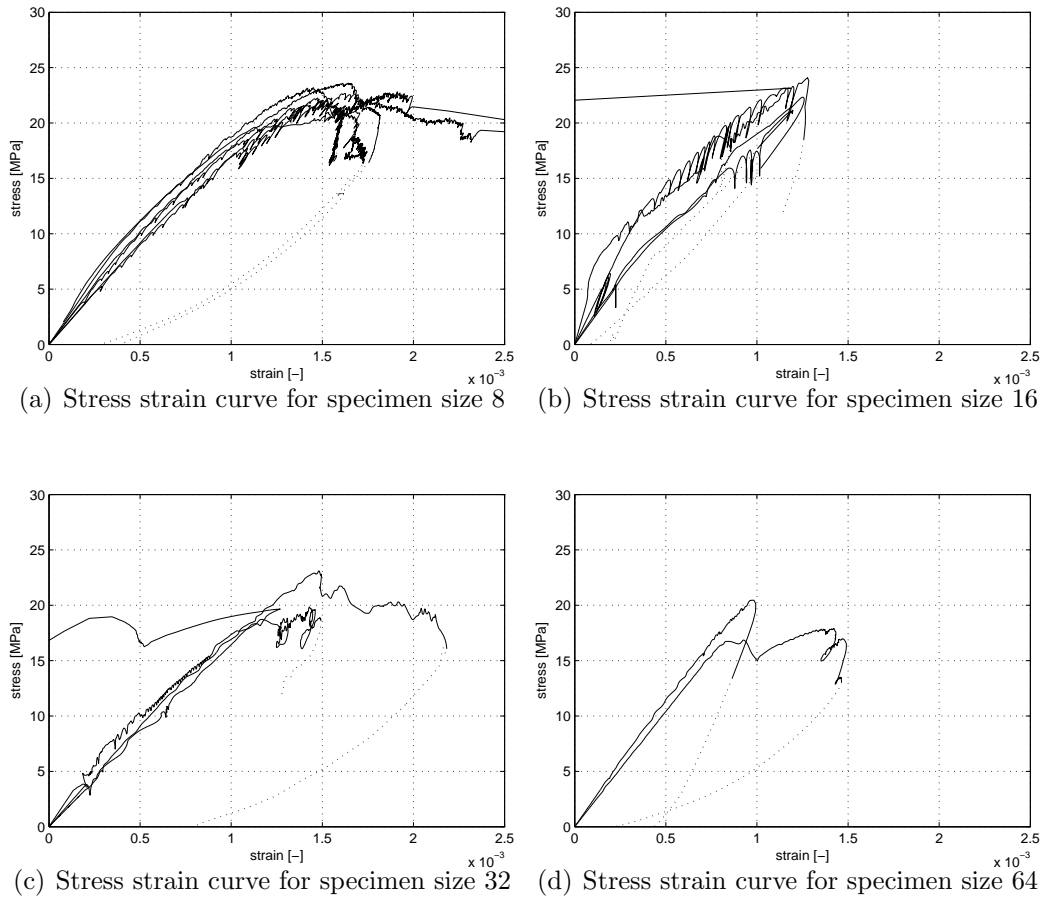
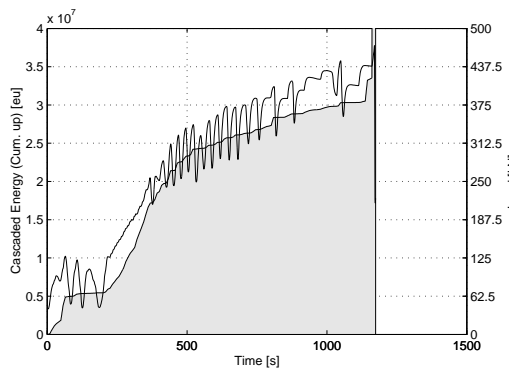


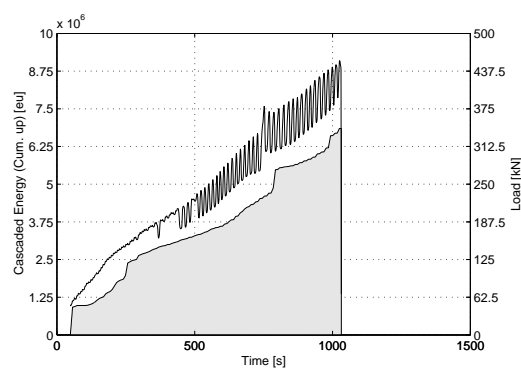
Figure 5.16: Stress strain curves different specimen sizes

The load (right axis) and the cascaded energy (left axis) are plotted versus time for each specimen in figure 5.17 to 5.19. The cascaded energy is given in cumulative and differential presentation. In the cumulative presentation the whole activity that happened in the test is presented, the differential plots provide information about the activity of damage evaluation at the moment. The cumulative cascaded energy increased from the beginning up to peak load for most specimen and goes mainly with the trend of the load. At the beginning there were sometimes some higher activities, that were attributed to positioning of the plate at the interface. For most cases the differential plot of the cascaded energy was increasing from the beginning of the experiment to peak load. Shortly before peak the energy increased stronger, which was also audible due to the loudspeaker of the acquisition equipment. But also constant and decreasing trends can be observed

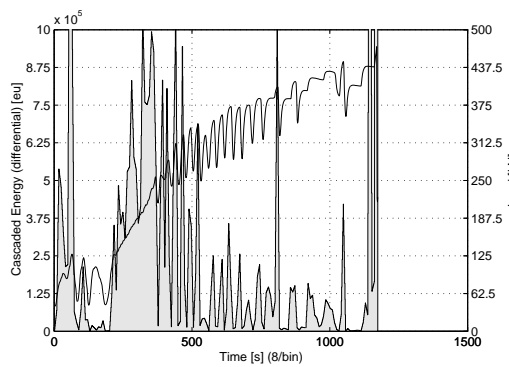
in the differential plots. The energy is a measure for damage and indicates that the damage starts with the beginning of loading, has no or a very low damage threshold and is continuously growing with the application of load.



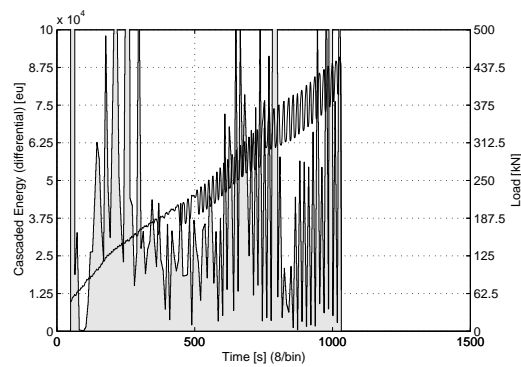
(a) Cum. casc. energy of specimen 16a



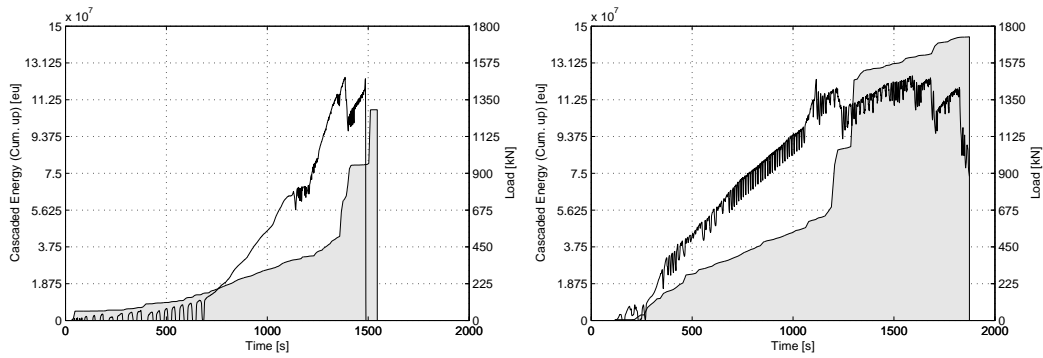
(b) Cum. casc. energy of specimen 16b



(c) Diff. casc. energy of specimen 16a

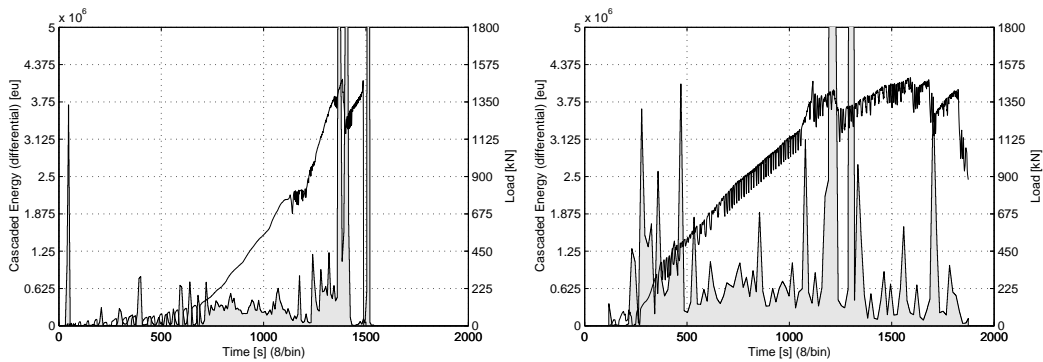


(d) Diff. casc. energy of specimen 16b



(e) Cum. casc. energy of specimen 32a

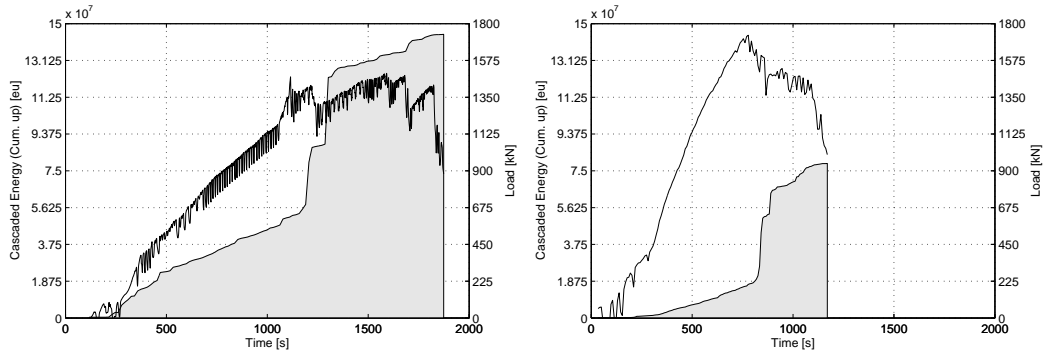
(f) Cum. casc. energy of specimen 32b



(g) Diff. casc. energy of specimen 32a

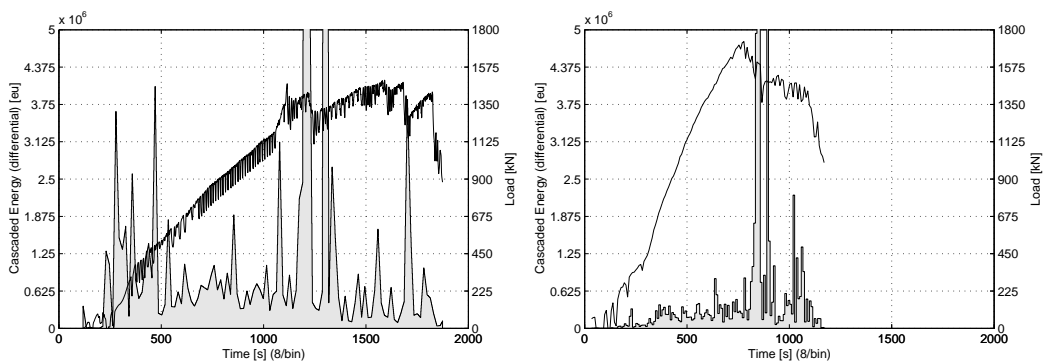
(h) Diff. casc. energy of specimen 32b

Figure 5.17: Cascaded energy in cumulative and differential presentation for specimens 16a, 16b, 32a, 32b



(a) Cum. casc. energy of specimen 32b

(b) Cum. casc. energy of specimen 32c



(c) Diff. casc. energy of specimen 32b

(d) Diff. casc. energy of specimen 32c

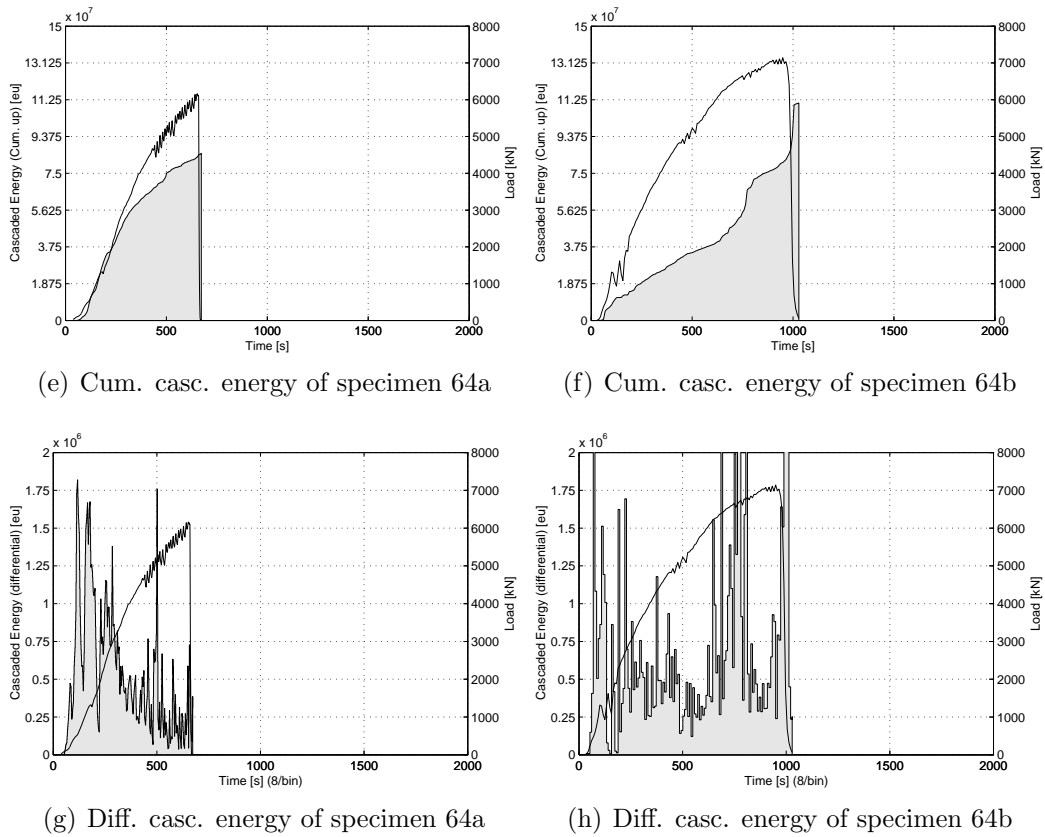


Figure 5.18: Cascaded energy in cumulative and differential presentation for specimens 32b, 32c, 64a, 64b

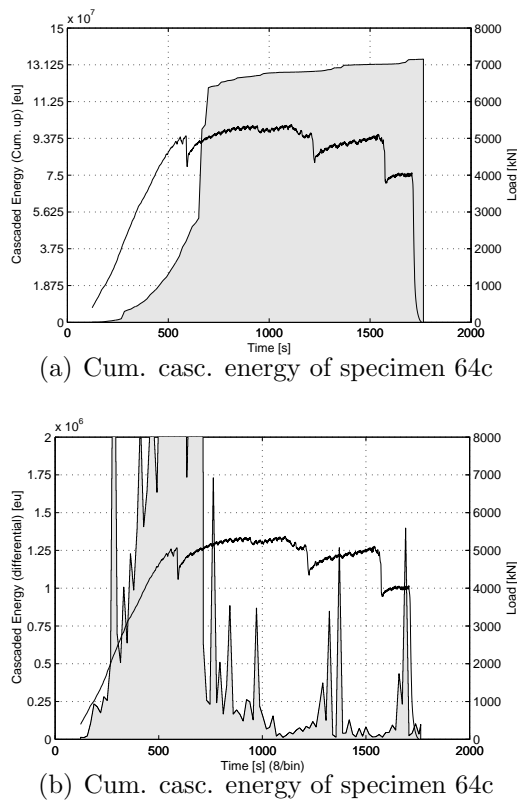


Figure 5.19: Cascaded energy in cumulative and differential presentation for specimens 64c

Chapter 6

Verification series on sandstone

6.1 Introduction

The aim of this test series was to clarify the influence of loading rate and density on strength, and most important the change of strength from size XS to L. In the *tests series on sizes XS to XXL* the strength of the sizes XS and S was much higher than for sizes M and L. In this *verification series* the sizes XS, S, M and L were tested again. The specimen had equal dimensions, notches and were tested under the same boundary conditions. The sandstone used for testing was from the same quarry, but from a different sandstone block. To compare the results of the XS and S size of this series with other series the sizes M and L were also tested.

6.2 Specimen dimensions and geometry

The specimens of sizes XS to L had dimensions from $2x2x4$ cm up to $16x16x32$ cm, see figure 6.1. All specimens were weighed and depending on the density they were assigned to series A or B. At last the specimen were provided with notches and the loading faces were polished. An overview of the sizes is drawn in figure 6.1. A total amount of 130 specimen was produced and tested. For a listing of the specimen sizes, dimensions, number, weight and density see table 6.1.

6.3 Homogeneity of specimen

The specimen were sawed from one block of dimensions $87x66x32$ cm, according to the scheme in figure 6.2. With this scheme it was possible to determine regions

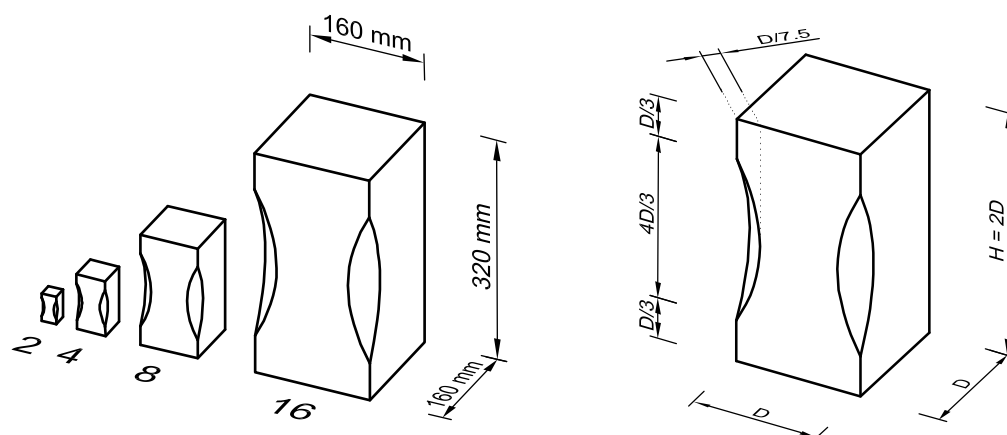


Figure 6.1: Geometry and dimensions of verification test series

Table 6.1: Size, series, labelling, number, dimension, weight and density of the tested sandstone specimens in the verification series

Size	Specimen Series	Labelling of specimens	Number	Dimension [mm]	Weight [kg]	Density [g/cm ³]
XS	2A	02-01 to 02-28	28	20x20x40	0.04	2.09 - 2.27
XS	2B	02-29 to 02-42	14	20x20x40	0.04	1.84 - 2.17
S	4A	04-01 to 04-18	18	40x40x80	0.3	1.94 - 2.01
S	4B	04-19 to 04-45	27	40x40x80	0.3	2.02 - 2.11
M	8A	08-XX ¹⁾	19	80x80x160	2.3	2.03 - 2.15
M	8B	08-XX ¹⁾	13	80x80x160	2.3	2.03 - 2.15
L	16	16-01 to 16-12	11	160x160x320	18	2.10 - 2.12

¹⁾ labels disordered

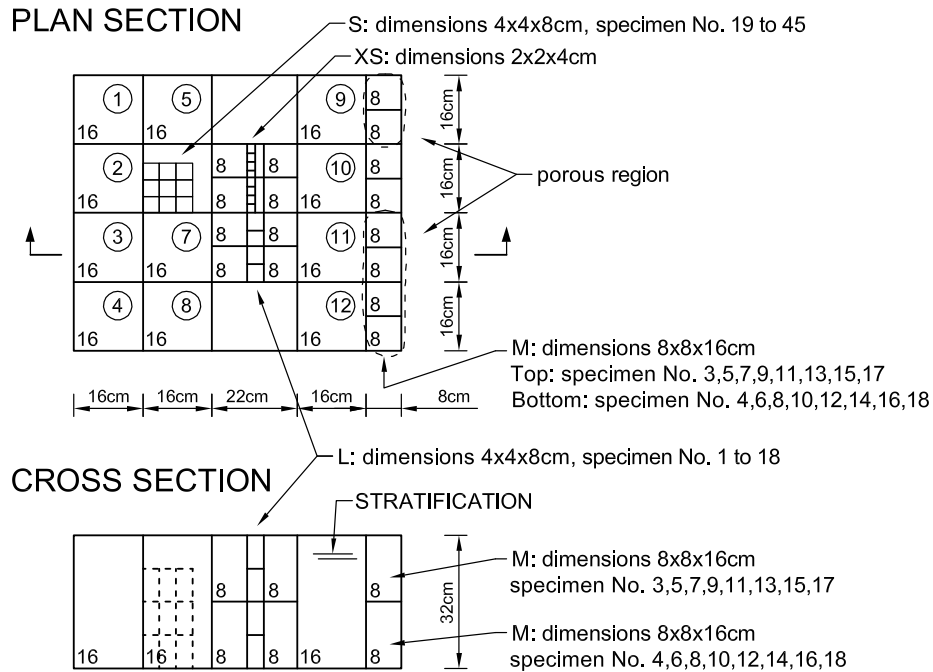


Figure 6.2: Scheme of specimens of verification series sawed from the sandstone block

of inhomogeneities, of different strength in horizontal direction and in different strata planes.

The sandstone block showed a perfectly homogeneous surface. After cutting it turned out that a porous region was in the interior of the block. Therefore the specimen of the size M (8x8x16 cm), which were taken from the interior of the block, had a porous region on one end of the specimen. The homogeneous specimens were assigned to series 8A and the inhomogeneous to 8B.

The size S specimen were taken from the center and the density of these specimen was lower (Series 4A). In order not to start with deviations, one specimen of size L (specimen No. 6) with a density that corresponded with the other specimens was sawed in 27 specimen of size S (Series 4B). The density of series 4B was the same as the other sizes. The XS sizes were also subdivided into series 2A and 2B because of different densities.

6.4 Boundary conditions and testing machines

6.4.1 Loading arrangement

The specimens were loaded with a predefined eccentricity. The eccentricity in that series was $e_{notch} = D/22$ ($e = D/33$). In the *test series on sizes XS to XXL* the eccentricity was $e_{notch} = D/20$ ($e = D/30$).

The sizes XS, S and M were tested in the D2 machine. The L specimens had higher strength than the specimens from the two previous series and the ultimate load exceeded the loading capacity of the D2 machine. Thus size L was tested at the TVFA with a machine from J. Amsler - Laffon & Sohn, Schaffhausen. The eccentricity was introduced like in the *test series on sizes XS to XXL* by a lateral shift of the specimen with respect to the axis of the machine, for details see section 5.4.1.

6.4.2 Interface between loading platen and specimen

The interface used in the *test series on sizes XS to XXL* performed well and was also applied for the *verification series on sizes XS to L*. For details see section 5.4.2 and 4.3.2.

6.5 Arrangement of displacement transducers

The displacement transducers were attached to the specimens like in the *test series on sizes XS to XXL*, see figure 5.6 on page 53. The specimens of size L (16) were tested in the testing machine at the TVFA. These experiments were performed under load control. The displacement transducers are vulnerable to damage and therefore a video extensometer measurement on the compressed side only was used during the tests.

In the *test series on sizes XS to XXL* the displacements for specimen XS and S were not measured. In this series a special apparatus was built to measure the displacements. The problem was to perform an accurate measurement with high accuracy over a measuring length of 7.2 cm (S-size) and 3.6 cm (XS-size) with displacement transducers with a length of 16cm.

6.6 Test control

The test control in the verification series was slightly different from the test control of the *test series*. In this series only small specimen were tested and the control was performed by the longitudinal displacement on the compressed side

only (*DT 1* in figure 5.6 on page 53). The lateral displacements were measured but not used for control of the experiment. This was possible because only small specimen were tested and the displacement transducers were protected with a special construction. The specimen of sizes L were tested under load control (manually). The loading rate was chosen according to the stress rate of the tests performed under displacement control.

6.7 Results of verification series on sizes XS to L

In this section only the specimens that showed fracture patterns A, B or C (according to section 5.8.4) are included. The series 8A was excluded because of the porous regions. The series 4A and 2B were also excluded because of the lower density.

6.7.1 Specimens after testing

The specimens were photographed after testing and the fracture pattern was determined. The cracks were colored with a black pencil. All specimen surfaces were brushed with a smooth brush after testing to make cracks visible. Only results that showed the fracture pattern A, B or C were used for comparison of the results (except if differently stated).

6.7.2 Strength versus loading rate

The higher loading rate of the specimens XS and S was still low and it was questionable if there was an influence of loading rate on the failure load. The normal strain rate was $1e - 6 \text{ strain/s}$. The high strain rate in the *test series on sizes XS to XXL* for the size XS was four times the normal strain rate $4e - 6 \text{ strain/s}$ and for the size S it was five times the normal strain rate $5e - 6 \text{ strain/s}$. Some specimens of the *verification series* were also tested at this loading rate. In the size effect plot in figure 6.6 all strengths were plotted independent of loading rate. In figure 6.3 the influence of the strength on the loading rate was plotted. Figure 6.3 clearly shows that there was no influence of this higher loading rates on the strength of the specimen.

6.7.3 Density versus strength

In figure 6.4 the density was plotted versus strength for all specimens of every specimen size, including the porous (2B, 4A, 8B) and dense specimens at high and low loading rate. The data displayed in figure 6.4 was fitted to a curve

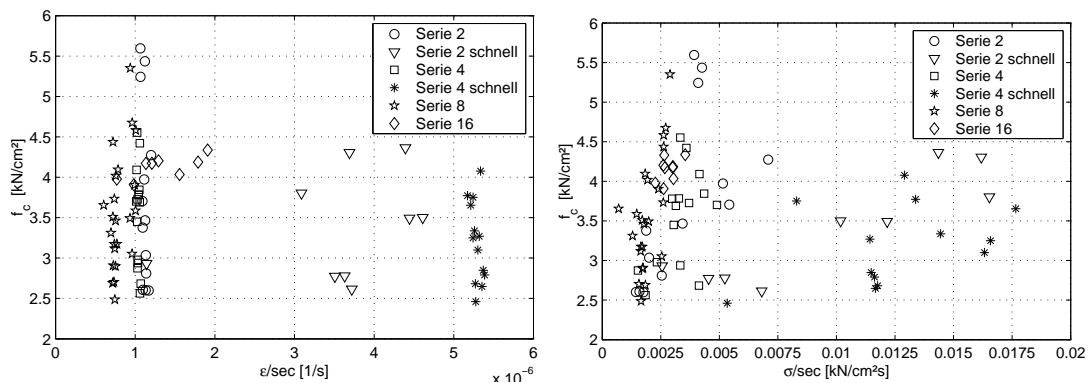


Figure 6.3: Strength versus loading rate

with linear regression and the strength values at a density of 2.1 g/cm^3 were determined for the sizes and potted in figure 6.7. Figure 6.4a, b, c indicates an increasing strength with density for the sizes XS, S and M. The deviation of the density of the L size was very low and so was the strength.

6.7.4 Density versus Young's modulus

The Young's modulus E was determined according to equation 4.8 in section 4.4.2 for every specimen and plotted for all series of each size in figure 6.5. The Young's modulus was for all specimen in a range between 1500 and 4000 kN/cm^2 . In the graphs in figure 6.5 no clear trend of density on Young's modulus could be detected.

6.7.5 Strength versus specimen size

The influence of strength on size is displayed in figure 6.6. In this comparison all specimens with proper fracture pattern and density are displayed. The strength did not change with increasing size. Therefore no size effect was detected.

In the *test series* the sizes XS and S were tested at a higher loading rate than the larger sizes. The higher loading rate was still relatively low, but to determine if there was any influence the size XS and S were tested at both loading rates. Figure 6.6 and more detailed section 6.7.2 shows that the loading rate did not have any influence on the strength.

Another influence on the strength is the density of the material, which was also investigated, see section 6.7.3. There the strength with varying density was determined for every size. In figure 6.7 the strength values at a density of 2.1 g/cm^3

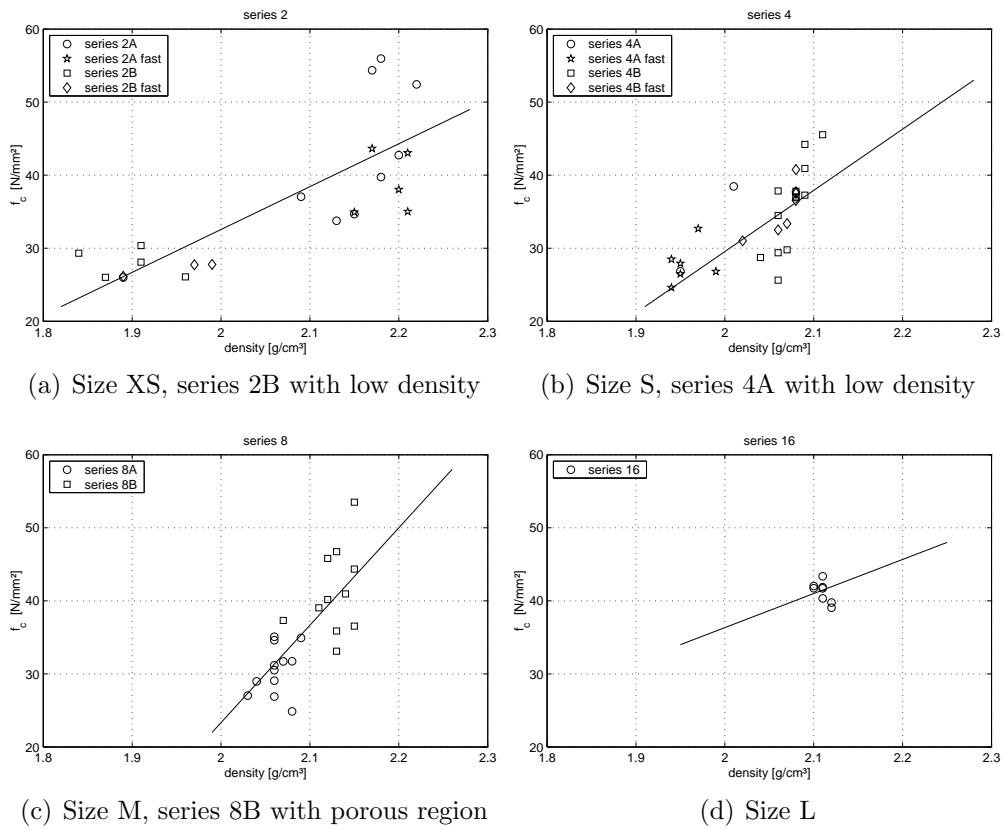


Figure 6.4: Strength versus density for all specimen sizes of *verification series*, including the porous and dense specimen and specimen tested at high and low loading rate

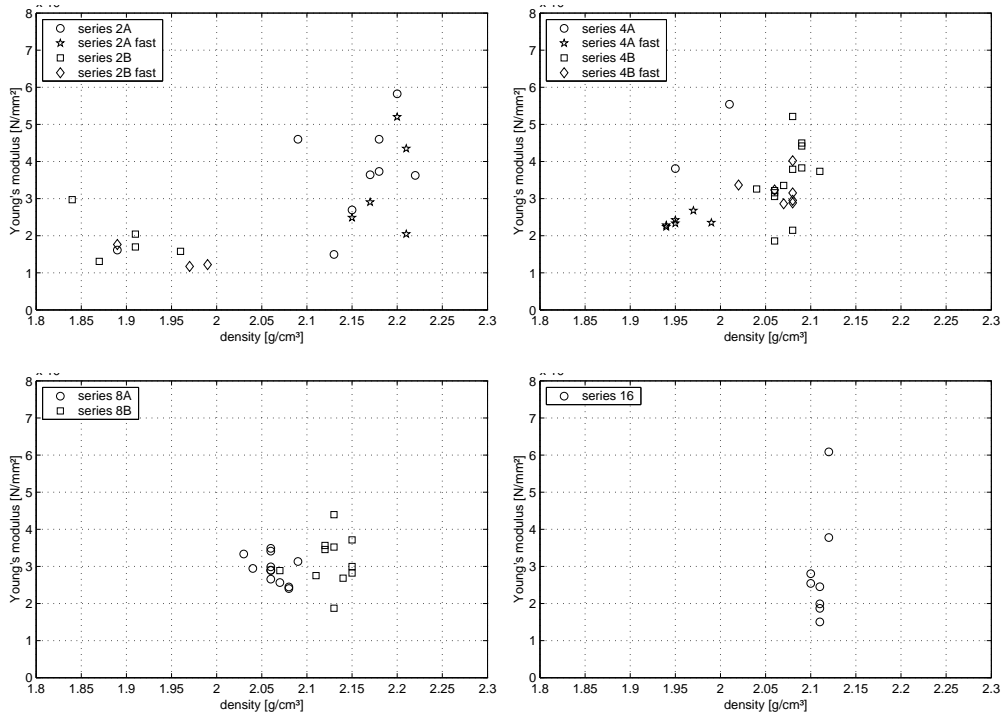


Figure 6.5: Young's Modulus versus density for all series of each size of *verification series*

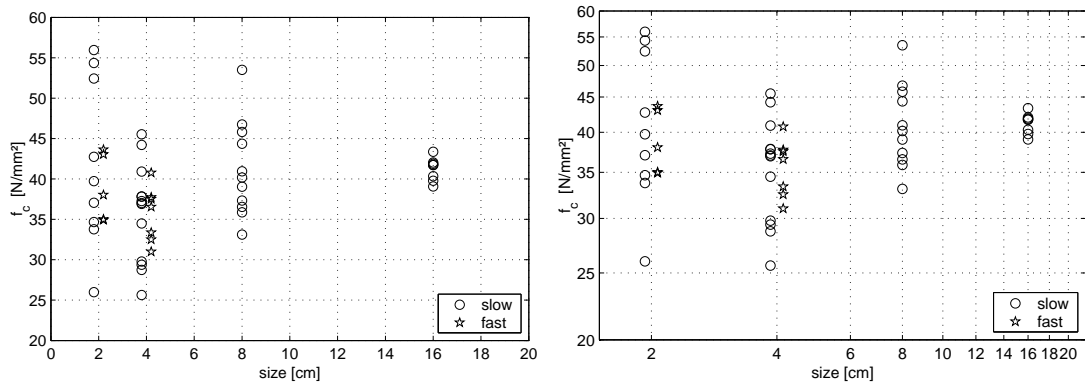


Figure 6.6: Strength vs Specimen size in linear (left) and logarithmic scale(right). The specimen were tested with two different loading rates

were plotted against size. Regarding only the XS, S and M size in the size effect plot in figure 6.7 the strength is relatively constant, with a slightly lower strength for size M and S. The strength of the L size was higher than for the rest of the other specimens, which could be due to the different loading machine and different test control.

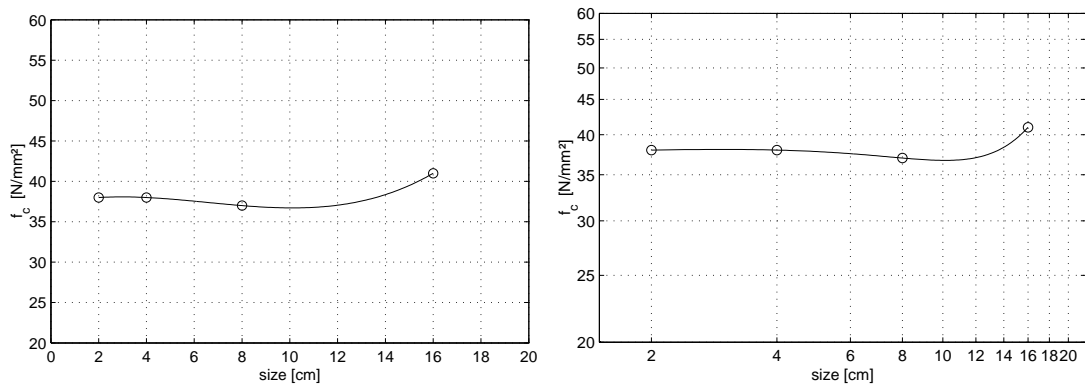


Figure 6.7: Strength vs. Specimen size in linear (left) and logarithmic scale(right). The strength was determined form all reliable data at a density of 2.1 g/cm^3

6.7.6 Stress strain plots for each size

The stresses were calculated according to equation 4.6, the strains following equation 4.7. The strains on the compressed side consider the influence of the notch,

Table 6.2: Specimen of individual series tested at high or low loading rate

Sandstone Series	Specimen label		Comment
	normal loading rate	high loading rate	
2A	1, 2, 4-7, 9-12, 15-18	19-25, 27, 28	
2B	31 - 36	29, 38-42	low density
4A	2, 4, 5, 7, 9, 10, 16	11-15, 18	low density
4B	23-37	38-44	
8A	1, 3-6, 11, 13-19, 24, 28-32		dense
8B	2, 7-10, 20-22, 25, 26, 27		porous
16	1, 3, 4, 5, 7, 8, 9, 10, 12		

which is 3.5% higher than the mean strain. In Figure 6.8 the stress strain curves of the different series were plotted in one graph, including the mean curve. The stress strain curves of the individual specimen are given in Burtscher et al. (2003a).

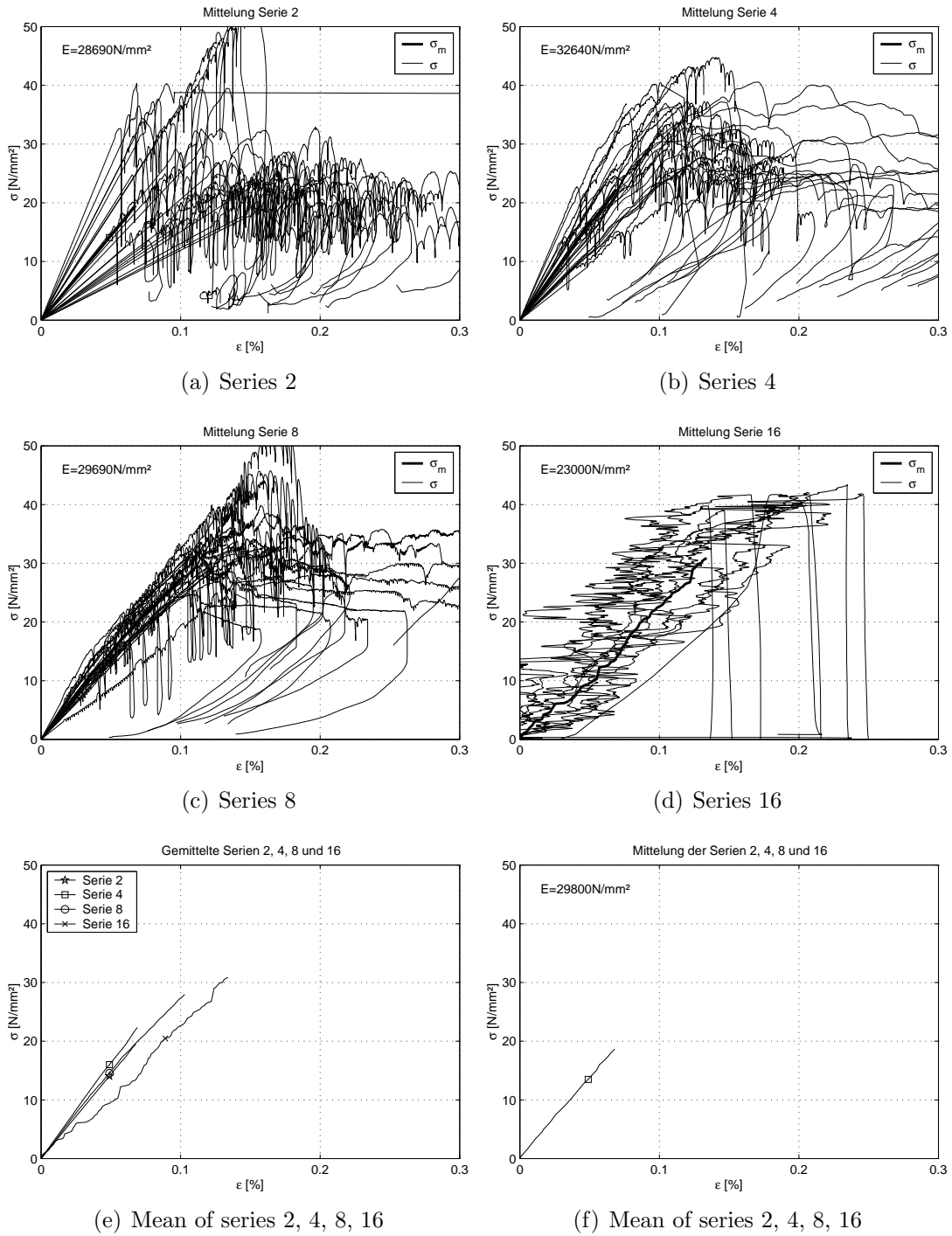


Figure 6.8: Stress strain diagram of series 2, 4, 8 and 16, including mean curve (thick line)

Chapter 7

Size effect in compression of sandstone

7.1 Collection of strength versus size data

In figures 7.1 and 7.2 the strength versus size from the preliminary series, the *test series* and the *verification series* are presented for the individual specimen and the mean value for each size. The data is always presented with linear (left) and double logarithmic scaling (right). The mean values were determined from the *preliminary series* and the size effect series by the arithmetic mean. In the *verification series* a vast number of specimens with varying density were tested. The mean strengths were taken from the resulting trend at a density of 2.1g/cm^3 , see figure 6.4 on page 77 or figure 6.7 on page 78. The standard deviation is plotted with the mean values. For the results of the individual specimens only specimens with a density between 2.05 and 2.15 g/cm^3 were displayed for the *verification series*.

7.1.1 Scatter of experimental results

The specimens in the *preliminary series* showed low scatter, see figure 7.4. In the test series the scatter was higher for the XS and S sizes and was lower for larger specimens. In the verification series the standard deviation is first increasing and afterwards decreasing. The trend for the small sizes is strongly dependent on the density range used for the calculation of the standard deviation.

The deviation of mean strength from the small sizes (XS and S) was pronounced for the *test series* on sandstone, see figure 7.2. Thus the verification series was performed on a very high number of specimens of sizes XS, S, M and L. In this investigation only the small sizes were tested again because their in-

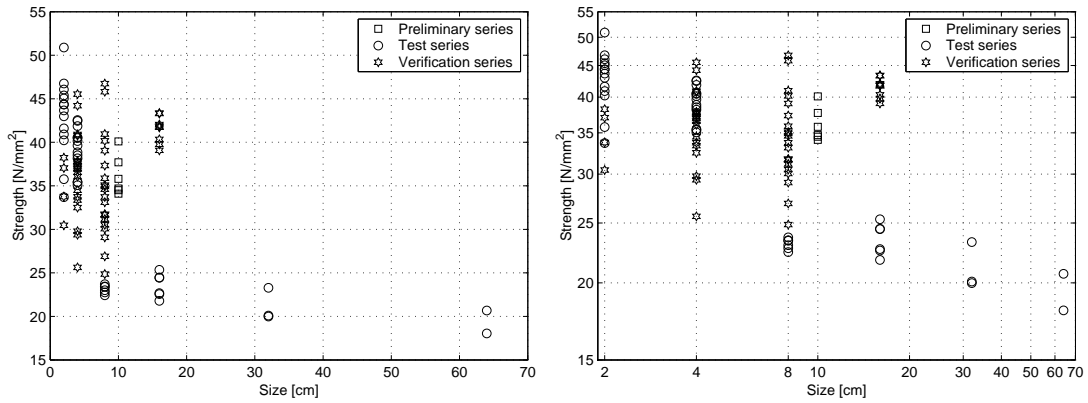


Figure 7.1: Strength of individual specimens versus size in linear (left) and logarithmic scaling (right)

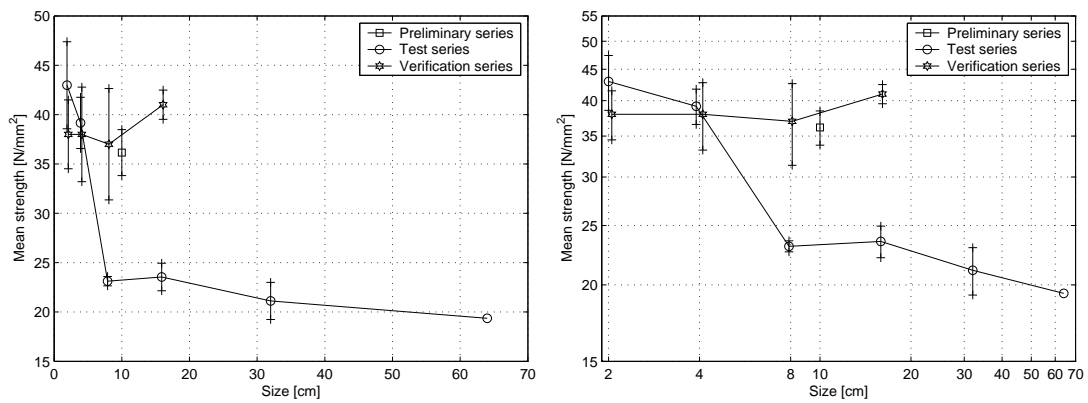


Figure 7.2: Mean strength versus specimen size in linear (left) and logarithmic scaling (right)

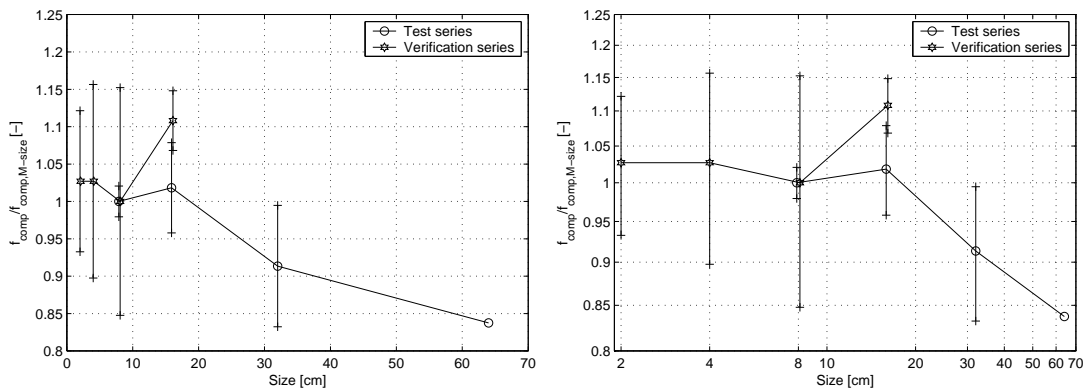


Figure 7.3: Normalized mean strength versus size of *size effect series* and *verification series* (XS and S from *test series* excluded) in linear (left) and logarithmic scaling (right)

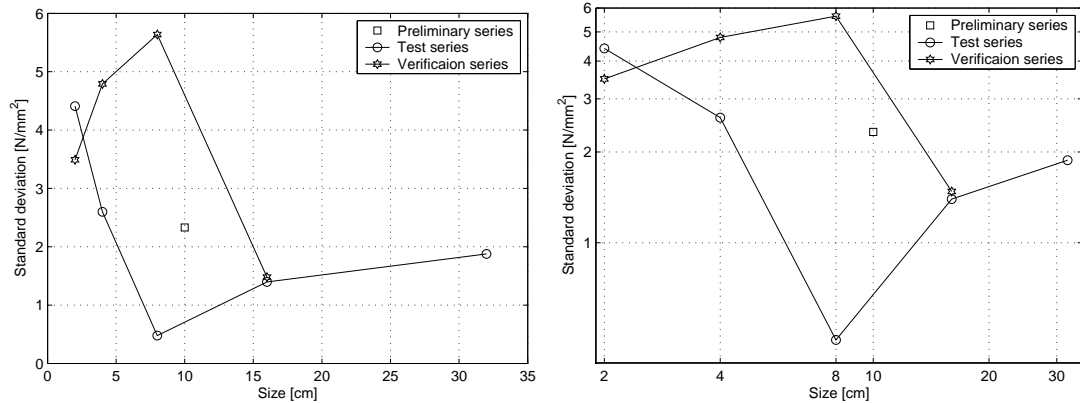


Figure 7.4: Standard deviation versus specimen size in linear (left) and logarithmic scale (right)

fluence of density on strength is more pronounced than for bigger ones. To end up with a more accurate mean value the number of specimens was increased considerably. In these observations it turned out that the strength is dependent on density.

The influence of strength on size at a certain density (2.1 g/cm^3) was found to be nearly constant for all sizes of the *verification series*, see figure 7.2 and figure 6.7 on page 78. Except the strength of specimen L (16 cm) was higher, which could be due to different loading machine. The higher strengths of the sizes XS and S of the *test series* were not confirmed. With the results from the *verification series* at density of 2.1 it was possible to determine the trend of the small sizes as nearly constant.

7.2 Normalized strength versus size of all series

The sandstone from the three series were from different blocks in the quarry and therefore they all had different strengths. To compare the trends in the different series the individual strengths were divided by the strength of specimen of size M (8 cm) of each series, see figure 7.3.

7.3 Fitting of data to SEL and MFSL

The Size Effect Law from Bažant see equation 2.1 on page 9 and the Size Effect Law for Compression 2.4 on page 12 were fitted to the normalized data of figure 7.3. The equation 2.4 was rearranged and used in similar form as 2.1, see

Table 7.1: Table of parameters of different size effect laws. D_0, l_{ch} in cm

SEL	SEL compression	MFSL
$\sigma_N = \frac{Bf_t}{(1+\frac{D}{D_0})^{\frac{1}{2}}}$	$\sigma_N = \frac{Bf_t}{(1+\frac{D}{D_0})^{\frac{2}{5}}}$	$\sigma_N = \sqrt{A + \frac{B}{D}}$
$B f_t = 1.053$ $D_0 = 117.54$ $r=0.0069$	$B f_t = 1.054$ $D_0 = 89.54$ $r=0.0071$	$A=0.8783 \quad f_c=0.30$ $B=0.4868 \quad l_{ch}=0.554$ $r=0.0266$

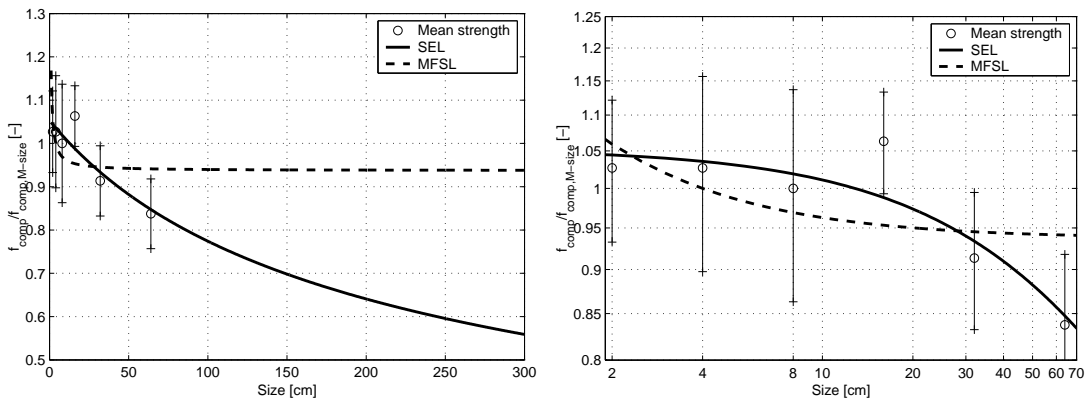


Figure 7.5: Mean strength of specimens versus size (XS and S for *test series* excluded) and data fit with MFSL and SEL

equations in table 7.1. The parameters for both size effect laws were found using the Levenberg-Marquardt nonlinear fitting algorithm and are listed in table 7.1.

The graphs are given together with the normalized data in figure 7.5. The data was also fitted to the Multi Fractal Scaling Law (MFSL) by Carpinteri. The law and the parameters are given in table 7.1. The SEL law with a power of $\frac{1}{2}$ and $\frac{2}{5}$ were on the same line. The SEL laws describe the trend of the data much better than the MFSL. The residuals in table 7.1 are for the SEL law much smaller than for the MFSL. Contrary to the observations in Bažant and Xiang (1997), also discussed in section 2.4 the SEL with a slope of $\frac{1}{2}$ shows slightly lower residual than with slope $\frac{2}{5}$. Finally the slope between XXL, XL and XXL, L was determined as $\frac{1}{5.8}$ and $\frac{1}{8.0}$ in double logarithmic plot.

Chapter 8

Test series on concrete

8.1 Introduction

In the concrete series 5 different sizes from S to XXL with a total size range of 1:16 were tested. All dimensions were scaled for every size by the same factor, thus geometrical similarity was provided. The aim of the series was to find the influence of size on strength, namely the size effect.

8.2 Specimen dimensions

The columns tested had a circular cross section. The diameter of the cross sections varied from 5 *cm* to 80 *cm*, see table 8.1 for the test program. The specimen length was always four times the diameter. All dimensions were scaled by a scaling factor. Therefore the specimens of the different sizes were all geometrically equal, see figures 8.1, 8.2, 8.3. In order to prevent failure and to ensure a proper load transfer from the loading platen to the specimen, the specimen were equipped with steel plates on both ends and spiral reinforcement. The spiral reinforcement was placed over the height of the diameter on both ends of the specimen and was scaled for the different sizes. The steel plates were scaled for all sizes except size XXL.

It is favorable to test specimens over a large size range to determine the influence of strength on size. The size of the smallest specimen is limited, because it has to be larger than the representative volume. Thus the smallest dimension has to be a multiple of the maximum aggregate size (8 *mm*). The ratio of the smallest dimension (50 *mm*) and the aggregate size was 6.25. It is stated in literature that this ratio is high enough to describe a representative volume. The maximum size of the largest specimen is limited by the capability of the testing equipment. The largest specimen tested in this series was the XXL size with a

Table 8.1: Geometric dimensions, eccentricity, weight testing machine of the concrete size effect series

Specimen	Number	Diameter [cm]	Length [cm]	Eccent. [cm]	Weight [kg]	Testing Machine
XXL	3	80	320	2.	4020	Column Tester
XL	3	40	160	1.	500	Column Tester
L	3	20	80	0.5	65	Column Tester
L	2	20	80	0.5	65	Inova Prague
M	3	10	40	0.25	8	Inova Prague
M	3	10	40	0.25	8	D2
S	6	5	20	0.125	1	D2

maximum load of 14380 kN . The size range from size S to XXL was 1:16. If the size range of the series would have been increased from 1:16 to 1:32 the maximum load of the XXXL size (not regarding the size effect) would have been approximately 58000 kN , which is beyond testing capabilities at Vienna University of Technology. The XXL size specimen of this series increased the effort for producing the formwork, the handling and the testing enormously. The weight of one XXL specimen was 4280 kg including steel plates, see table 8.1. For the smallest size the number of specimen was increased, because small dimensions and the small eccentricities may lead to larger scatter of the experimental values. The specimen of size L were tested in the Column Tester and in the Inova machine. The specimen of size M were tested in the Inova machine and the D2 machine. With these tests the influence of the testing machine was also determined. One specimen of size L was broken, therefore only 2 specimen of that size were tested in the Inova machine in Prague.

8.2.1 Concrete cylinders for determination of strength

Additionally concrete cylinders with a diameter of 10 cm and a length of 20 cm were produced to determine the evolution of strength with time and with specimen height. The concrete cylinders were concreted in tubes with a diameter of 10 cm and a length of 102 cm . For comparison with the other specimen the same foil was used inside this tubes. After 30 days 4 concrete cylinders with a length of

20 cm were sawed from the 102 cm tube. After sawing the cardboard cover and the foil was removed. During the size effect experiments the cylinders were tested.

8.3 Specimen preparation

8.3.1 Concrete formwork and concreting

The specimens were produced in a standing position. The first step was to establish a horizontal platform made of concrete. The cardboard tubes were positioned vertically and were fixed by a support construction made of wood, see figure 8.4.

First the cardboard tubes for the diameter 80 cm were positioned and afterwards the tubes for diameters 40 and 20 cm, see figure 8.4. The cardboard tubes were fixed by the support construction in horizontal direction on their basis and top. At the top the tubes were also fixed in vertical direction to prevent any movement during concreting.

All specimens were cast using one batch of concrete. 7 m³ were necessary to produce the specimens. Because of this high amount of concrete and the big formwork that was necessary, the specimen were produced at the concrete plant *Ready Mix* in Vienna's 22nd district. The formwork was made of cardboard tube with 400 μm PVC foil inside, see specimen XXL in figure 1.1. The foil was advantageous for several reasons:

- The formwork did not absorb water at the beginning, which would have led to drying of the concrete surface at very early ages.
- No moisture gradient could develop and therefore no diffusion phenomena could take place.
- The water that was available for the concrete to hydrate was for every specimen the water that was added during mixing.
- The cardboard tube was a good isolator. Therefore no temperature gradient could develop, that could influence the hydration and produce regions with different microcracks. However the temperature due to hydration was higher in the XXL specimens than in the S size specimens.

The formwork was removed between one hour and 8 hours before testing. The specimens were sealed during curing and no diffusion phenomena could take place before testing.

Another problem was that the concrete at the top has a lower strength than the concrete below, see section 2.2. For the XXL and the XL specimen this was

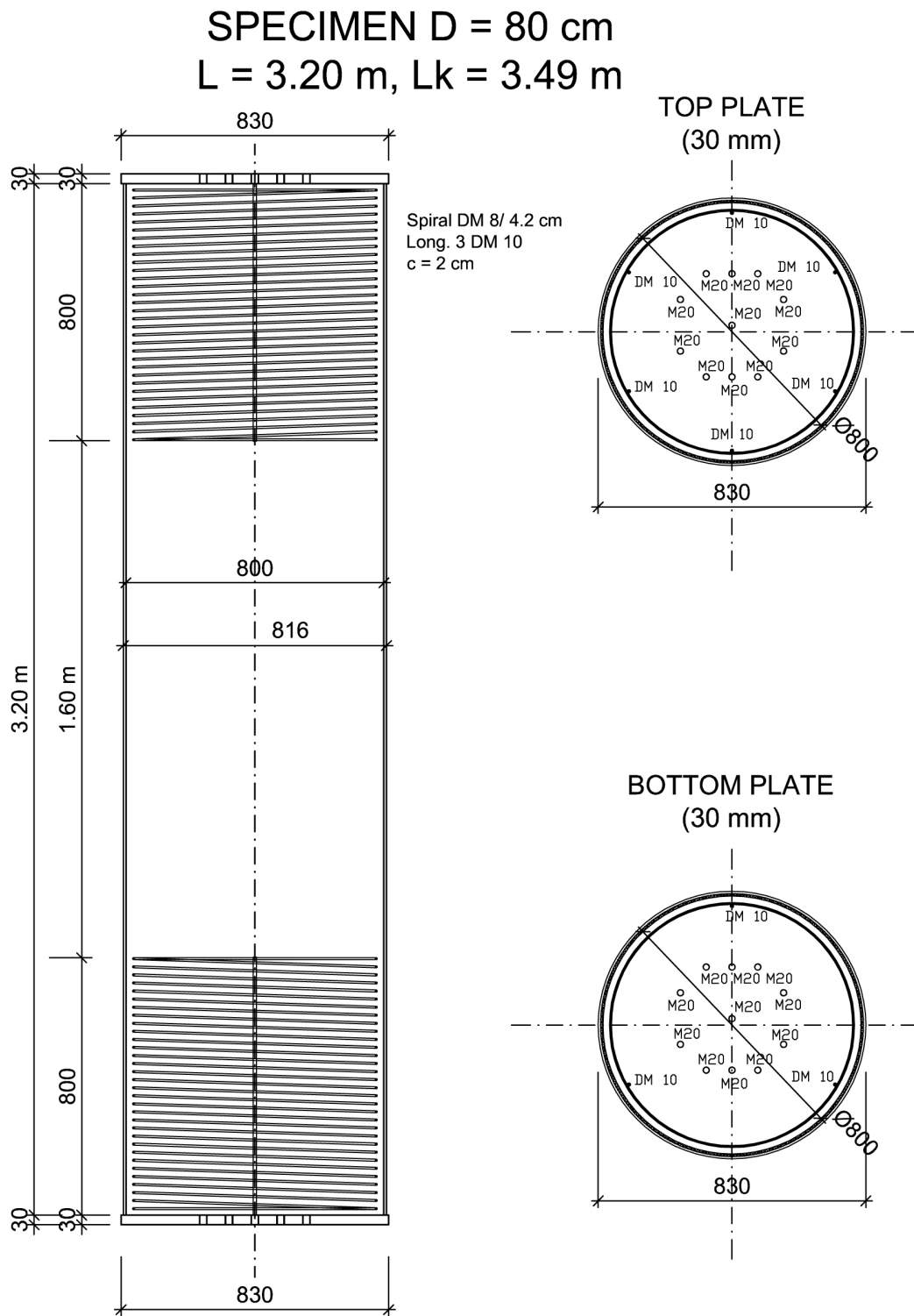


Figure 8.1: Formwork, reinforcement and end plates for specimen XXL (diameter 80 cm)

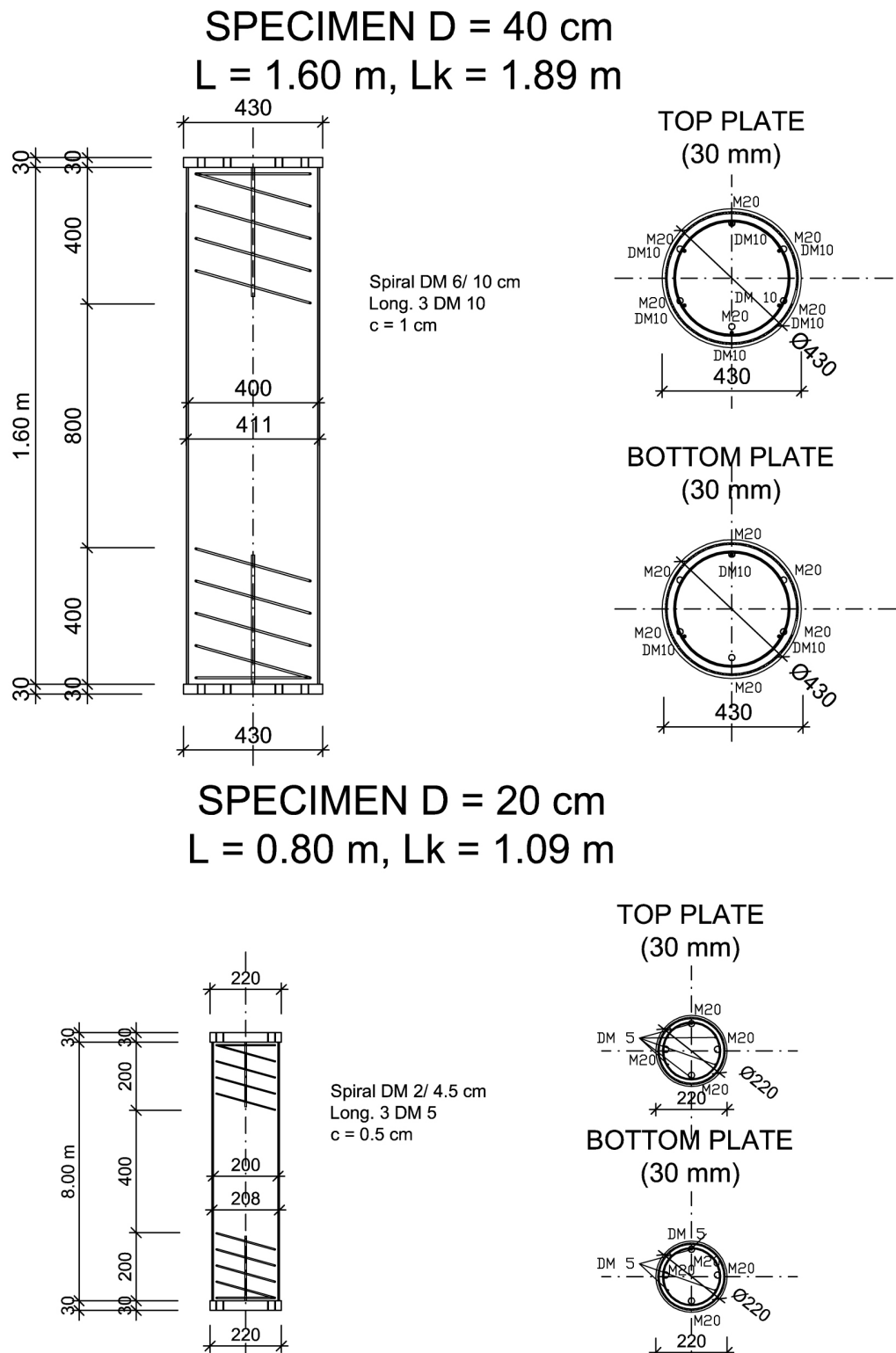
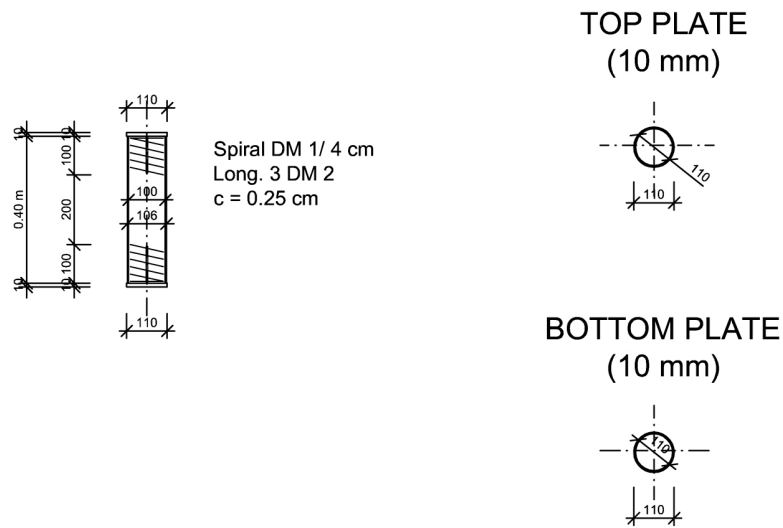


Figure 8.2: Formwork, reinforcement and end plates for specimen XL and L (diameter 40 and 20 cm)

SPECIMEN D = 10 cm
L = 0.40 m, Lk = 0.494 m



SPECIMEN D = 5 cm
L = 0.20 m, Lk = 0.294 m

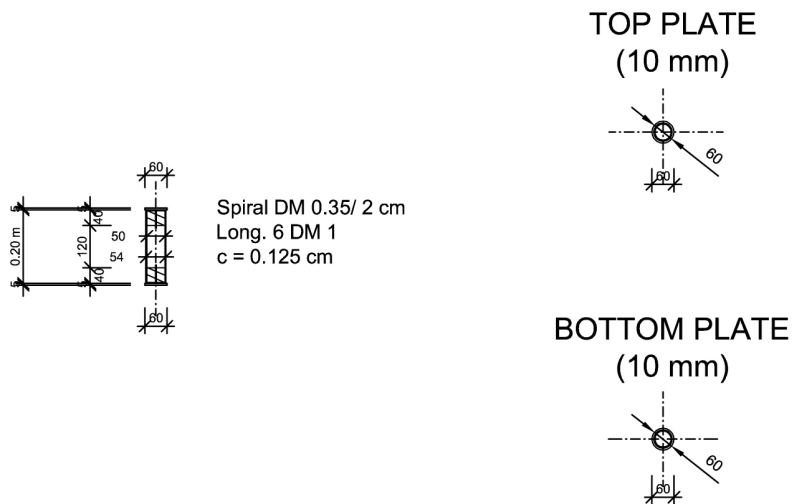


Figure 8.3: Formwork, reinforcement and end plates for specimen M and S (diameter 10 and 5 cm)



Figure 8.4: Construction of the formwork.

not a problem because the weak region was inside the reinforced region. For the sizes L, M and S the weak part would have been in the unreinforced region and the strength of the specimen would have been reduced due to the preparation process. This was prevented by adding an additional cardboard tube with a length of 20cm at the top. This cardboard tube and the concrete was removed after approximately 30 minutes.

8.3.2 Placing the reinforcement and attaching the steel plate

The specimens had reinforcement and a steel plate on both ends, see figure 8.5 left. The steel plate and the lower reinforcement were positioned at the bottom of the tube. The tube was filled with concrete from the top and therefore it was not possible to fix the top steel plate at that time. The top steel plate was fixed three weeks later in the laboratory. But the top reinforcement had to be inserted prior to concreting. This was done with a fixing construction displayed in figure 8.5 right. This construction fixed the concrete tube in vertical direction at the same time.

8.3.3 Concrete batch

The concrete specimen were produced from one batch of concrete at the concrete plant *Ready Mix*, where the formwork was erected. The concrete was mixed according to table 8.3. The maximum aggregate size was 8 mm, the consistency was K4 and the amount was $7m^3$. The day of concreting was the April 5th 2002.

Table 8.2: Concrete cover, longitudinal and spiral reinforcement, and thickness of steel plates used for the different specimen sizes

Specimen	Specimen diameter [cm]	Concrete cover [cm]	Spiral reinforcement	Longitudinal reinforcement	Steel plate thickness [mm]
XXL	80	2	\emptyset 8/4.2 cm	3 \emptyset 10	30
XL	40	1	\emptyset 6/10 cm	3 \emptyset 10	30
L	20	0.5	\emptyset 2/4.5 cm	3 \emptyset 5	30
M	10	0.25	\emptyset 1/4.0 cm	3 \emptyset 2	10
S	5	0.125	\emptyset 0.35/2 cm	6 \emptyset 1	5



Figure 8.5: Reinforcement which was inserted at bottom of the specimen(left). The construction for fixing the reinforcement at the top of the specimen and at the same time for fixing the cardboard tube in vertical direction (right)



Figure 8.6: Producing the specimen with the concrete pump

Table 8.3: Listing of the concrete batch

RK 4/8 [kg]	RK 0/4 [kg]	Cement I 42.5 R [kg]	Water added [kg]	Water total [kg]	W/C factor [—]	Temp. [°C]	Duration of mixing [sec]
715	1103	330	138	200	0.6	14.1	93

8.3.4 Concreting of specimens

The concrete was brought with a concrete transporter and was filled into the formwork with a concrete pump, see figure 8.6. For compaction vibrating units with diameter 4 cm were used for the XXL specimens and diameter 2 cm for XL, the L sizes and the concrete cylinders for evaluation of strength with time. The size M and S were compacted using a shaking table. In the following week the concrete was watered and covered with foil to prevent drying at young age.

8.4 Boundary conditions and loading

8.4.1 Loading arrangement

All specimen were tested under eccentric loading. The eccentricity was scaled with the specimen size and was always $e = D/40$, see table 8.1. The reasons for loading the specimens under eccentric loading were already discussed in section 5.4.1. For the tests on concrete the same set-up was used as for the test series performed on sandstone.

8.4.2 Interface between loading platen and specimen

The loaded faces of the specimens had to obey special accuracy and evenness. With the concrete face itself this would not have been possible, therefore steel plates were used on both ends to provide the specimens with an even surface. Additionally reinforcement was inserted in a height of the specimen diameter to increase the strength in that region and compensate inaccuracies due to lack of right angles of the steel plates and disturbances from the testing machine.

8.5 Test set-up

8.5.1 Set-up for sizes XXL, XL and L tested in the Column Tester

In figure 8.7 the arrangement of the displacement transducers is shown. On the compressed and the tensed side the displacement were measured over the whole specimen length (DW1, DW2) and over the unreinforced region in the middle of the specimen (DW3, IW1). The whole specimen length was always four times the diameter and the unreinforced region was two times the diameter. The displacement transducer IW2 was positioned behind the loading plate and was only used for positioning of the plate. The displacement transducers DW1 to DW3 were digital displacement transducers with an accuracy of $\pm 1 \mu m$ and IW1 and IW2 were linear variable displacement transducers (LVDT).

The specimens were implemented in the Column Tester in horizontal position with the predefined eccentricities $e = D/40$ for every specimen size, see table 8.1. The eccentricity was arranged that the more compressed side was on the top surface of the specimen. The exact eccentricity of the specimen was established for the sizes L, XL, and XXL with different support constructions in the testing machine, see figures 8.8 and 8.9. The fine tuning of the position was done with thin steel plates, that were inserted below the specimen. The specimens were placed

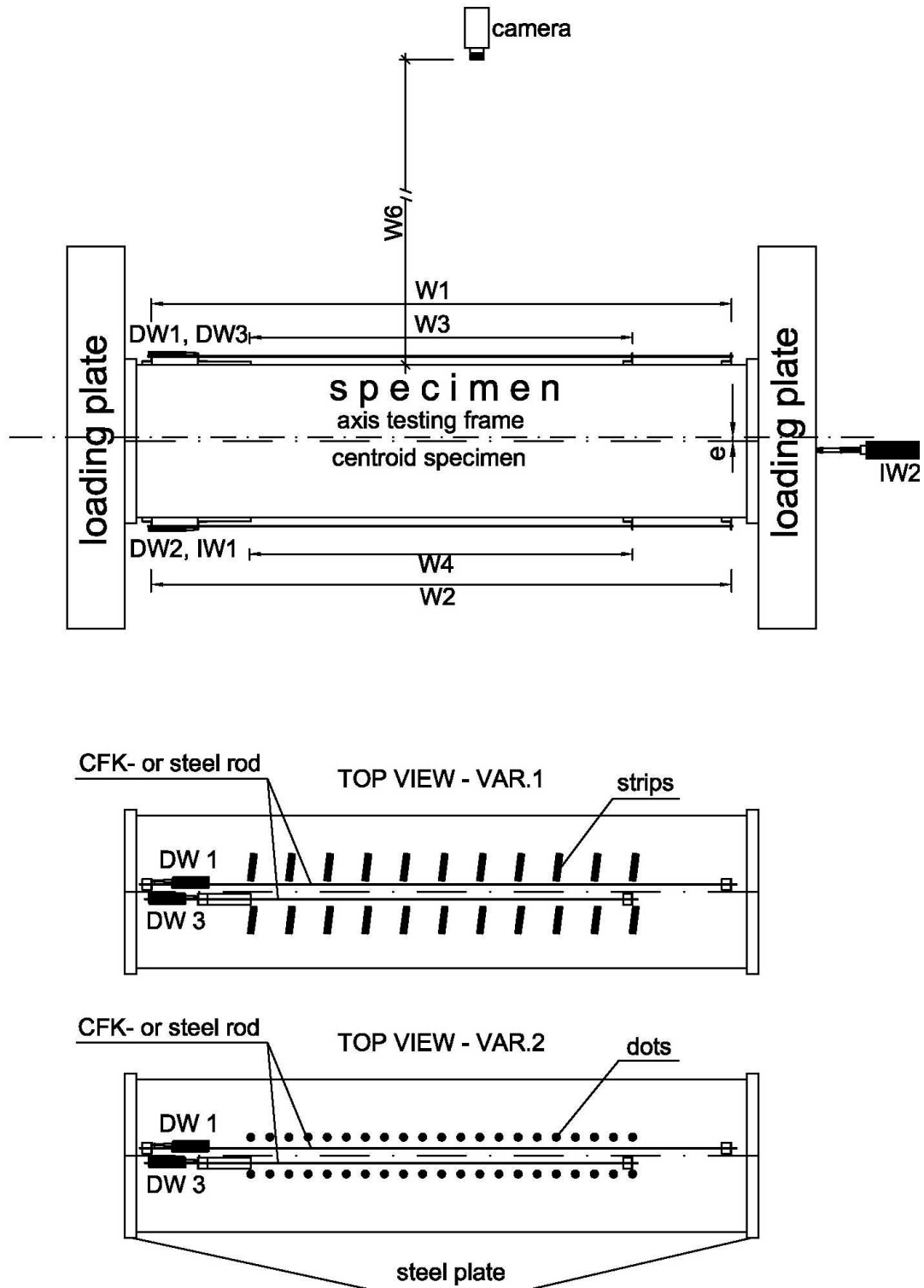


Figure 8.7: Experimental setup in Column Tester with Displacement transducers DW1 to DW3, IW1, IW2 and video extensometer camera

Table 8.4: Expected maximum accuracy of eccentricity for different sizes

Specimen	Diameter [mm]	e [mm]	Δe [mm]	Factor $D/\Delta e$ [-]	Testing frame
XXL	800	20	± 2	400	Column Tester
XL	400	10	± 1	400	Column Tester
L	200	5	± 0.5	400	D2
M	100	2.5	± 0.1	1000	D2
S	50	1.25	± 0.1	1000	D2

with high accuracy because the position defined the eccentricity of loading. The assumed maximum deviations in eccentricity (Δe) are listed in table 8.4.

8.5.2 Setup for sizes M and S tested in the D2 machine

The arrangement of the displacement transducers, the loading device and the positioning of the specimen is shown for size S in figures 8.10 and 8.11. For the M and the S size two digital displacement transducers were used to measure the displacements. Transducer DW1 was measuring on the more compressed side, where the fracture started and DW2 on the opposite side. The displacement transducers were attached to the specimen with needles onto the surface. DW3 was used only for positioning of the machine. The measuring length of the displacement transducers was approximately 5 % less than the specimen length. The displacements plotted in the graphs were converted to the total specimen length. For the sizes M and S only the displacements over the whole specimen length were measured.

8.5.3 Set-up for sizes M and L tested in the Inova machine

The arrangement of the displacement transducers, the loading device and the positioning of the specimen is shown for sizes M and L in figure 8.12. For the M and the L size four displacement transducers were used. On the more compressed and the tensed side the displacements were measured over the whole specimen length (WA1, WA2) and over the unreinforced region in the middle of the specimen (WA3, WA1). The displacement transducer WA1 and WA3 were measuring on the more compressed side, where the fracture started and WA2 and WA4 on

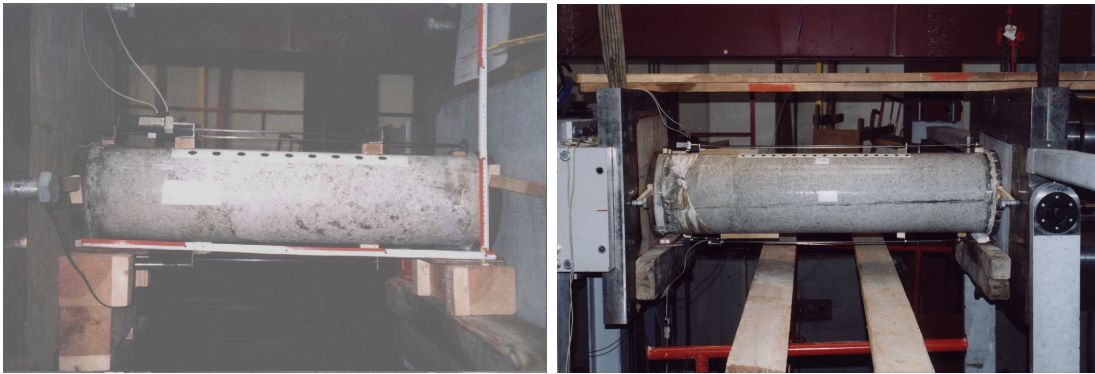


Figure 8.8: Specimen 20 C (left) and 40 C (right) ready for testing



Figure 8.9: Installing of specimen 80b in the Column Tester (left). Specimen 80 b prior to testing (right)

the opposite side. The displacement transducers were attached to elongation bars that were pressed with needles onto the specimen surface. An additional displacement transducer was attached at the cylinder to measure the piston stroke. For the tests in the Inova machine the displacement transducer measuring the piston stroke was used for test control.

The specimens were tested in vertical position and the eccentricity was introduced by the lateral shift. The loading devices were very similar to the devices used in the D2 machine. The eccentricity of loading for every specimen are listed in table 8.1.

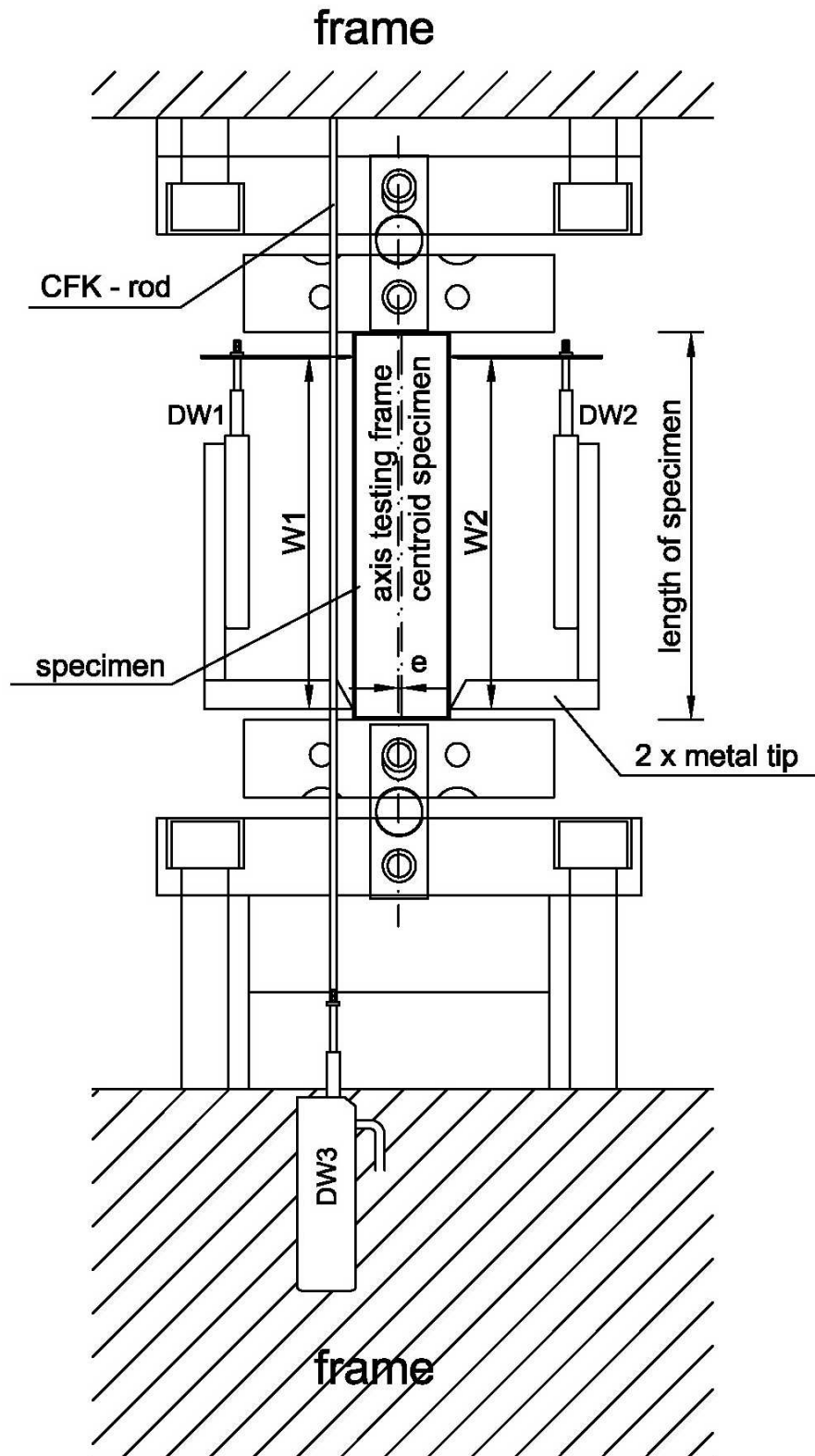


Figure 8.10: Experimental setup in D2 machine with Displacement transducers DW1 to DW3

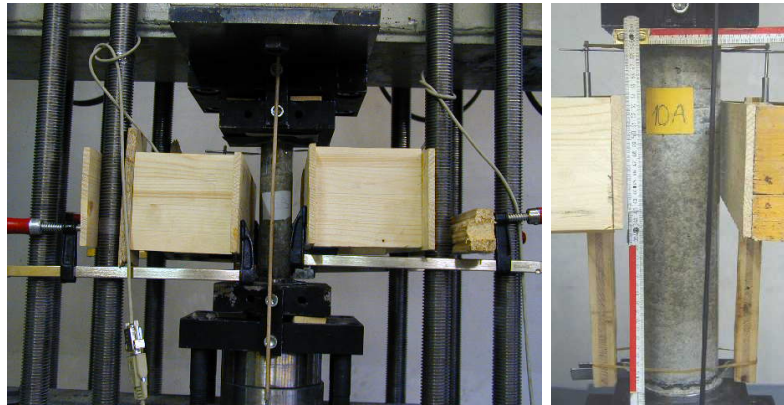


Figure 8.11: Specimen 5b (left) and 10a (right) ready for testing

8.5.4 Set-up for tests on the concrete cylinders

The tests on concrete cylinders were performed in the D2 machine. The specimen had a height of 20 cm and a diameter of 10 cm and were tested under uniaxial compression under displacement control. Spherical bearings were used which were able to rotate during the whole experiment.

8.6 Test control

In the sandstone series the lateral displacement measurements were used to guarantee a stable experiment, see section 5.7. This was possible because the specimen was notched. In this series the two longitudinal displacements on the compressed side (DW1 and DW3) were used for control. The two displacement transducers measured over the whole specimen length and over half of the specimen length where the specimen was unreinforced. The displacement transducer with the higher strain was responsible for control. Close to the maximum load the unreinforced region showed always the larger deformation and this displacement transducer was responsible for control at and after peak. The experiment was usually stopped when the load dropped between 30 to 50 % of maximum load. The specimens were always loaded with a predefined strain rate of $2 \mu\text{strain}/\text{s}$. For the tests in the Column Tester and the D2 machine the displacements were controlled by displacements on the specimen surface. In the Inova machine the displacement was controlled at the hydraulic actuator.

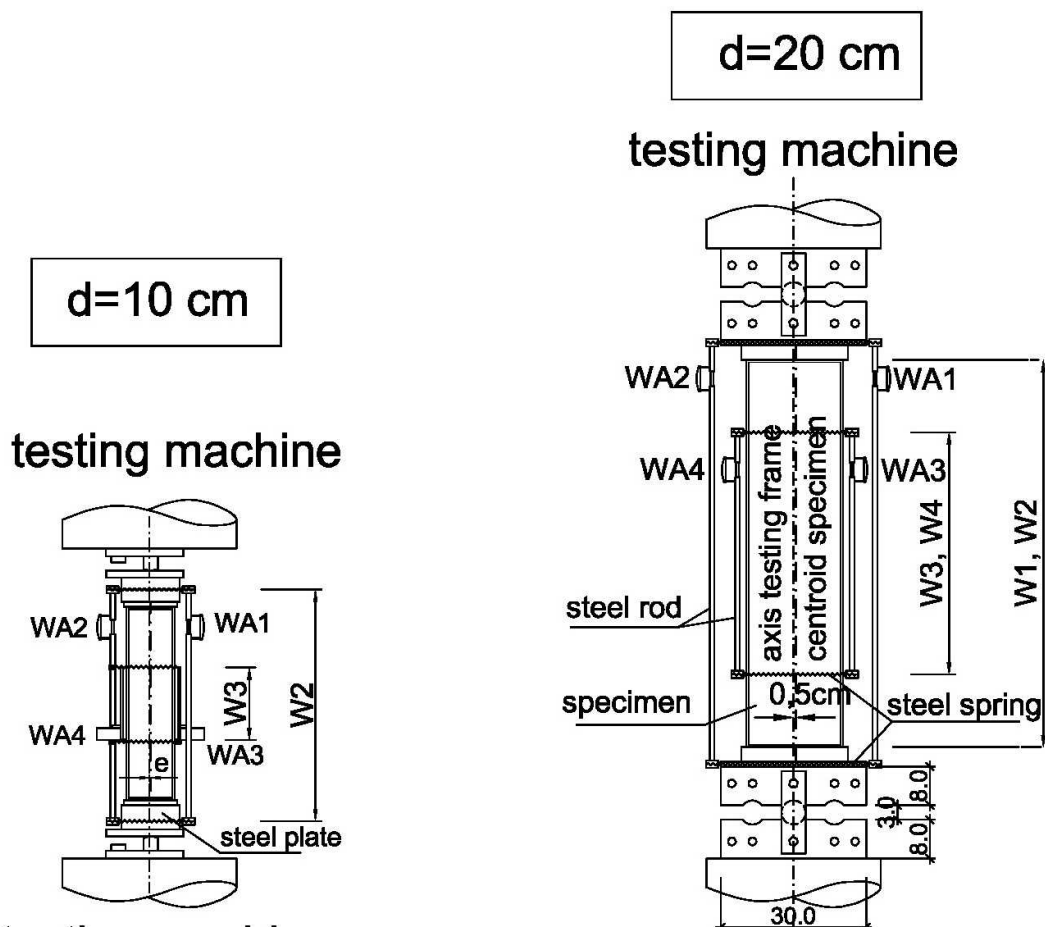


Figure 8.12: Experimental setup in Inova machine with displacement transducers WA1 to WA4

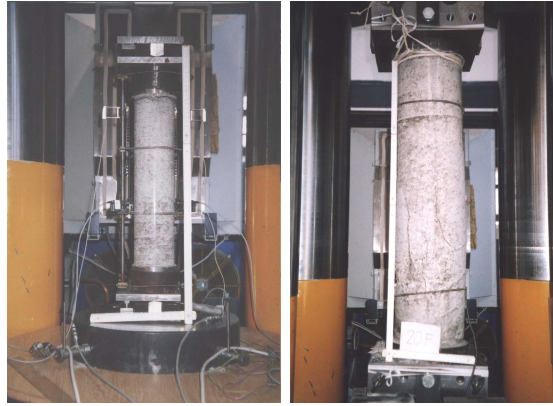


Figure 8.13: Specimen 10a (left) and 20f (right) ready for testing

8.7 Determination of material parameters from displacements and loads

First the measured data was corrected and moved to the origin with the same algorithm as used in the sandstone series, see section 4.4. The stresses σ were calculated in the unreinforced region on the compressed and tensile side according to linear elasticity theory. The area A , the moment of inertia I and the distances of the centroid y were calculated. The stresses were calculated as

$$\sigma = \frac{F}{A} \pm \frac{F \cdot e}{W} \quad , \quad \text{with:} \quad A = \frac{D^2 \cdot \pi}{4} \quad \text{and} \quad W = \frac{d^4 \cdot \pi}{64} \quad . \quad (8.1)$$

The strains were calculated on the compressed and tensile side by simply dividing the measured displacement by the measuring length. With $DT3$ and $DT4$ the strains ε_3 and ε_4 were calculated in the unreinforced region. The strains ε_1 and ε_2 were calculated as mean strains of the reinforced and the unreinforced region by simply dividing the measured displacement Δl by its measuring length l_0 . The length l_0 was always measured prior to testing and was approximately four times the diameter for the displacements w_1 and w_2 or 2 times the diameter for the displacements w_3 and w_4 . The strains were calculated as

$$\varepsilon_i = \frac{\Delta l}{l_0} \quad . \quad (8.2)$$

The stress strain diagrams are given for all specimen in figures 9.16. For the modulus of elasticity the stresses and strains were determined at $\frac{1}{3}$ and $\frac{1}{6}$ of the maximum load. The modulus of elasticity E_{mean} was calculated as

$$E_{mean} = \frac{\sigma_{\frac{1}{3}F_{max}} - \sigma_{\frac{1}{6}F_{max}}}{\varepsilon_{\frac{1}{3}F_{max}} - \varepsilon_{\frac{1}{6}F_{max}}} \quad . \quad (8.3)$$

The loading rate was determined in terms of stress rate and strain rate. The according measurements are taken at $\frac{1}{3}$ of maximum load and at maximum load. The stress rate writes

$$\dot{\sigma} = \frac{\sigma_{F_{max}} - \sigma_{\frac{1}{3}F_{max}}}{t_{F_{max}} - t_{\frac{1}{3}F_{max}}} \quad (8.4)$$

and the strain rate

$$\dot{\varepsilon} = \frac{\varepsilon_{F_{max}} - \varepsilon_{\frac{1}{3}F_{max}}}{t_{F_{max}} - t_{\frac{1}{3}F_{max}}} \quad (8.5)$$

Chapter 9

Size effect in compression of concrete

9.1 Strength versus specimen size

One of the main issues of the size effect theory is the influence of size on the strength of the specimen. The strength was determined as maximum stress following equation 8.1. The strengths for the individual specimens tested with the D2-machine, the Column Tester and the Inova machine at the TU Prague are plotted in figure 9.1. The results are displayed with linear (left) and logarithmic scaling (right). A tabular presentation of the results can be found in tables 9.1 and 9.4. The mean values are shown in figure 9.2 for every specimen size and every testing machine. In figure 9.3 the mean values are determined for every specimen size not considering the different testing machines. The standard deviation is shown for every mean value in both plots by an error bar. One can easily see that the strength reduces with specimen size. The standard deviations from figures 9.2 and 9.3 were plotted separately versus specimen size in figure 9.4. The maximum standard deviation was 7 MPa for size S (50mm). For the other sizes the standard deviation was rather low for a heterogeneous material like concrete. Interesting to mention here is that the standard deviation is decreasing with increasing size, see figure 9.4.

9.2 Strength versus loading rate

It is described in literature that the loading rate affects the strength of specimens. For easier comparison of the different sizes, the loading rate was calculated as normalized loading in terms of applied strain per second $\dot{\epsilon}$ and stress per second $\dot{\sigma}$. The values were obtained from the data using equations 8.4 and 8.5. This

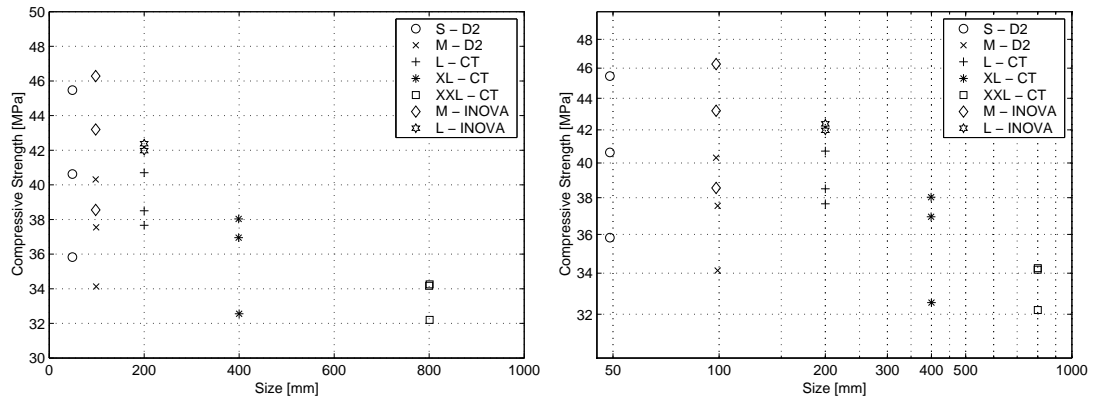


Figure 9.1: Strength vs specimen size in linear (left) and logarithmic scale(right)

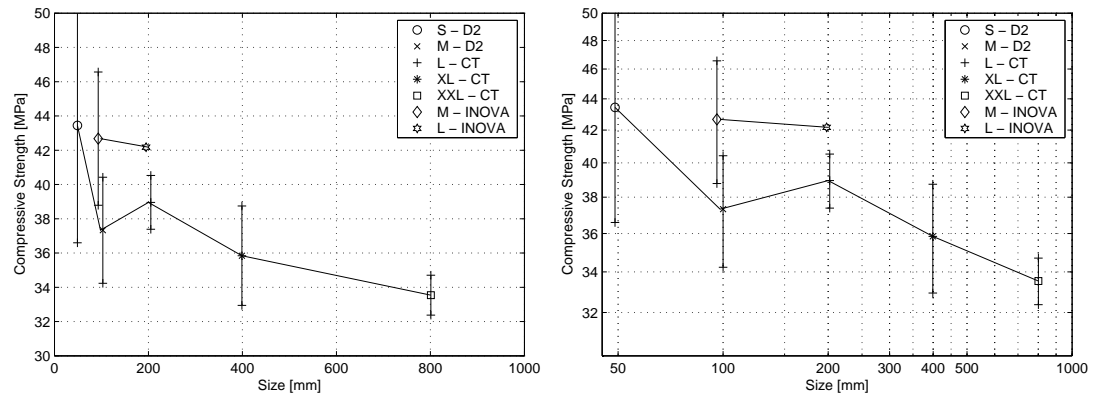


Figure 9.2: Mean strength with standard deviation from Prague tests and from Vienna tests versus specimen size in linear (left) and logarithmic scale(right)

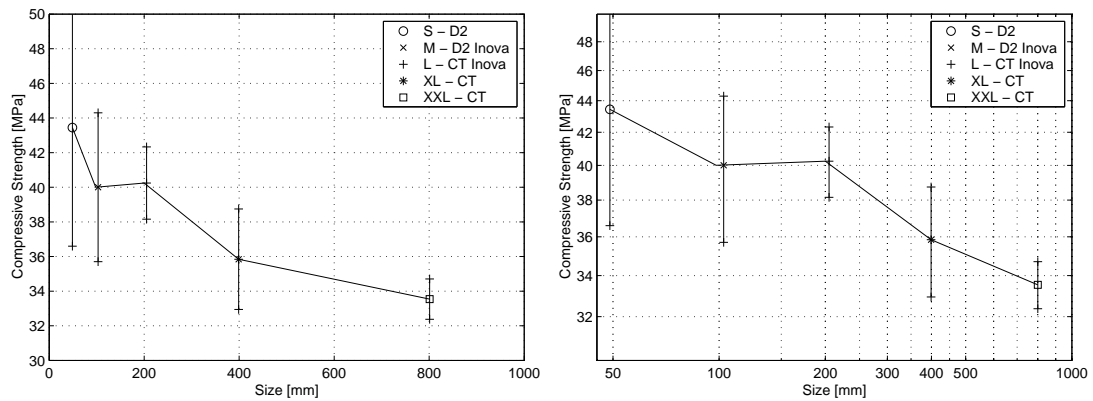


Figure 9.3: Mean strength with standard deviation from Prague and Vienna tests versus specimen size in linear (left) and logarithmic scale(right)

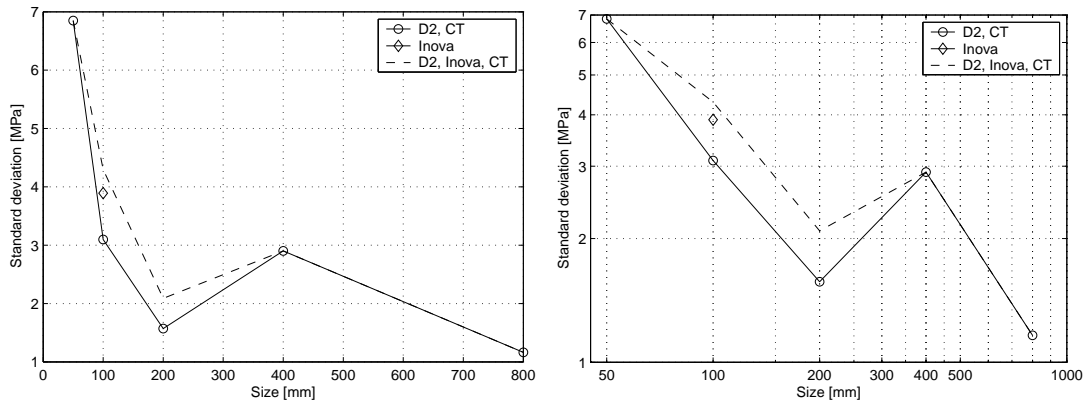


Figure 9.4: Standard deviation of the strength versus specimen size in linear (left) and logarithmic scale(right)

rate should be the same for all specimen sizes. In figure 9.5 the strength versus loading rate is displayed. The strain rate in figure 9.5 (right) shows a mean strain rate of $2 \mu\text{strain}/s$ and a stress rate between 0.01 to $0.03 \text{ MPa}/s$ for the specimens tested in the D2 machine and the Column Tester. The specimens tested in the Inova machine in Prague showed a higher stress rate between 0.036 and $0.046 \text{ MPa}/s$ and a strain rate between 4 and $8.5 \mu\text{strain}/s$

The difference in the loading rate of the D2 machine and the Column Tester was so small that it was assumed that these deviations did not affect the strength of the specimens. Additionally, the plot shows no trend of increasing or decreasing strength with strain rate.

9.3 Development of cylinder strength with time

48 concrete cylinders were tested on different days in the D2 machine, see figure 9.6. The first concrete cylinder was tested on the 49th day and the last on the 67th day. The strength between the 48th and the 55th day was between 31 and $42 \text{ N}/\text{mm}^2$. The data was fitted with linear curve fitting and the trend was a slightly increasing strength with age, see figure 9.6. The increase was determined in the observed time range as $0.16 \text{ N}/\text{mm}^2 \text{ per day}$.

9.4 Influence of age on strength of specimen

The tested specimens are described in section 8.2.1. The testing of specimens began in the Column Tester with the L sizes at the 48th and 49th day after

Table 9.1: Age, mean strength at the day of testing f_c and at the 52nd day $f_{c,52thday}$, with standard deviation $\sigma_{f_{c,52thday}}$ for each specimen size and testing machine.

Specimen	Diameter [cm]	Quantity	Age [days]	f_c [kN]	$f_{c,52thday}$ [N/mm ²]	$\sigma_{f_{c,52thday}}$ [N/mm ²]	Testing machine
XXL	80	3	58	33.6	32.6	1.37	CT
XL	40	3	53	35.9	35.7	3.01	CT
L	20	3	48	39.0	39.6	1.66	CT
L	20	2	75	42.2	38.3	-	Inova
L	20	5	59	40.3	39.1	1.38	CT,Inova
M	10	3	74	42.7	38.8	3.52	Inova
M	10	6	71	40.0	36.8	3.58	D2,Inova
M	10	3	67	37.3	34.9	2.90	D2
S	5	3	60	43.5	41.7	5.60	D2

casting. Then followed the XL sizes on the 52nd till the 54th day and the XXL sizes from the 56th till the 60th day. Afterwards in the D2 frame the sizes S and M were tested on the 66th and the 67th day, except for specimens 5a and 5b, which were tested at the 55th day, see table 9.1 and 9.4. The tests in the Inova machine in Prague were performed at the 74 and the 75 day. The testing machine used are indicated in figure 9.11 by different colors and the testing sequence is indicated by ascending numbers.

As shown in section 9.3 the strength of the concrete cylinders increased during the testing. The tests in Vienna (D2 and Column Tester) were performed over a time range of 19 days. The development of the strength determined on cylinders was calculated by the fitted function displayed in figure 9.6. The strength of the concrete cylinders were extrapolated from specimens tested between the 49th and the 67th day to the 74th day.

To eliminate the effect of strength increase of the specimens, the strengths were all calculated for the 52nd day of testing. This calculation was performed linearly by simply dividing the strength of the specimens determined in the test f_{test} by

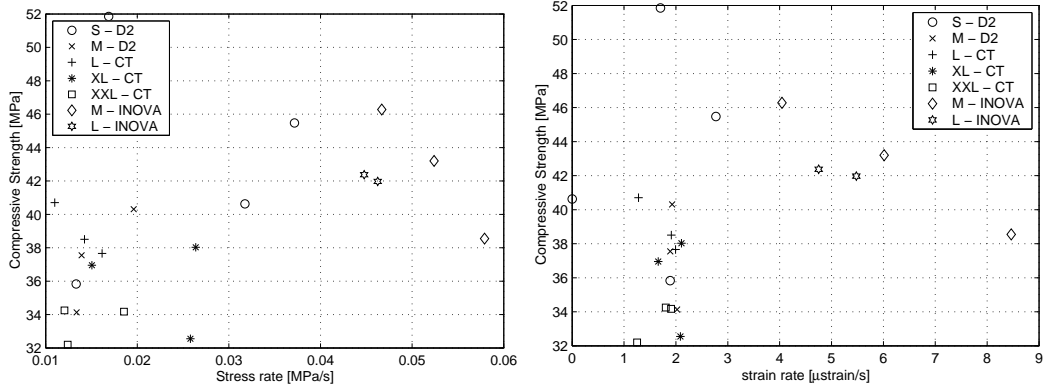


Figure 9.5: Strength vs. loading rate

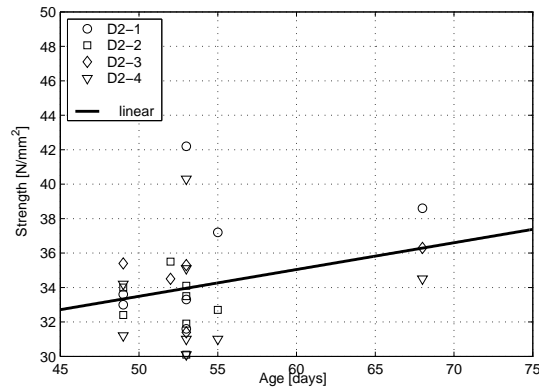


Figure 9.6: The strength of concrete cylinders with a diameter of 10 cm and length of 20 cm was determined at different age

the cylinder strength $f_{cylinder, day}$ and multiplying with the cylinder strength at the 52nd day $f_{cylinder, 52nd day}$

$$f_{52nd day} = \frac{f_{test}}{f_{cylinder, day}} f_{cylinder, 52nd day} \quad , \quad (9.1)$$

where $f_{cylinder, day}$ was calculated by the linear interpolation displayed in figure 9.6. The cylinder strength at the 52nd day $f_{cylinder, 52nd day}$ was 33.80 MPa.

The strengths calculated for the 52nd day are given in figure 9.7 in linear and double logarithmic scaling and in table 9.4. In figures 9.8 and 9.9 the mean values of the strength at the 52nd day were calculated and are shown with their standard deviation. The mean values plotted in figure 9.8 were determined for every specimen size and every testing machine separately. In figure 9.9 the mean

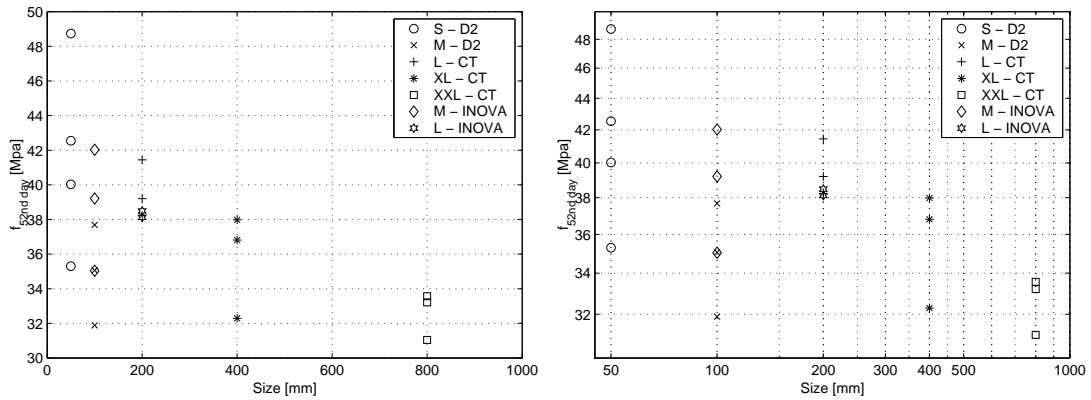


Figure 9.7: Strength calculated for 52nd day vs. specimen size in linear (left) and logarithmic scale (right)

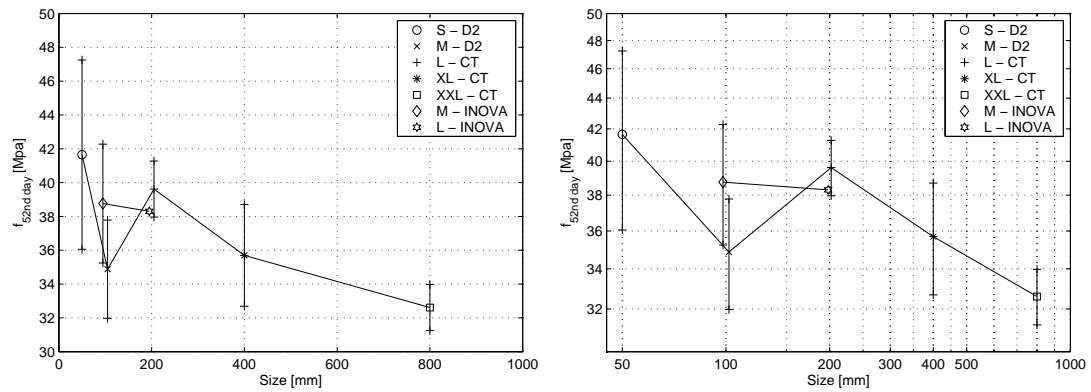


Figure 9.8: Mean strength with standard deviation calculated for 52nd day from Prague tests and from Vienna tests versus specimen size in linear (left) and logarithmic scale(right)

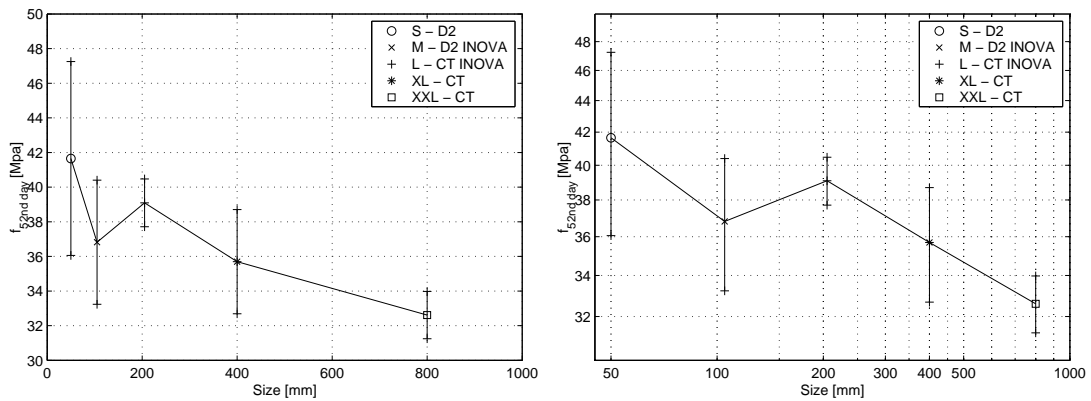


Figure 9.9: Mean strength with standard deviation calculated for 52nd day from Prague and from Vienna tests versus specimen size in linear (left) and logarithmic scale(right)

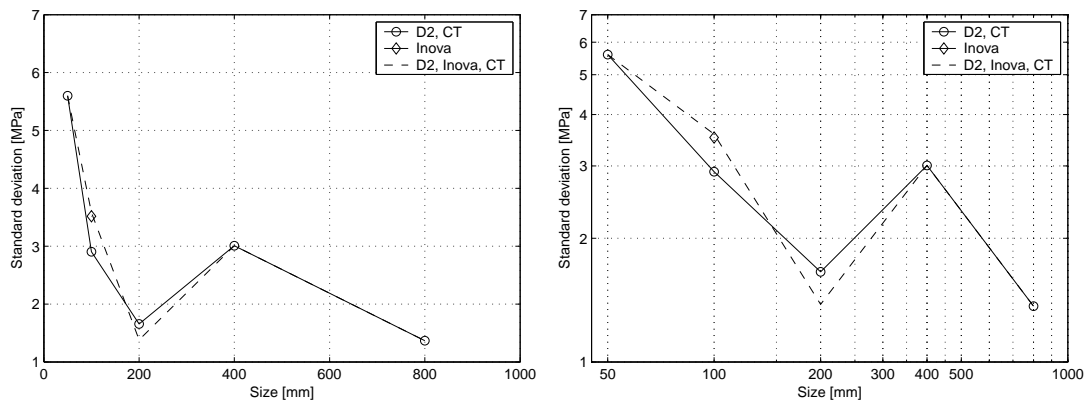


Figure 9.10: Standard deviation of the strength calculated for 52nd day versus specimen size in linear (left) and logarithmic scale (right)

strength were plotted for every specimen size, not considering the different testing machines. The longest time period was between the L size tested in the Column Tester in Vienna and the Inova machine in Prague. The tests on the cylinders showed that the strength increased by 4 *Mpa* during the whole testing time. In figure 9.2 the L sizes tested in Prague were much higher, but with consideration of strength increase with time the strengths of the size effect specimens are in a narrow range now, see figure 9.8.

In figure 9.10 the standard deviation is plotted versus size and again shows a decreasing trend. Comparing the standard deviations considering strength increase with time (figure 9.10) and not considering strength increase (figure 9.4) one can see that the standard deviation for the calculation of mean values from the D2, Column Tester (CT) and the Inova machine became lower.

It is interesting to note that the strength under eccentric loading is higher than the strength under centric loading for all specimen, except for specimens XXL. This was also earlier observed in the preliminary series for sandstone in compression, see figure 4.13 on page 40.

9.5 Influence of testing machine

In this size effect series specimens with maximum loads from 60 *kN* to 14300 *kN* were tested. These specimens cannot be tested in one machine. Regarding the proper measurement of load and experiment control it was sufficient to use two testing machines. In literature it is stated that a testing machine can have an influence on the maximum strength (Van Mier et al., 1997). In a size effect series

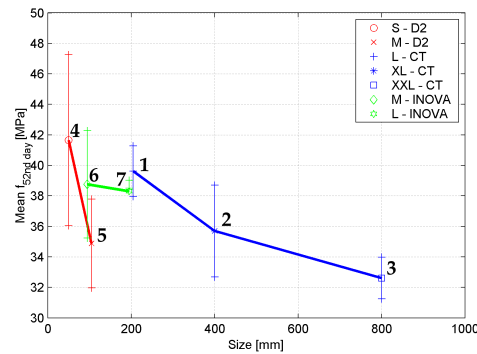


Figure 9.11: Strength at 52nd day. The testing machines are indicated by different colors and the testing sequence is given by consecutive numbers. The test sequence is given by ascending numbers

it is very important that no influences of testing machines are present. In order to make comparisons possible additional tests on a testing equipment that has its maximum load between the big (the Column Tester) and the small machine (D2 machine) were necessary. The Inova machine at TU Prague was perfect for that purpose because of the maximum load of 2000 kN and the similar loading devices available.

All tests in the Inova machine were performed within two days. The size L in the Column Tester were the first and the M size in the D2 machine were the last sizes that were tested in Vienna. 19 days were between these tests. Thus the strength increase with time was considered by dividing the strength of the specimens by the cylinder strength at the day of testing, as done previously in section 9.4.

To compare the results from the D2 machine to the Column Tester, three specimens of the M (diameter 100mm) size were tested in the D2 machine and another three in the Inova machine. Additionally, three specimens of L (diameter 200mm) size were tested in the Column Tester and another two were tested in the Inova machine. The mean strengths for the 52nd day were plotted in figure 9.11, where the testing machines are indicated by different colors. The individual strength, the mean strength and the standard deviation are given in table 9.2 for the tests performed in Vienna and the tests performed in Prague. The deviations and the strengths listed are usual for concrete. The tested cylinders showed a standard deviation of 2.9 MPa. The slopes of the lines between sizes M and L for the Inova machine and the slope for D2 and Column tester are different in figure 9.11. The testing machines are indicated by individual colors. Nevertheless, the mean strength are strongly influenced by individual strength of specimen, i.e.

Specimen 10b tested in the D2 machine has lowest strength, increases the scatter and changes the slope strongly. A influence of testing machine was not detectable. The ranges of the strengths are in figure 9.11 close and an influence of the machine was rather small or not present.

9.6 Fitting of data to SEL and MFSL

The strengths plotted in figures 9.2, 9.3 and the strengths at the 52nd day shown in figures 9.8 and 9.9 were used for the fitting procedures. Thus the strength at testing (indicated as test day) and the strength at the 52nd day (indicated as 52nd day) was used (after section 9.4). One set of data was from the tests performed in the D2 machine and the Column Tester and another set of data contained all mean values from all three machines.

For fitting the Size Effect Law by Bažant (SEL), the Size Effect Law for compression (SEL-compression) and the Multifractal Scaling Law (MFSL) were applied. The three laws were shortly described in section 2.3. The equation 2.4 was rearranged and used in similar form as 2.1, see equations in table 9.3. The data sets were fitted with the nonlinear Levenberg-Marquardt algorithm. In table 9.3 the fitted parameters of the size effect laws are given with their residual norm r .

In figures 9.12, 9.13, 9.14, 9.15 the laws are plotted for the different data sets. The residual norm r is a measure how close the fitted function is to the data and varies depending on the data set used, see table 9.3. These values are not a clear indicator for the suitability of a law. The SEL plots and the SEL-compression are on the same line. However, the trend of the Bažant SEL law seems to describe the trend of the data more accurately. There are deviations from the data in the ranges of the M and the L sizes, that deviate. For the three largest sizes the SEL goes with the trend of the data, which is not the case for the MFSL. To get information of the slope in the logarithmic plot the mean values of the two largest sizes were used to determine the slope in double logarithmic presentation. The slope was determined as $\frac{1}{7.7}$.

9.7 Stress strain diagrams

In figure 9.16 the stress strain diagrams are shown for each size in one graph. The stress is plotted on the compressed side versus the strain on the compressed side in the unreinforced region of the specimens. The machine used for testing is indicated in the legend.

Table 9.2: Strengths of sizes M and L tested in D2 machine (D2), Column Tester (CT) and Inova Machine(Inova) with and without consideration of increasing strength with time

	Strength of specimens [Mpa]			Mean strength [MPa]	Standard deviation [MPa]
D2 machine and CT strength results at test days					
M 100mm	40.3	34.1	37.5	37.3	3.11
L 200mm	40.7	37.7	38.5	39.0	1.55
D2 machine and CT strength results calculated for 52nd day					
M 100mm	37.7	31.9	35.1	34.9	2.90
L 200mm	41.4	38.2	39.2	39.6	1.66
Inova strength results at test days					
M 100mm	43.2	46.3	38.6	42.7	3.87
L 200mm	42.0	42.4	-	42.2	-
Inova strength results calculated for 52nd day					
M 100mm	35.0	38.1	38.5	37.2	1.92
L 200mm	39.2	42.0	-	40.6	-

Table 9.3: Table of parameters of different size effect laws. D_0, l_{ch} in cm, Bf_t, f_c in N/mm^2

SEL	SEL compression	MFSL
$\sigma_N = \frac{Bf_t}{\left(1+\frac{D}{D_0}\right)^{\frac{1}{2}}}$	$\sigma_N = \frac{Bf_t}{\left(1+\frac{D}{D_0}\right)^{\frac{2}{5}}}$	$\sigma_N = \sqrt{A + \frac{B}{D}}$
Mean of D2 and CT strength results see figure 9.12		
$B f_t = 41.6$ $D_0 = 132.4$ r=15.4	$B f_t = 41.7$ $D_0 = 97.8$ r= 15.4	A=1171.3 $f_c = 34.22$ B=3463.4 $l_{ch} = 2.96$ r=15.1
Mean of D2, CT and Inova strength results see figure 9.13		
$B f_t = 43.3$ $D_0 = 108.8$ r=5.7	$B f_t = 43.4$ $D_0 = 79.7$ r=15.1	A=1221.2 $f_c = 34.95$ B=3670.3 $l_{ch} = 3.00$ r=9.8
Mean of D2 and CT strength results calculated for 52nd day, see figure 9.14		
$B f_t = 40.0$ $D_0 = 160.2$ r=24.2	$B f_t = 40.1$ $D_0 = 120.9$ r=24.2	A=1163.7 $f_c = 34.11$ B=2616.2 $l_{ch} = 2.25$ r=26.2
Mean of D2, CT and Inova strength results calculated for 52nd day, see figure 9.15		
$B f_t = 40.7$ $D_0 = 140.1$ r=10.1	$B f_t = 40.8$ $D_0 = 104.8$ r=10.1	A=1166.5 $f_c = 34.15$ B=2861.4 $l_{ch} = 2.46$ r=14.7

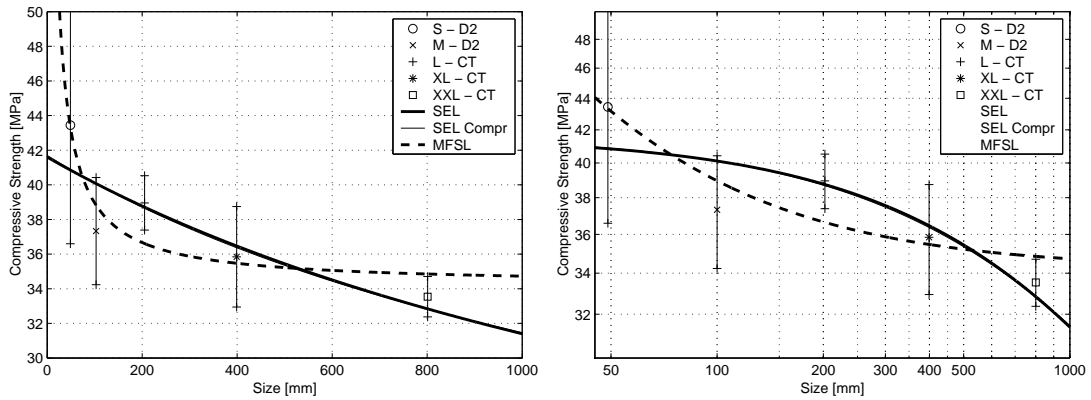


Figure 9.12: Fitting of size effect laws for results from Column Tester and D2 machine at the day of testing. For comparison the mean values and the standard deviation is plotted

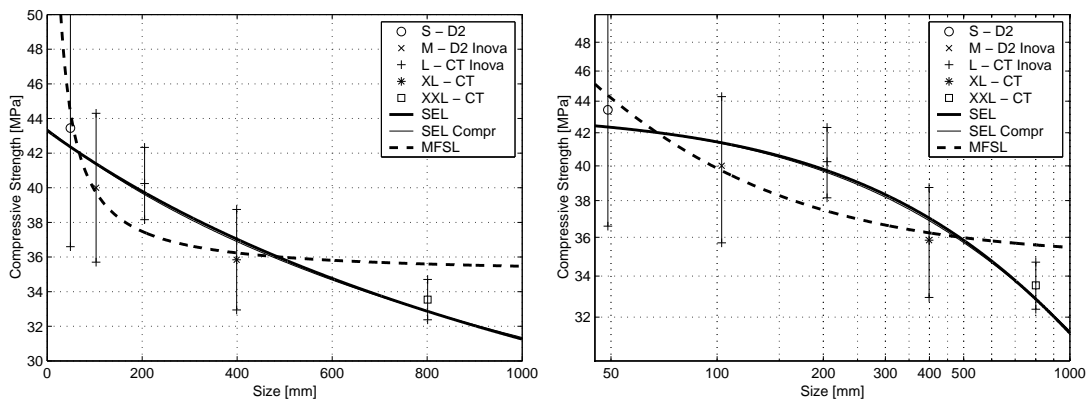


Figure 9.13: Fitting of size effect laws for results from Column Tester, D2 machine and Inova machine at the day of testing. For comparison the mean values and the standard deviation is plotted

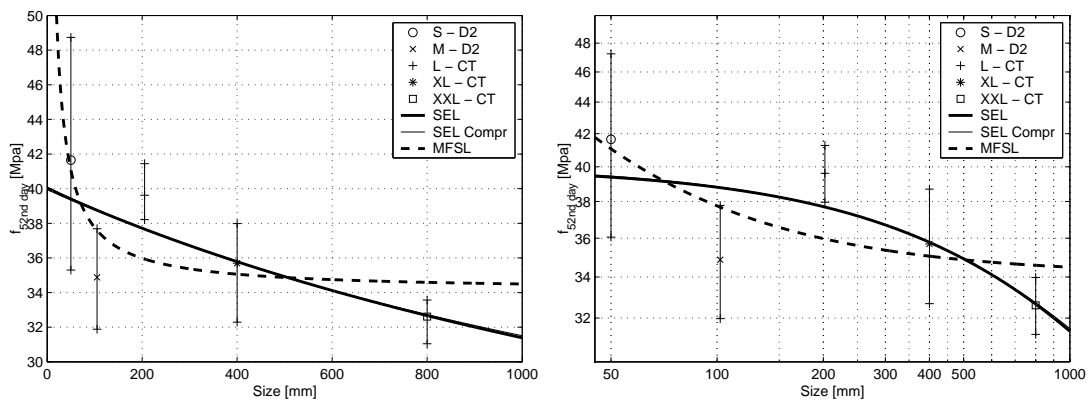


Figure 9.14: Fitting of size effect laws for results calculated for 52nd day from Column Tester and D2 machine only. For comparison the mean values and the standard deviation is plotted

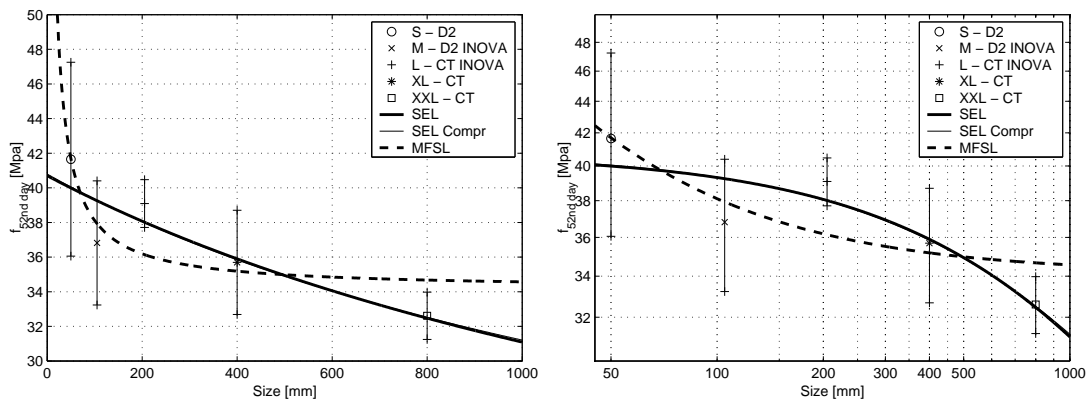


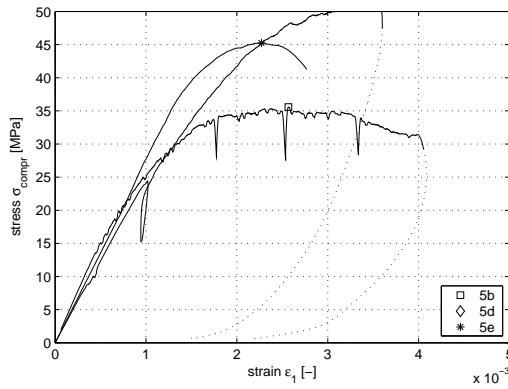
Figure 9.15: Fitting of size effect laws for results calculated for 52nd day from Column Tester, D2 machine and Inova machine. For comparison the mean values and the standard deviation is plotted

9.8 Tabular results for individual specimens

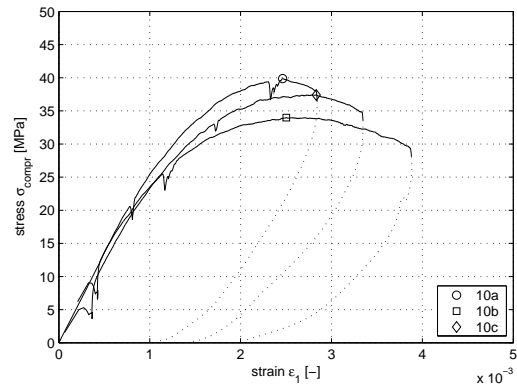
In table 9.4 the main results determined from tests in the D2 machine, the Column Tester in Vienna and the Inova machine at the TU Prague are summarized for every specimen. The listed results are the Young's modulus E , the strength at the day of testing f_{day} , strength at 52nd day $f_{52nd\ day}$ calculated according to section 9.4, the mean strain at peak over the whole specimen length $\varepsilon_{1,peak}$, the stress rate $\dot{\sigma}$ and the strain rate $\dot{\varepsilon}$, calculated between $2/3$ and maximum load, see section 8.7 for details on the determination of results.

9.9 Specimens after testing and crack patterns

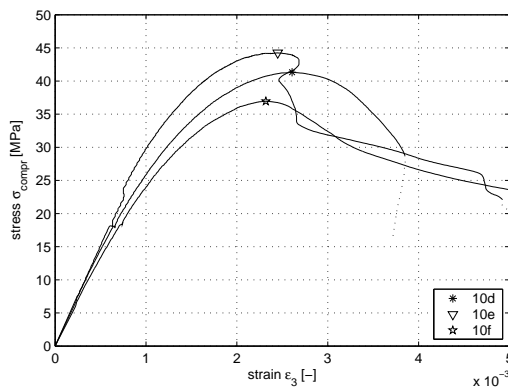
The fracture patterns of the specimens are shown in figures 9.17 to 9.19 and photos of selected specimens after testing are shown in 9.20. However, the crack patterns shown represent the state of the specimens after completion of the test. Since the loading of the specimens in the range after the maximum load had been reached was different (see figure 9.16), a different damage situation is shown for each specimen. Therefore it is rather difficult to draw conclusions regarding the failure mechanisms from the different fracture patterns shown in figure 9.17 to 9.19. There were no fractures close to the interface and it was concluded that the interface performed well for all specimen. The specimens 40a and 40c showed two fracture fronts after testing.



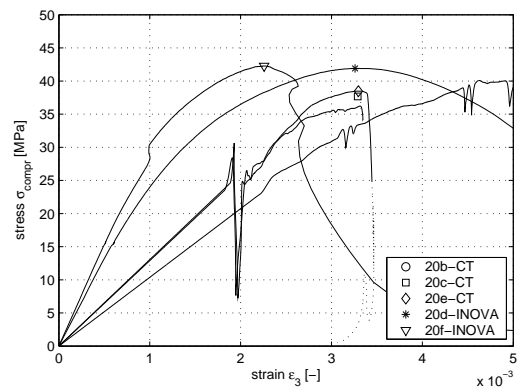
(a) Stress strain curve on compressed side for specimens of size S ($D=50$ mm, D2)



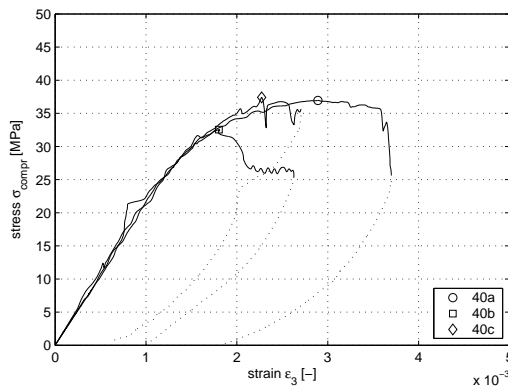
(b) Stress strain curve on compressed side for specimens of size M ($D=100$ mm, D2)



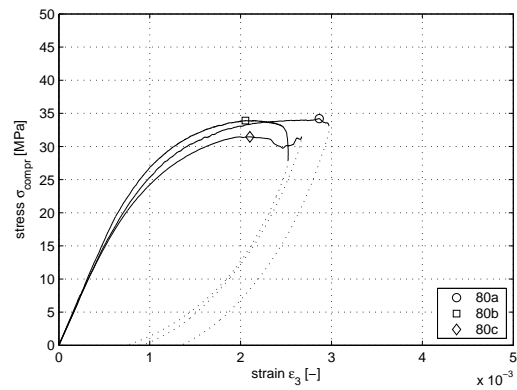
(c) Stress strain curve on compressed side for specimens of size M ($D=100$ mm, Inova)



(d) Stress strain curve on compressed side for specimens of size L ($D=200$ mm, CT and Inova)



(e) Stress strain curve on compressed side for specimens of size XL ($D=400$ mm, CT)



(f) Stress strain curve on compressed side for specimens of size XXL ($D=800$ mm, CT)

Figure 9.16: Strain in unreinforced region ϵ_3 versus stress σ_{compr} for each specimen size

Table 9.4: Experimental data for the individual specimens tested in D2 frame (D2), Column Tester (CT) and Inova machine at the CVUT Prague (Inova)

	E [MPa]	$f_{52nd\ day}$ [kN]	f_{day} [MPa]	$\varepsilon_{1,peak}$ [%]	$\dot{\sigma}$ [MPa/s]	$\dot{\varepsilon}$ [10 ⁶ /s]	age [days]	
S 5a	-	40.03	40.6	-	-	-	55	D2
S 5b	49106	35.30	35.8	2.57	0.0107	1.89	55	D2
S 5d	25446	48.74	51.9	3.29	0.0135	1.70	66	D2
S 5e	61365	42.54	45.5	1.86	0.0297	2.77	67	D2
M 10a	26571	37.68	40.3	2.40	0.0157	1.93	67	D2
M 10b	-	31.88	34.1	2.67	0.0109	2.02	67	D2
M 10c	23730	35.06	37.5	2.79	0.0114	1.89	67	D2
L 20b	10367	41.44	40.7	3.46	0.0092	1.26	48	CT
L 20c	12886	38.21	37.7	2.92	0.0135	1.99	49	CT
L 20e	13044	39.20	38.5	3.98	0.0119	1.91	48	CT
XL 40a	21063	36.81	37.0	2.51	0.0124	1.65	53	CT
XL 40b	22403	32.29	32.6	1.87	0.0215	2.09	54	CT
XL 40c	20556	37.98	38.0	2.21	0.0219	2.10	52	CT
XXL 80a	30539	33.21	34.3	2.45	0.0101	1.81	59	CT
XXL 80b	32537	33.57	34.2	1.89	0.0155	1.91	56	CT
XXL 80c	30725	31.04	32.2	1.83	0.0104	1.25	60	CT
M 10d	26843	39.21	43.2	2.79	0.0419	6.03	74	Inova
M 10e	-	42.03	46.3	1.45	0.0373	4.05	74	Inova
M 10f	19372	35.04	38.6	3.22	0.0463	8.48	74	Inova
L 20d	23739	38.12	42.0	2.96	0.0385	5.48	74	Inova
L 20f	26957	38.49	42.4	2.65	0.0373	4.75	75	Inova

$f_{52nd\ day}$: strength calculated for 52nd day, strength increase with time considered
 f_{day} : strength determined in test, no consideration of strength increase with time

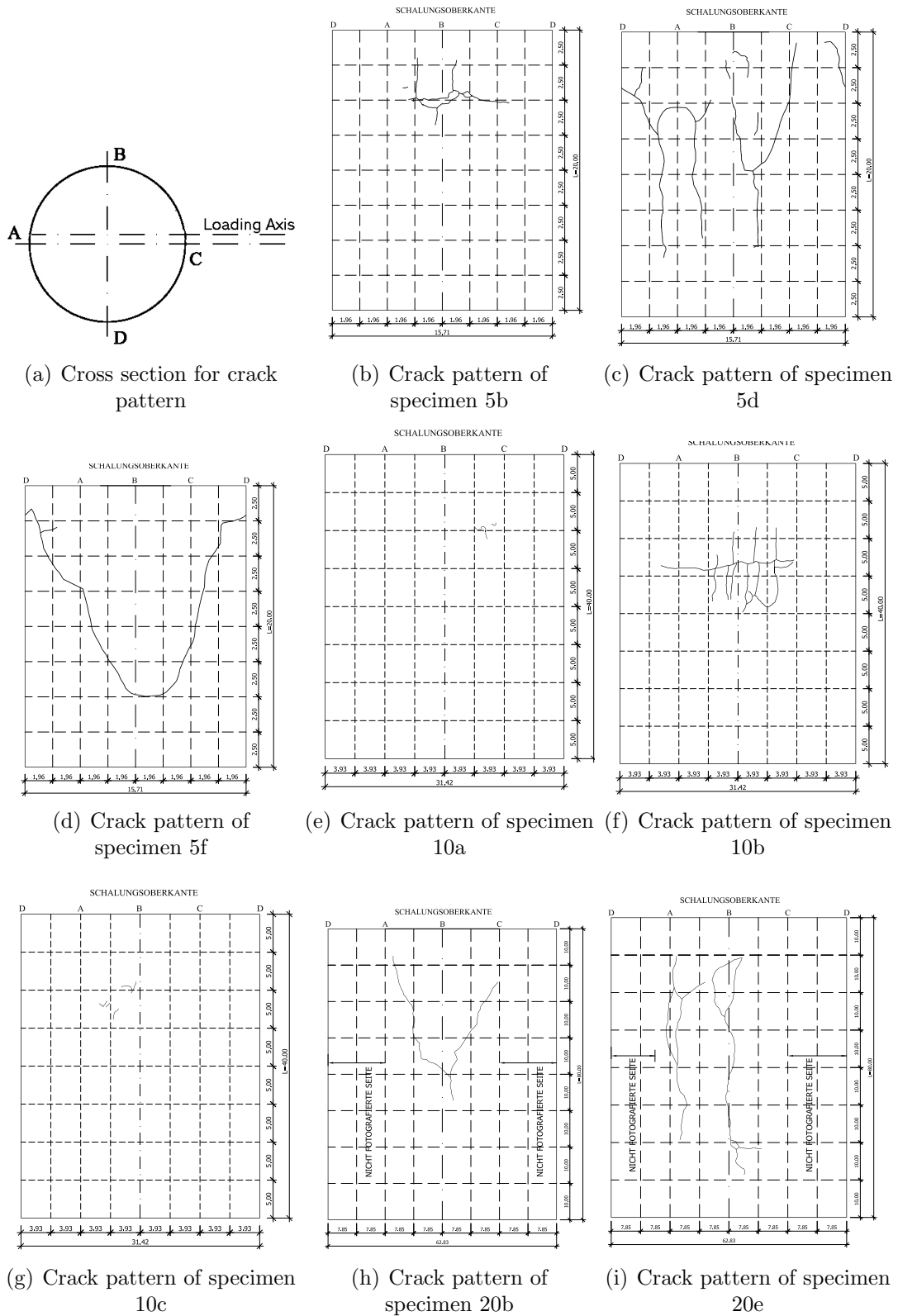


Figure 9.17: Crack patterns of specimens with size S, M and L

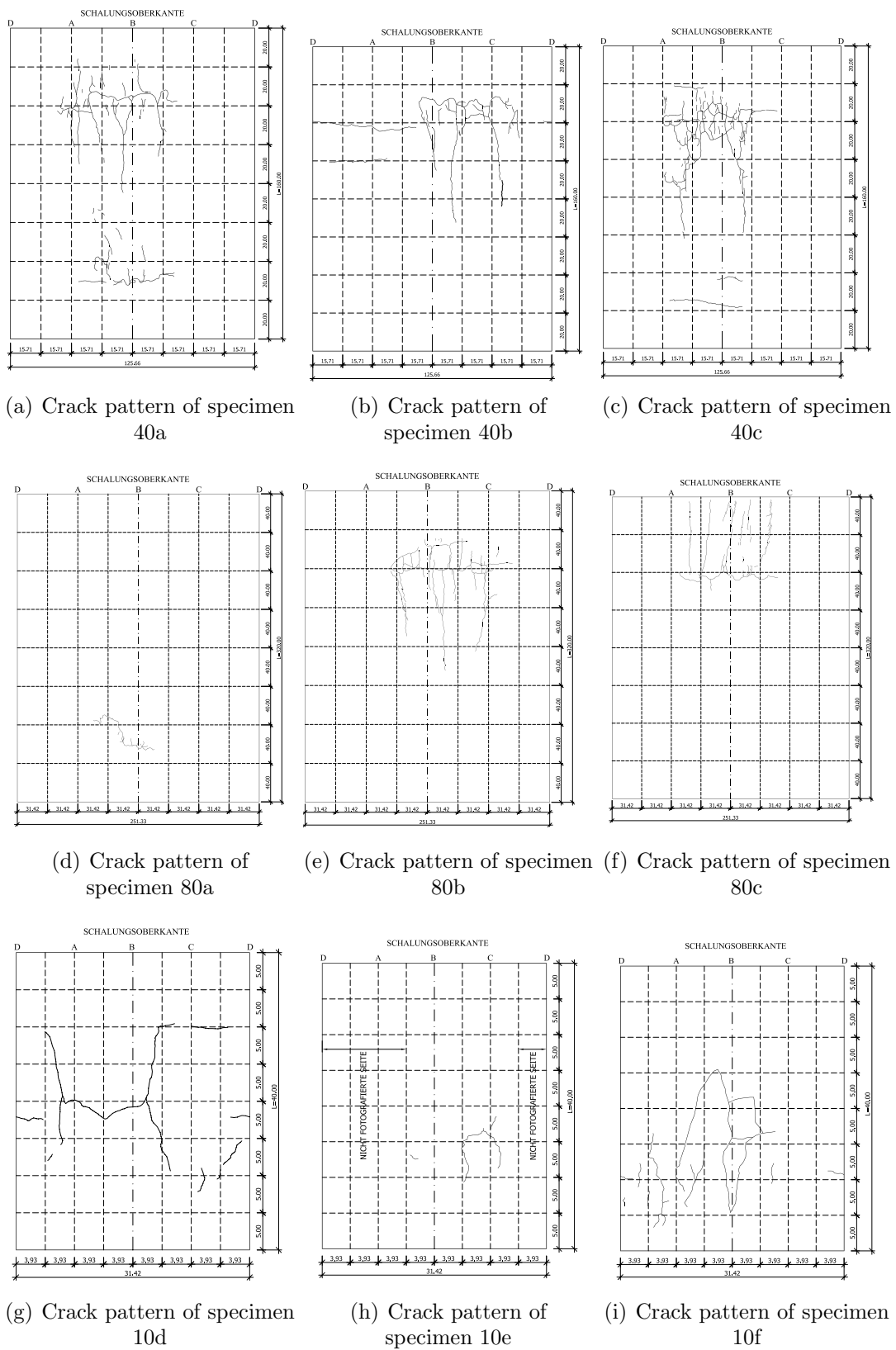


Figure 9.18: Crack patterns of specimens with size XL, XXL and M tested in Inova machine

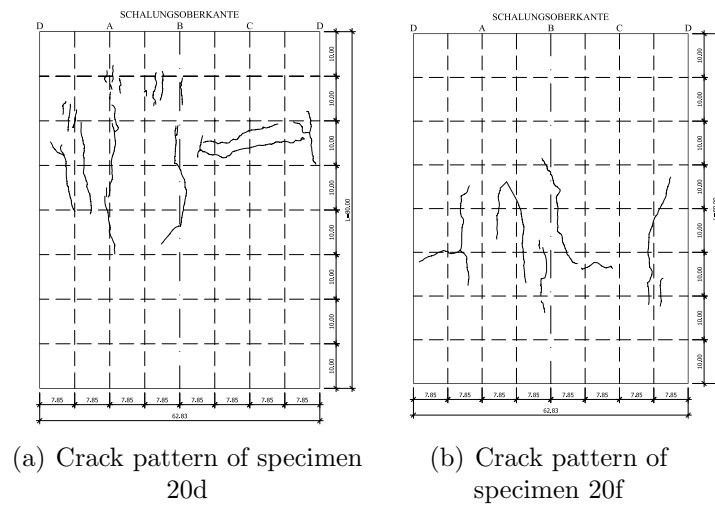


Figure 9.19: Crack patterns of specimens with size L tested in Inova machine at TU Prague

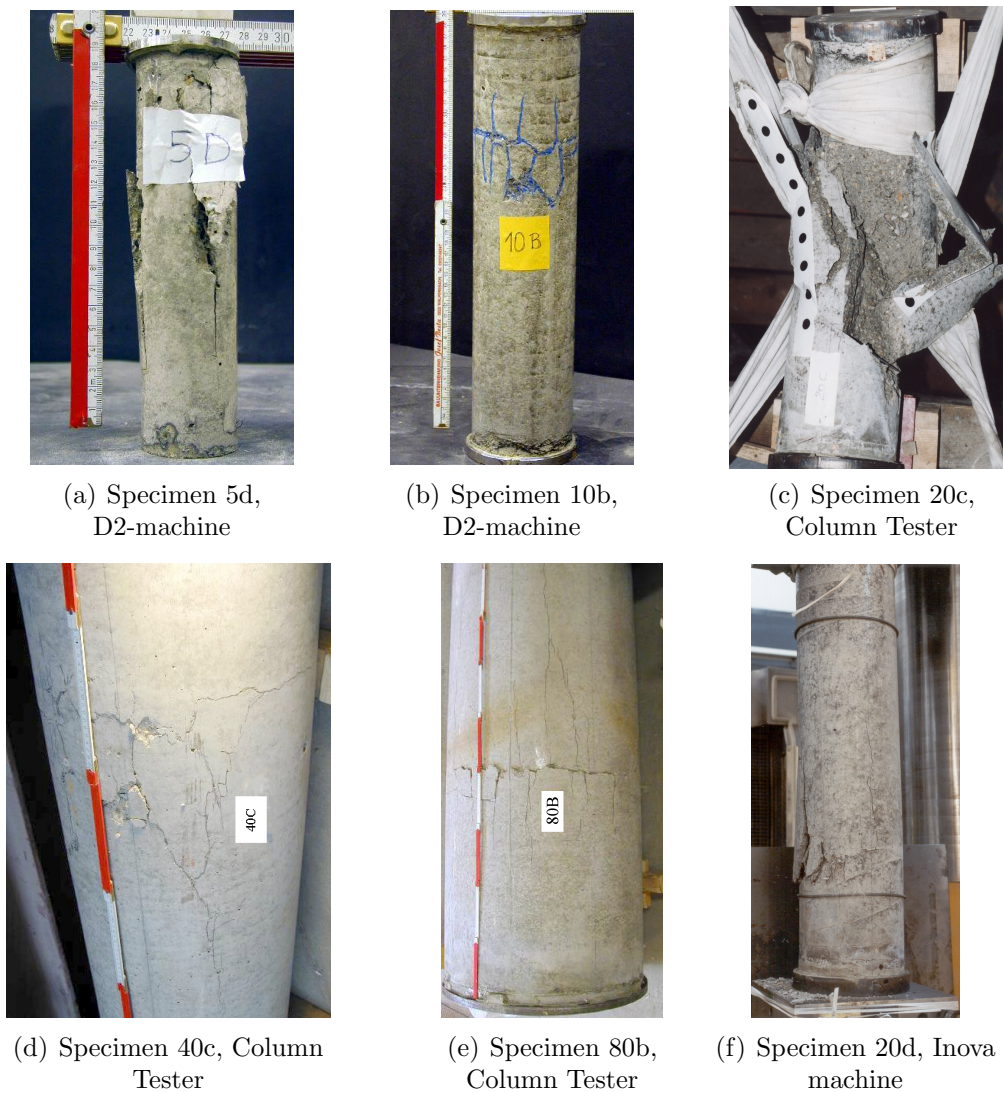


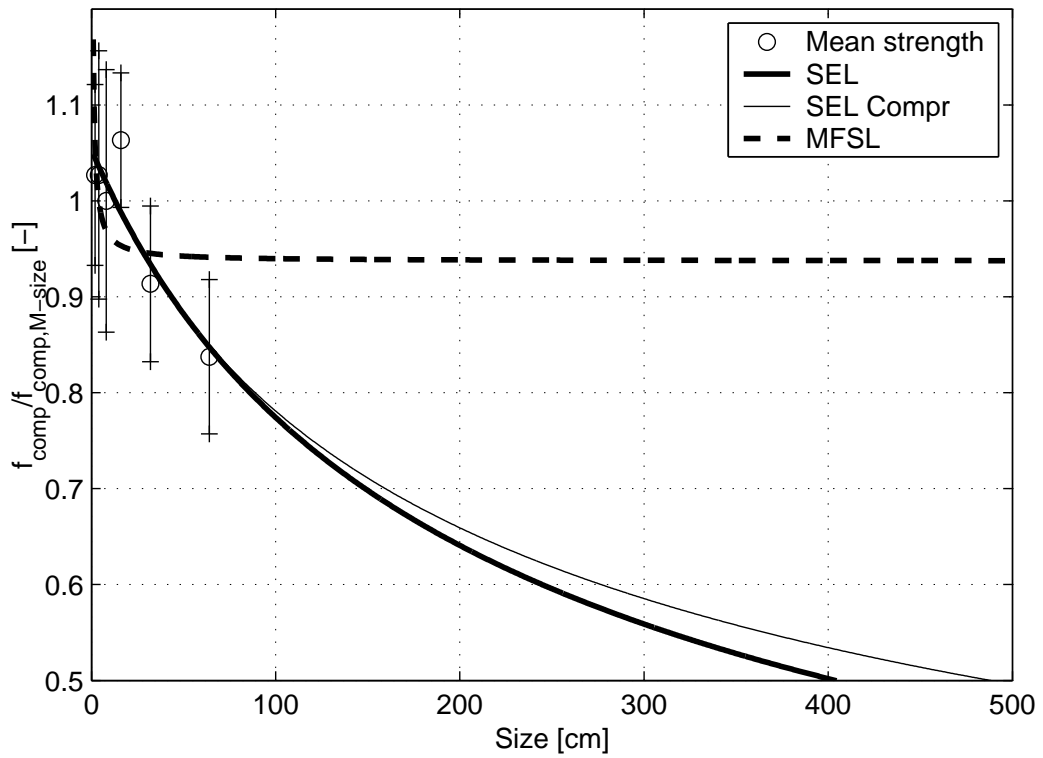
Figure 9.20: Specimens photographed after testing

Chapter 10

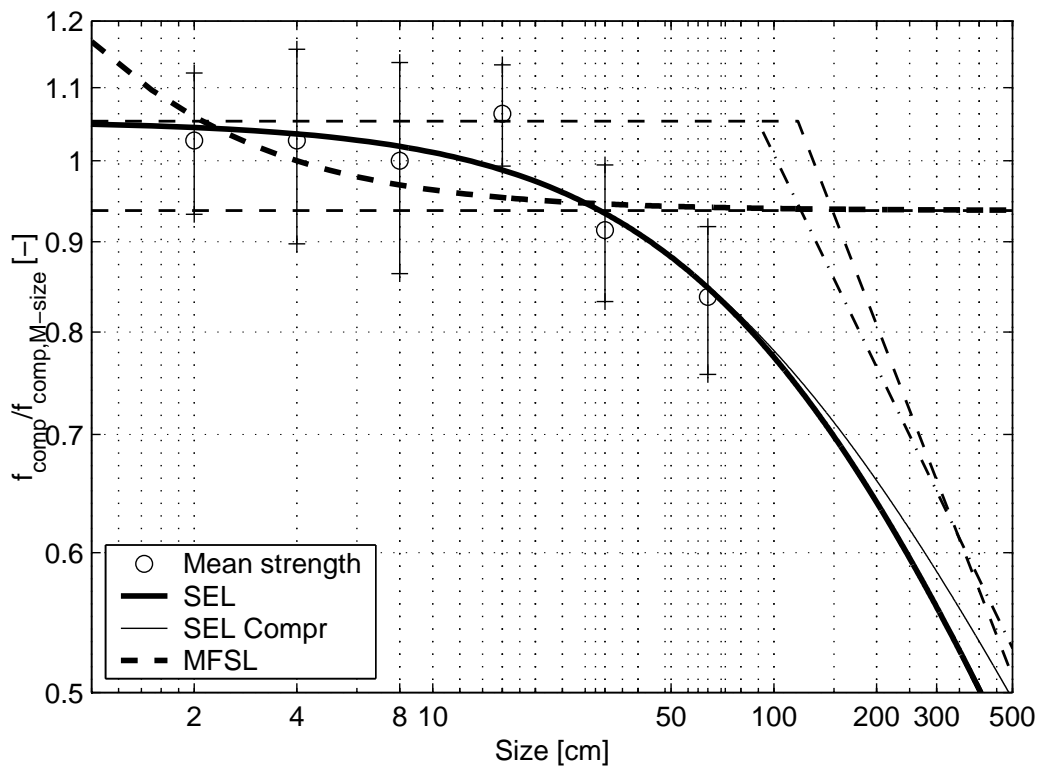
Summary of main results

10.1 Sandstone experiments

Specimens with a height to width ratio of 2:1 were tested under eccentric loading. On the compressed side the specimen had a smooth notch to predefine the location where failure started. The specimens were geometrically equal. All dimensions of the specimens were scaled by a factor from one size to the other. The size range in the *test series* was 1:32 and in the *verification series* it was 1:8. A size effect on strength was determined in the sandstone for larger sizes. For the small sizes the verification series showed that the strength is dependent on density of the material. For specimens of equal density the strength did not change with specimen size. The sandstones of the *preliminary series*, the *test series* and the *verification series* were from different locations in the quarry and had different maximum strengths. Thus the strength values were normalized (divided by the mean strength of specimens M, D= 8cm). In figure 10.1 the Size Effect Laws by Bažant (SEL, SEL-compression) and the Multifractal Scaling Law by Carpinteri (MFSL) were fitted to the data. The normalized strength versus size is given in linear (a) and double logarithmic scaling (b). A detailed description of results is given in section 7. The SEL and the SEL-compression laws are on the same line inside the tested range and show only small differences at the maximum size plotted. In figure 10.1 the laws are also drawn for sizes that were larger than the tested ones. The trend from the SEL and SEL-compression follows better the data than the trend from the MFSL.



(a) Data presented with linear scaling.



(b) Data presented with double logarithmic scaling.

Figure 10.1: Strength of individual specimens versus size and data fit with MFSL and SEL

10.2 Concrete experiments

The concrete tests were performed on specimens with circular cross section and a height to diameter ratio of 4:1. 5 different sizes were tested which were all geometrically equal. The size range was 1:16. All tests were performed between the 48th and the 75th day after moulding. The increase of concrete strength in this time range was determined on accompanying tests on concrete cylinders. It was assumed that the strength of the cylinders increased by the same ratio as the strength of the specimens. The strength were all calculated for the 52nd day after moulding and plotted in figure 10.2. The SEL and the MFSL were fitted to the data and plotted in figure 10.2. The results are similar to the results of the sandstone series. The trend of the large sizes shows clearly a decreasing strength with size. The difference between SEL and SEL-compression is little for small and large sizes. In the range of experimental data both laws are on a line. When extrapolating the laws to larger sizes one can see clearly in the double logarithmic plot, that the SEL and the SEL-compression follow the trend indicated by the data. The MFSL does not follow this trend. In section 9.6 the laws were fitted to different data sets. The residual norm is a measure how close the fitted function is to the data and varied depending on the data set used. These values were not a clear indicator for the suitability of a law, because a low value does not assure that the trend of the data was captured by the model.

The SEL laws follow the trend of the data, but MFSL does not, see figure 10.2. See chapter 9 for a detailed discussion of results. As already mentioned for the sandstone series, the standard deviations showed a decreasing trend with increasing specimen size.

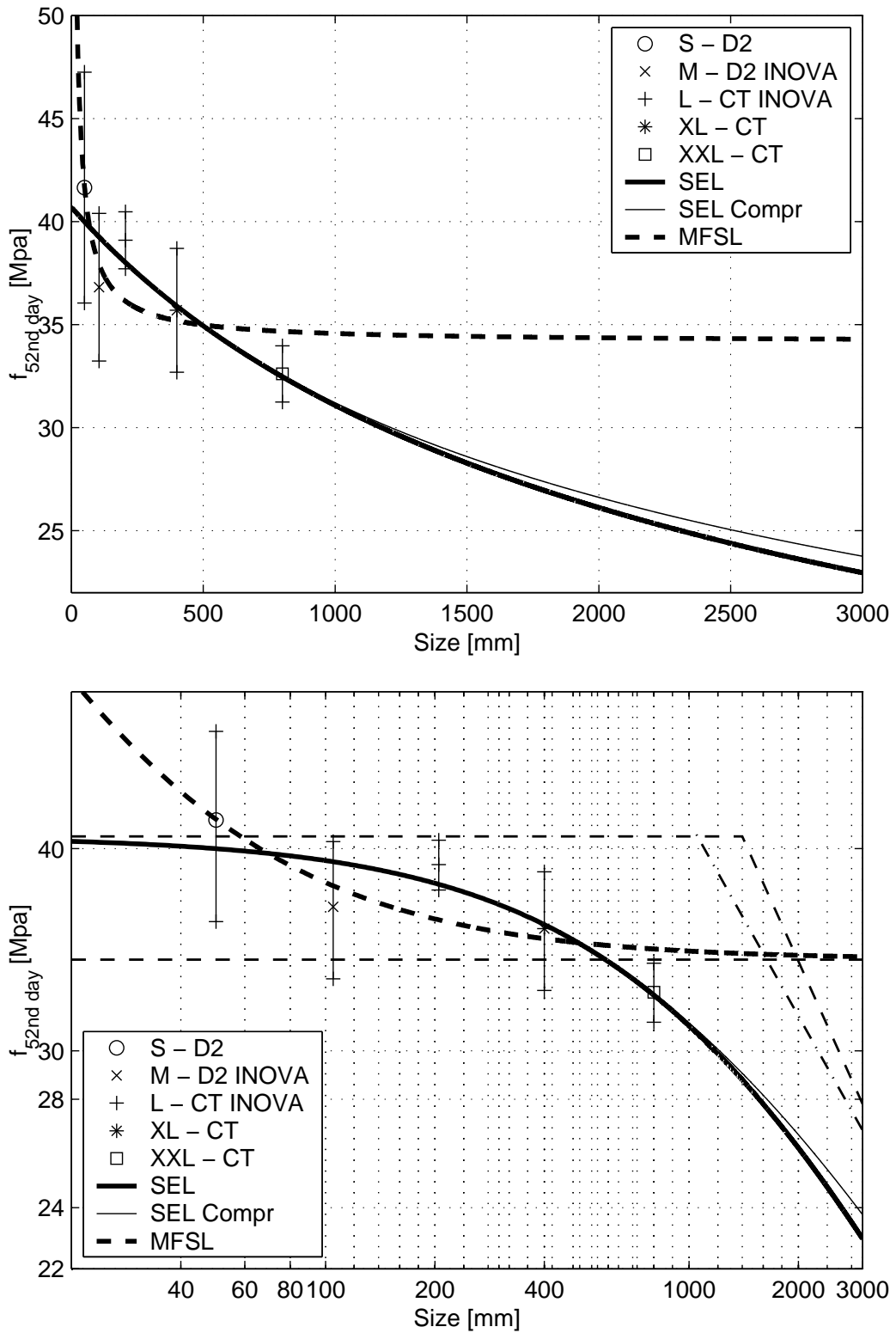


Figure 10.2: The mean strength of the specimens at 52nd day and data fit with MFSL and SEL

Bibliography

- Bažant, Z. (1997). Scaling of quasibrittle fracture: Asymptotic analysis. *International Journal of Fracture*, 83(1):19–40.
- Bažant, Z. (1999). Size effect on structural strength: A review. *Archive of Applied Mechanics*, 69:703–725.
- Bažant, Z. and Chen, E. (1997). Scaling of structural failure. *Applied Mechanics Reviews*, 50(10):593–627.
- Bažant, Z., Kim, J.-J. H., Daniel, I. M., Becq-Giraudon, E., and Zi, G. (1999). Size effect on compression strength of fiber composites failing by kink band propagation. *International Journal of Fracture*, 95:103–141.
- Bažant, Z. and Kwon, Y. (1994). Failure of slender and stocky reinforced concrete columns: tests of size effect. *Materials and Structures, RILEM*, 27.
- Bažant, Z., Lin, F.-B., and Lippmann, H. (1993). Fracture energy release and size effect in borehole breakout. *Int. J. Numerical and Analytical Methods in Geomechanics*, 17:1–14.
- Bažant, Z. and Ožbolt, J. (1992). Compression failure of quasi-brittle material: Nonlocal microplane model. *Journal of Engineering Mechanics, ASCE*, 118(3):540–556.
- Bažant, Z. and Planas, J. (1998). *Fracture and size effect in concrete and other quasibrittle materials*. CRC Press LLC.
- Bažant, Z. and Xiang, Y. (1997). Size effect in compression fracture: Splitting crack band propagation. *J. Eng. Mech.-ASCE*, 123(2):162–172.
- Bažant, Z. P. (1984). Size effect in blunt fracture: Concrete, rock, metal. *Journal of Engineering Mechanics*, 110(4):518–535.

- Burtscher, S. L., Aus der Schmitt, H., Watzl, B., and Kollegger, J. (2003a). Experiments on the size effect in sandstone under compression. Technical Report 4, Institut for Structural Concrete, Vienna University of Technology. ISBN 3-902089-03-2.
- Burtscher, S. L., Kollegger, J., Rinnhofer, G., and Barnas, A. (2002). Schleuderbetonstützen mit hoher Tragfähigkeit für Bauvorhaben in Österreich. *OIB aktuell*, 3. Jahrgang(3):9–13.
- Burtscher, S. L., Suda, G., Mihaylov, V., and Kollegger, J. (2003b). Size effect tests on concrete columns. Technical Report 5, Institute for Structural Concrete, Vienna University of Technology. ISBN 3-902089-04-0.
- Carpinteri, A. (1994). Scaling laws and renormalization groups for strength and toughness of disordered materials. *International Journal of Solids and Structures*, 31(3):291–302.
- Carpinteri, A. and Ferro, G. (1994). Size effects on tensile fracture properties: A unified explanation based on disorder and fractality of concrete microstructure. *Materials and Structures*, 27:563–571.
- Carpinteri, A., Ferro, G., and Monetto, I. (1999). Scale effects in uniaxially compressed concrete specimen. *Magazine of Concrete Research*, 51(3):217–225.
- Choi, S., Thienel, K.-C., and Shah, S. (1996). Strain softening of concrete in compression under different end constraints. *Magazine of Concrete Research*, 48(175):103–115.
- Dempsey, J., Adamson, R., and Mulmule, S. (1995). Scale effects on the in-situ tensile strength and fracture of sea ice. Part II: First-year sea ice at Resolute, N.W.T. *International Journal of Fracture*, 95(1/4):347–366.
- Gonnerman, H. F. (1925). Effect of size and shape of test specimen on compressive strength of concrete. *ASTM*, 25(2):237–250.
- Griffith, A. (1921). The phenomena of rupture and flow in solids. *Phil. trans.*, 221A:179–180.
- Hillerborg, A., Modéer, M., and Petersson, P. (1976). Crack growth and development of fracture zones in plain concrete and similar materials. *Cement and Concrete Research*, 6:773–782.
- Hollingworth, S. (1998). *Structural and mechanical properties of high strength concrete*. PhD thesis, Division of Civil Engineering, Cardiff, University of Wales.

- Jansen, D. and Shah, S. (1997). Effect of length on compressive strain softening of concrete. *Journal of Engineering Mechanics*, 123(1):25–35.
- Kim, J.-K., Yi, S.-T., Park, C.-K., and Eo, S.-H. (1999). Size effect on compressive strength of plain and spirally reinforced concrete cylinders. *ACI Structural Journal*, 96(1):88–94.
- Leaird, J. D. (1997). *Acoustic Emission Training Guide. How to Ensure an Accurate and Valid Acoustic Emission Test*. Greensland Publishing Company, P.O. Box 254531, Sacramento, CA 95825.4531.
- Linsbauer, H. N. and Šanjna, A. (1999). Horizontal wedge splitting test method (HWST) - a new method for the fracture mechanics testing of large samples. In *Euromat 99, European Congress on Advanced Materials and Process*, München.
- Mariotte, E. (1718). *Traité du mouvement des eaux.*, page 249. Posthumously Edited by M. De la Hire, transl. by J.T. Desvagliers, London.
- Marti, P. (1989). Size effect in double-punch tests on concrete cylinders. *ACI Materials Journal*, 86(6):597–601.
- Miller, R. K. and McIntire, P., editors (1987). *Nondestructive Testing Handbook*, volume 5. American Society for Nondestructive Testing, U.S.
- Müller, R. (2001). Size effect im Betonbau. Master's thesis, Vienna University of Technology, Institute for Structural Concrete.
- Němeček, J. (2000). *Modeling of compressive softening of concrete*. PhD thesis, CTU Prag, in: CTU Reports. ISBN 80-01-02298-6.
- Okubo, S. and Nishimatsu, Y. (1985). Uniaxial compression testing using a linear combination of stress and strain as the control variable. *Int. J. of Rock Mechanics Mining Sciences and Geomechanics*, 22(5):323–330.
- Palmquist, M. and Jansen, D. (2001). Postpeak strain-stress relationship for concrete in compression. *ACI Materials Journal*, 98(3):213–219.
- Piller, W. and Vavra, N. (1991). St. Margarethen "Römersteinbruch" bzw. Steinbrüche "Hummel" und "Kummer". *Exkursionen im Tertiär Österreichs*, pages 200–202.
- Rohatsch, A. (1997). St. Margarethen: Leithakalk (Mittleres bis oberes Badenium). *Gesteinskunde in der Denkmalpflege*, page 62.

- Schickert, G. (1980). Schwellenwerte beim Betondruckversuch. *Deutscher Ausschuß für Stahlbeton, Berlin*, 312.
- Schwarz, L. (1987). Neue Möglichkeiten der Experimentellen Tragwerksuntersuchung an der Abteilung für Angewandte Modellstatik im Stahlbau der TU-Wien. *Stahlbau Rundschau*, 68:2–8.
- Sener, S. (1997). Size effect tests of high strength concrete. *Journal of Materials in Civil Engineering*, 9(1):46–48.
- Sener, S., Barr, B., and Abusiaf, H. (1999). Size-effect tests in unreinforced concrete columns. *Magazine of Concrete Research*, 51(1):3–11.
- Slowik, V. (1995). Beiträge zur experimentellen Bestimmung bruchmechanischer Materialparameter von Beton. Technical Report 3, ETH, Laboratory for Building Materials.
- Tschegg, E., Elser, M., and Stanzl-Tschegg, S. (1995). Biaxial fracture tests on concrete - development and experience. *Cement and Concrete Research*, 17:57–75.
- Vallen Systeme, G. (1994). *Focus three: The AMS3 Hit-Cascade-Processing*. Vallen - Systeme, GmbH, Icking, Germany.
- Vallen Systeme, G. (2000). *Schallemissionsprüfung: Grundlagen, Gerätetechnik, Anwendungen*. Vallen - Systeme, GmbH, Icking, Germany.
- Van Mier, J., Shah, S., Arnaud, M., Balayassac, J., Bascoul, A., Choi, S., Dasenbrock, D., French, G. F. C., Gobbi, M., Karihaloo, B., König, G., Kotsovos, M., Labuz, J., Lange-Kornbak, D., Markeset, G., Pavlovic, M., Simsch, G., Thienel, K.-C., Turatsinze, A., Ulmer, M., Geel, H. V., Vliet, M. V., and Zisopoulos, D. (1997). Fracture processes of concrete. *Materials and Structures, Rilem*, 30:195–209.
- Van Vliet, M. (2000). *Size Effects in Tensile Fracture of Concrete and Rock*. PhD thesis, Technical University Delft.
- van Vliet, M. and van Mier, J. (1996). Experimental investigation of concrete fracture under uniaxial compression. *Mechanics of Cohesive-Frictional Materials*, 1:115–127.
- Walsh, P. (1972). Fracture of plain concrete. *Indian Concrete Journal*, 46(11):469–470.

- Weibull, W. (1939). The phenomenon of rupture in solids. *Proc. Royal Swedish Inst. Eng. Res. (Ingenioersvetenskaps)*, 153:1–55.
- Williams, E. (1957). Some observations of Leonardo, Galileo, Mariotte and others relative to size effect. *Annals of Science*, 13:23–29.
- Zisopoulos, P., Kotsovos, M., and Pavlovic, M. (2000). Deformational behaviour of concrete specimens in uniaxial compression under different boundary conditions. *Cement and Concrete Research*, 30:153–159.